

On the pulse-width statistics in radio pulsars. I. Importance of the interpulse emission

Krzysztof Maciesiak¹*, Janusz Gil¹ and Valério A. R. M. Ribeiro²

¹*Kepler Institute of Astronomy, University of Zielona Góra, Lubuska 2, 65-265 Zielona Góra, Poland*

²*Astrophysics Research Institute, Liverpool John Moores University, Twelve Quays House, Egerton Wharf, Birkenhead, CH41 1LD*

Accepted . Received ; in original form

ABSTRACT

We performed Monte Carlo simulations of different properties of pulsar radio emission, such as: pulsar periods, pulse-widths, inclination angles and rates of occurrence of interpulse emission (IP). We used recently available large data sets of the pulsar periods P , the pulse profile widths W and the magnetic inclination angle α . We also compiled the largest ever database of pulsars with interpulse emission, divided into the double-pole (DP-IP) and the single-pole (SP-IP) cases. We identified 31 (about 2%) and 13 (about 1%) of the former and the latter, respectively, in the population of 1520 normal pulsars. Their distribution on the $P - \dot{P}$ diagram strongly suggests a secular alignment of the magnetic axis from the originally random orientation. We derived possible parent distribution functions of important pulsar parameters by means of the Kolmogorov-Smirnov significance test using the available data sets (P , W , α and IP), different models of pulsar radio beam $\rho = \rho(P)$ as well as different trial distribution functions of pulsar period P and the inclination angles α . The best suited parent period distribution function is the log-normal distribution, although the gamma function distribution cannot be excluded. The strongest constraint on derived model distribution functions was the requirement that the numbers of interpulses generated by means of Monte Carlo simulations (both DP-IP and SP-IP cases) were exactly (within 1σ errors) at the observed level of occurrences. We found that a suitable model distribution function for the inclination angle is the complicated trigonometric function which has two local maxima, one near 0° and the other near 90° . The former and the latter implies the right rates of IP, occurrence, single-pole (almost aligned rotator) and double-pole (almost orthogonal rotator), respectively. It is very unlikely that the pulsar beam deviates significantly from the circular cross-section. We found that the upper limit for the average beaming factor f_b describing a fraction of the full sphere (called also beaming fraction) covered by a pulsar beam is about 10%. This implies that the number of the neutron stars in the Galaxy might be underestimated.

Key words: stars: pulsars: general – stars: neutron – stars: rotation

1 INTRODUCTION

Although the number of pulsars discovered recently in modern search campaigns increased enormously, the observed pulsar population is still a small fraction of the neutron star population in the Galaxy. Most of them will never be detected as radio pulsars due to misalignment of their beams with our line-of-sight (l-o-s). However, many of those whose beams point towards the Earth still await detection in future, more sensitive pulsar surveys. Therefore, a more or less complete knowledge about Galactic pulsar population can be obtained only by means of statistical considera-

tions. Statistical studies of the pulse-width in mean profiles of radio pulsars is an important tool for investigations of the geometry of pulsar radiation. One especially important parameter that can be derived from such studies is the inclination angle between the magnetic and the spin pulsar axes. Early studies were carried out by Henry & Paik (1969), Roberts & Sturrock (1972, 1973), Backer (1976) and Manchester & Lyne (1977, hereafter ML77). Since the amount of the available data was small, these papers suffered from problems of small number statistics. A more complete work was performed by Prószyński (1979) and Lyne & Manchester (1988), who analyzed samples of about 200 pulse-width data measured near 400 MHz. Although the database used in these papers was quite rich, the pulse-

* E-mail:jezyk@astro.ia.uz.zgora.pl

width measurements were contaminated by the interstellar scattering dominating at low radio frequencies. More recently Gil & Han (1996; hereafter GH96) compiled a new database of 242 pulse-widths W_{10} (corresponding to about 10 per cent of the maximum intensity) measured at a higher radio frequency (near 1.4 GHz), which was relatively unbiased compared to the lower frequency data. GH96 used their pulse-width database to perform Monte Carlo simulations in an attempt to derive the distribution statistics of pulsar periods, pulse-widths, magnetic inclination angles and rates of interpulses. By comparing the simulated and observed (or observationally derived) quantities they concluded that the observed distribution of the inclination angles resembles a sine function following from the flat (random) distribution in the parent population, and that the probability (beaming fraction) of observing a pulsar was about 0.16. GH96 also pointed out that the rates of interpulse occurrence should be considered as an important aspect of pulsar population studies.

On the other hand, Tauris & Manchester (1998, hereafter TM98) using a different method based on an analysis of the indirectly derived polarization position angles and magnetic inclination angles concluded that the observed distribution of the latter is cosine-like rather than sine-like as suggested by GH96. They also obtained the beaming fraction 0.10 ± 0.02 , considerably lower than 0.16 obtained by GH96. TM98 pointed out a likely source of this discrepancy, namely the incorrect assumption used by GH96 that the observed distribution and the parent distribution of pulsar periods are similar. Recently, Zhang, Jiang & Mei (2003, hereafter ZJM03) followed the Monte Carlo simulation scheme developed by GH96. ZJM03 argued that both the parent distribution function and the observed distribution of pulsar periods can be modelled by the gamma function but with different values of the free parameters, and their Monte Carlo simulations included searching for a 2-D grid of these parameters. As a result, ZJM03 concluded that indeed the cosine-like distribution (suggested by TM98) is much more suitable to model the inclination angles in the parent pulsar population than the flat distribution (suggested by GH96). They argued that the most plausible parent distribution is a modified cosine function (see Section 2.1.1), which has a peak around 25° and another weaker peak near 90° . They also obtained the beaming fraction ~ 0.12 , consistent with the result of TM98.

As emphasized by ZJM03 in the conclusions of their paper, neither they nor TM98 considered potentially important constraints related to the observable interpulse emission. Kolonko et al. (2004, KGM04 hereafter) corrected this shortcoming of analysis of ZJM03 and included the rates of occurrences of the interpulse emission, divided into categories of single-pole and double-pole origin. In this paper we follow the scheme developed by KGM04 but with a few important improvements. We used much richer databases of pulsar periods, pulse-widths and interpulse occurrences. Moreover, we use broader spectrum of trial distribution functions in our Monte Carlo simulations.

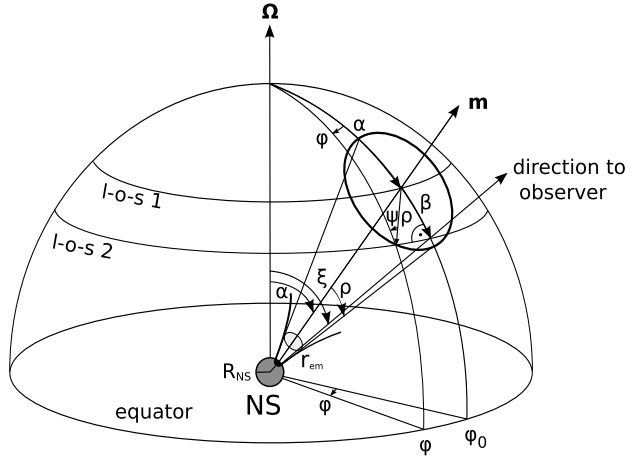


Figure 1. Geometry of the pulsar radiation presented schematically on the "celestial" hemisphere centred on the neutron star (NS) with the radius R_{NS} . The polar cap is marked as a black area on the shadow NS surface. The radio emission region is marked at the altitude r_{em} . The fiducial plane $\varphi_0 = 0$ contains the rotation Ω and the magnetic \mathbf{m} axes as well as the observer's direction. The following angles are marked: the longitudinal phase φ measured from the fiducial phase $\varphi = 0$, the inclination angle α between the magnetic \mathbf{m} and the spin Ω axes, the impact angle β of the closest approach of the observer to the magnetic axis, the observer's angle $\xi = \alpha + \beta$, the opening angle of the radiation beam ρ and the polarisation position angle ψ . Two exemplary line-of-sights are marked: l-o-s 1 passing through the magnetic axis ($\beta = 0$) and l-o-s 2 corresponding to a grazing impact angle $\beta \sim \rho$.

2 GEOMETRY OF THE PULSAR RADIATION

The basic condition for the pulsar to be detected is that it should be bright enough for sensitivity of the observing system used in the radio observatory. In this paper we assume that this condition is always satisfied (some consequences of this assumption are discussed in Appendix A (in the on-line materials)) and our main concern is geometrical detection conditions. Pulsar can be detected if its narrow beam sweeps through the observer. We use this geometrical detection method in our Monte Carlo simulations, without taking into account the intrinsic pulsar luminosity (although we briefly discuss this problem in Section 5). However, we restrict our parameter space to quantities that should not be strongly affected by the luminosity problem.

The geometry of pulsar radiation is schematically shown in Fig. 1. The observed pulse-width W (ignoring dispersive and scattering broadening; see Section 3.2) depends on the intrinsic angular radius of the beam ρ , the inclination angle α and the impact angle β . Purely geometrical pulse-width W_l on the l -th level of the maximum intensity of the profile is

$$W_l = 2 \cdot \varphi_l =$$

$$4 \cdot \arcsin \left\{ \left[\frac{\sin((\rho_l + \beta)/2) \cdot \sin((\rho_l - \beta)/2)}{\sin \alpha \cdot \sin(\alpha + \beta)} \right]^{1/2} \right\} \quad (1)$$

(Gil 1981). For the impact angle $\beta = 0^\circ$ (corresponding to a very rare situation when the line-of-sight cuts through the centre of the beam) and the inclination angle $\alpha = 90^\circ$

(corresponding to the case of the orthogonal rotator), we get $W = 2\rho$. For non-orthogonal rotator this gives a very well known approximation $W = 2\rho/\cos \alpha$. Thus, roughly speaking the pulse-width is proportional to the angular radius of the beam ρ . We would like to emphasize that Eq. (1) assumes symmetry of the pulsar beam (and thus symmetry of the pulse-width but not necessarily the pulse shape) with respect to the fiducial phase φ_0 (Fig. 1). We paid special attention to selecting pulsars with relatively low dispersion measure DM , free from broadening features (see Section 3.2) that would introduce significant asymmetry into pulsar profiles.

2.1 Probability density distribution functions

The main aim of this work is to carry out statistical studies of emission properties of the normal radio pulsars. On the one hand, we have samples of different measurable (directly or indirectly) parameters obtained for a large number of pulsars. On the other, we can simulate these parameters and compare the simulated values with the measured ones. In each case the important question we try to answer is what the statistical distributions of these parameters are in the observed sample, and more generally in the whole pulsar population. Below we consider possible trial distribution functions of selected pulsar parameters. We present the so-called parent trial distribution functions, which should be distinguished from the observed distributions.

2.1.1 Inclination angle α and impact angle β

In an arbitrary coordinate system the spin axis of the neutron star and the viewer's line-of-sight are both randomly chosen uniformly on the surface of the sphere, resulting in an isotropic distribution of both. The correlated probability distribution of the observer's angle $\xi = \alpha + \beta$ relative to the spin axis is given by

$$f(\xi) = \sin(\xi) = \sin(\alpha + \beta), \quad (2)$$

where α and β are the inclination and the impact angles¹, respectively (Fig. 1). However, the actual distribution of the inclination angle α may depend on number of unknown factors. Therefore, we considered a number of trial probability density functions for the parent distribution of α , including flat distribution

$$f(\alpha) = \frac{2}{\pi}, \quad (3)$$

sine function

$$f(\alpha) = \sin \alpha, \quad (4)$$

¹ Range of the observer's angle ξ , inclination angle α and impact angle β is as follows: $0 \leq \xi \leq \pi$, $0 \leq \alpha \leq \pi/2$ and $-\pi/2 \leq \beta \leq \pi/2$. The observer's ξ angle is uniformly distributed on a sphere, however the inclination angle α is drawn from one of the trial probability density functions (Eqs. (3) – (7)). Thus, the impact angle β distribution is not uniform but depends on distribution of the inclination angle. Let us keep in mind that for the observed pulsars the impact angle $\beta \leq \rho$, where ρ is the angular width of the emission beam (Fig. 1). Although distributions of both α and β are unknown, their sum is uniformly distributed on a sphere.

or cosine function

$$f(\alpha) = \cos \alpha. \quad (5)$$

Apart from the simple functions presented above some more complicated probability density functions were considered as well. As a parent distribution function of the inclination angle α GH96 proposed the following function

$$f(\alpha) = \frac{5}{4} + \cos\left(\frac{5}{2}\alpha\right). \quad (6)$$

Later ZJM03 proposed even more complicated function

$$f(\alpha) = \frac{0.6}{\cosh(3.5(\alpha - 0.43))} + \frac{0.15}{\cosh(4.0(\alpha - 1.6))} \quad (7)$$

which they called the modified cosine function. This function is characterised by two local maxima, around $\alpha \approx 25^\circ$ and another weaker one around $\alpha \approx 90^\circ$. Interestingly ZJM03 did not consider rates of interpulse occurrence in their paper and their complicated cosine function was introduced to improve modelling of the parent inclination angles by means of Monte Carlo simulations. Later, KGM04 demonstrated that this function is also responsible for the occurrence of the proper amount of interpulses. We do not confirm this conclusion in the present paper, using much larger databases of the observed pulsar parameters and interpulses. We find that the most suitable parent distribution is that proposed by GH96 (6).

2.1.2 Period P

GH96 showed that the distribution function of the observed 516 pulsars with periods $0.05 < P < 4.2$ s can be fitted² by the gamma function

$$f(P) = \mathcal{N}_0 x^{a-1} e^{-x}, \quad (8)$$

where \mathcal{N}_0 is the normalisation constant, $x = P/m$ and, m and a are values of the free parameters. ZJM03 used this function to fit much larger sample of the 1165 period values from the same period range and obtained good result. They argued that the parent distribution of periods is different from the observed distribution and it is very convenient to use the gamma function with the values of m and a treated as free parameters of the model. We will use this approach, generalized by including a number of other trial probability density functions, like the Lorentz function

$$f(P) = \frac{\mathcal{C}_0}{1 + (P - x_0)^2/a_0^2}, \quad (9)$$

where \mathcal{C}_0 is the normalisation constant, x_0 and a_0 are free parameters. Another trial function that we considered was the Gauss function representing normal distribution

$$f(P) = \frac{1}{\sigma\sqrt{2\pi}} \exp\left(\frac{-(P - x_0)^2}{2\sigma^2}\right), \quad (10)$$

² Fit of this function to the observed data was obtained with the least square method, minimalising $\sum_i \left[N(x_i) - \mathcal{N}_0 \int_{x_i}^{x_{i+1}} x^{a-1} e^{-x} dx \right]^2$. They found values of free parameters m and a as well as the normalising constant \mathcal{N}_0 (details in GH96).

where x_0 and σ are free parameters. We also tried the log-normal distribution

$$f(P) = \frac{1}{P\sigma\sqrt{2\pi}} \exp\left[\frac{-(\log P - x_0)^2}{2\sigma^2}\right] \quad (11)$$

(suggested by Lorimer et al. (2006)), where x_0 and σ are free parameters of period probability distribution function whose logarithm is normally distributed.

2.1.3 Opening angle ρ

The opening angle (radius) of the pulsar beam can be calculated from the pulse-width W if α and β angles are known, either from the polarisation data (Manchester & Taylor 1977) or from the width of the core component (using Eq. (29) taken from Rankin (1990; hereafter R90)), or both. Inverting Eq. (1) one obtains the opening angle ρ as a function of α , β and W (Gil et al. 1984)

$$\rho_l = 2 \sin^{-1} \left[\sin \alpha \sin(\alpha + \beta) \sin^2 \frac{W_l}{4} + \sin^2 \left(\frac{\beta}{2} \right) \right]^{1/2}. \quad (12)$$

Lyne & Manchester (1988) were the first who applied this equation to a large number of 10 per cent pulse-width data W_{10} measured at 408 MHz. They argued that $\rho_{10}(408 \text{ MHz}) \approx 6^\circ.5 P^{-1/3}$, which scaled to the 1.4 GHz was

$$\rho_{10} = 5^\circ.8 P^{-1/3}. \quad (13)$$

Biggs (1990) reanalysed the same sample of data and argued that

$$\rho_{10} = 5^\circ.6 P^{-1/2}. \quad (14)$$

Rankin (1993a) analysed a large sample of pulse-widths data taken at different frequencies in different world radio observatories over a period of several years. She has interpolated all available data to frequency of about 1 GHz and divided them into different profile classes (according to Rankin (1983)). In each class she obtained a bimodal $\propto P^{-1/2}$ opening angle distribution. This result clearly indicated that pulsar beams consist one or two coaxial cones centred on the magnetic axis, with the opening angle ρ of each cone following $P^{-1/2}$ period dependence. Gil, Kijak & Seiradakis (1993; GKS93) and Kramer et al. (1994) have confirmed this result at frequency 1.4 GHz, using data obtained with the Effelsberg 100 m radiotelescope. Instead of dividing pulsars into different classes to reveal the bimodal $P^{-1/2}$ distribution of ρ , GKS93 performed a careful error analysis and rejected all data subject to large errors (broadening the apparent distribution). As a result they obtained that for given period P , the opening angle ρ can have two possible values:

$$\rho_{10} = \begin{cases} 6^\circ.3 P^{-1/2} \\ 4^\circ.9 P^{-1/2} \end{cases} \quad (15)$$

(see Fig. 2 in GKS93). Kramer et al. (1994) obtained exactly the same result, using an independent method for both the pulse-width measurements and error analysis. Examining Fig. 2 in GKS93 we can notice that the inner cone with $\rho = 4^\circ.9 P^{-1/2}$ seems to be preferred at shorter periods $P < 0.7$ s, while the outer cone with $\rho = 6^\circ.3 P^{-1/2}$ dominates at longer periods $P > 1.2$ s. However, the exact model of transition between cones is not known. This observational feature is crucial, and it has to be taken

into account in the statistical analysis to calculate the pulse-width in the synthetic population. We use Eq. (15) in two model variants:

a) based on Fig. 2 in GKS93 we established the period value $P = 0.7$ s below which the inner cone ($4^\circ.9 P^{-1/2}$), and above this value the outer cone ($6^\circ.3 P^{-1/2}$), is always chosen,

b) like in case a) but below period $P = 0.7$ s there is a 20 per cent chance to choose the outer cone and an 80 per cent chance for the inner cone.

It is worth noting that Eq. (15) was derived by GKS93 by means of geometrical analysis of a large number of conal profiles. We believe that it describes well the low intensity pulse-width measurements used in this paper.

2.2 Interpulse emission

At the time of writing the manuscript of this paper there were 1520 normal pulsars (with periods longer than 20 ms) known. In nearly 3 per cent of them the so-called interpulse (IP) emission could be identified, by which we understand features separated by about 180° (possible deviation could amount to about 40 per cent) from the main pulse (MP). The canonical lighthouse pulsar model naturally predicts the occurrence of interpulses. In this model two beams are collimated along the open lines of dipolar magnetic field. When the inclination angle $\alpha \approx 90^\circ$ (almost orthogonal rotator) the observer can detect both beams, associated with two opposite magnetic poles. This is the so-called double-pole interpulse model (hereafter DP-IP). In this case both pulse components are clearly separated (by about 180° of longitude) and there is not any kind of low level emission between them. Duty cycles of each component are small, typically several per cent of the pulsar period. Another possibility of generating the interpulse is described by the so-called single-pole model (SP-IP hereafter). This model requires a small inclination angle α (almost aligned rotator). In the SP-IP case pulse-widths are much broader than in DP-IP model, to the extent that they often fill the entire or most of the pulsar period (360°). Even if both components are separated, usually there is a low intensity bridge of emission between them. The first version of this model (Rickett & Lyne (1968)) assumes that MP and IP occur when the observer's line-of-sight cuts the wide hollow cone of radiation twice (ML77) at a distance of about 180° of longitude (Fig. C1 (Appendix C in the on-line materials)). In the other version of SP-IP model (Fig. C2 (Appendix C in the on-line materials)) the line-of-sight stays in a pulsar beam for the entire pulsar period and MP and IP correspond to cuts through two nested conical beams or through the arrangement of the core beam surrounded by the cone (Gil (1983); hereafter G83, Gil (1985)). In the latter version the separation between MP and IP is naturally close to 180° , and it does not depend on the observational frequency, while in the former version these properties are not natural.

In addition to information about profile shape and/or widths one can usually use polarisation angle (PA) curves to distinguish between different kinds of interpulses. In case of DP-IP (almost orthogonal rotators) swings of PA are steep across both MP and IP components, while for SP-IP cases PA curve is typically flat over the entire profile

(including MP, IP and weak emission bridge between them).

2.3 Beam shape

It is commonly assumed that the pulsar beam is circular in shape. Some authors however consider elliptical shapes with meridional compression or equatorial elongation. For example, Narayan & Vivekanand (1983) argued that the pulsar beam is elongated with the ratio of north-south (N-S) to east-west (E-W) dimension depending on pulsar period as

$$R \approx 1.8P^{-0.65}, \quad (16)$$

so the effect is predominant at shorter periods $P < 0.25$ s. On the other hand, Biggs (1990) and McKinnon (1993) considered the opposite tendency of the beam compression in meridional direction, with the ratio of minor (N-S) to major (E-W) ellipse axes depending on the inclination angle α

$$R \approx \cos \frac{\alpha}{3} \sqrt{\cos \left(\frac{2}{3}\alpha \right)}, \quad (17)$$

so this effect is predominant at large α close to $\pi/2$. Equations (1) and (12) are independent from the beam shape (if symmetry to the fiducial plane is conserved). The opening angle is always described by Eq. (12) or by its observational representations (Eq. (13), (14) or (15)). Taking into account ellipse geometry the following equation could be shown

$$r = \sqrt{\rho_0^2 + \beta^2 \left(\frac{1}{R^2} - 1 \right)} \quad (18)$$

and

$$rR = \sqrt{R^2\rho_0^2 + \beta^2(1-R^2)}. \quad (19)$$

Equation (19) describes circular beam when $R = 1$ and $r = \rho$. In this paper we argue that pulsar beam shape is circular or almost circular (a possible ellipticity can not be excluded but if it exists it is very small).

2.4 Detection conditions

For simplicity let us consider one hemisphere with $0 \leq \alpha \leq \pi/2$ (Fig. 1). Pulsar is detectable geometrically when the observer's l-o-s passes through its beam (independent of the actual beam shape). For circular or almost circular beam the detection condition is

$$|\beta| < \rho_0, \quad (20)$$

where ρ_0 is the opening angle of the beam corresponding to the last open field lines. The above condition is valid for the main pulse emission. For interpulse emission within DP-IP model (almost orthogonal rotator $\alpha \sim \pi/2$) the detection condition is

$$\rho_0 > \pi - 2\alpha - \beta. \quad (21)$$

In the SP-IP model, in which both MP and IP originate from single magnetic pole (almost aligned rotator $\alpha \sim 0$), we will consider two different versions of this model. In the

first MP and IP represent two cuts through one conical beam (ML77) and the detection condition is

$$\rho_0 > \sqrt{2\alpha^2 + \beta^2 + 2\alpha\beta}. \quad (22)$$

This version is presented in more details in Fig. C1. The second version corresponds to the case when the l-o-s remains inside the beam for the entire pulsar period, so the occurrence of both MP and IP result from the internal beam structure in the form of nested hollow-cones (G83). The detection condition for this case is

$$\rho_0 > 2\alpha + \beta. \quad (23)$$

This version is presented in more details in Fig. C2.

For elliptical pulsar beams the detection conditions expressed by equations (20), (21), (22) and (23) transform into equations (24), (25), (26) and (27), respectively, presented below:

$$|\beta| < [R^2\rho_0^2 + \beta^2(1-R^2)]^{1/2}, \quad (24)$$

$$rR > \pi - 2\alpha - \beta, \quad (25)$$

$$rR > \sqrt{2\alpha^2 + \beta^2 + 2\alpha\beta} \quad (26)$$

$$rR > 2\alpha + \beta. \quad (27)$$

In the case of SP-IP model, beside detection conditions (Eq. (22) or Eq. (26)) it is also important to apply some kind of morphological definition to avoid a danger of classifying just a broad double-peaked profiles as interpulses. By carefully reviewing our interpulse database we decided that the interpulse case has to have at least 100° of longitude separation between the component peaks, that is

$$100^\circ < \Delta\varphi_{sep}^{IP-MP} < 260^\circ. \quad (28)$$

2.5 Beam edge correction

KGM04 used the detection condition $\rho > |\beta|$ (Eq. (20)), where ρ was approximated by ρ_{10} obtained from observations (e.g. from models Eqs. (13) – (15)). Such an approach was justified only by the fact that it is difficult to measure pulse-width at the level lower than about 10% of the maximum intensity. It seems that this condition is too restrictive from the geometrical point of view, because the intensity level corresponding to the ρ_{10} beam radius could be much higher than the one that should be adopted as the edge of the beam. A simple model of the beam envelope is presented in Fig. 2. The two circles with different radii ρ_0 and ρ_{10} correspond to two different intensity levels with respect to the maximum intensity level I_{max} in the centre of the beam, namely 10 % and low intensity level corresponding to the beam edge. It is important to notice that the maximum of the observed profile (upper panel) does not generally correspond to the maximum intensity of the beam and in reality depends on the impact angle β . Thus I_{10} does not necessarily correspond to the cut of the beam at 10% of its maximum (it is just 10% of the maximum of the observed profile). If we use $\rho = \rho_{10}$ in detection conditions we can lose $\sim 10\%$ pulsars with intensity less than 0.1 of the absolute maximum

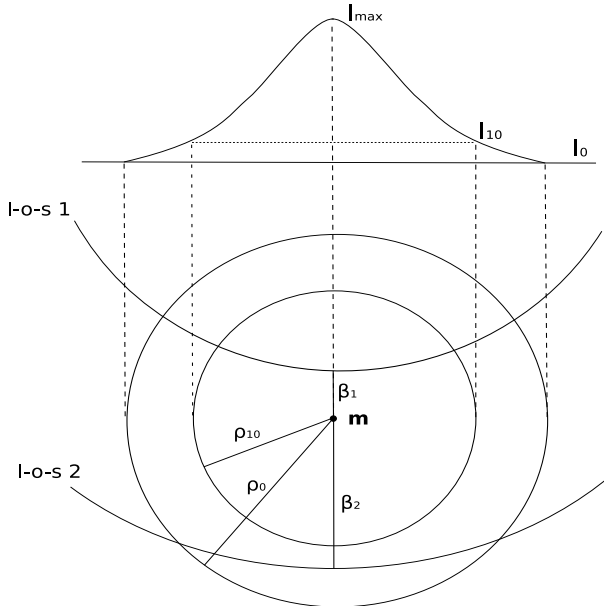


Figure 2. Schematic representation of the gaussian envelope of the beam intensity distribution. Two concentric circles centred on the magnetic axis \mathbf{m} with radii ρ_0 and ρ_{10} represent two intensity levels: edge of the beam and 10% of the maximum intensity in the beam centre, respectively. Two lines of sight trajectories l-o-s 1 and l-o-s 2 corresponding to different impact angles β_1 and β_2 are marked. One can notice that in the case of l-o-s 1 the detection independent of the actual values of ρ (ρ_0 or ρ_{10}) in the detection condition (Eq. (20)) is possible because $\beta < \rho_{10} < \rho_0$. However, in the case of l-o-s 2 the condition $\beta < \rho_{10}$ does now guarantee the detection, and new detection condition $\beta < \rho_0 = 1.1\rho_{10}$ should be introduced.

of the beam. To improve this situation, let us consider Tables 1a and 1b in Gil & Kijak (1993). These tables are very useful since they present the pulse-width measurements at 10% and 1% maximum intensity of the profile for a group of pulsars. The latter one can be considered as being close to the level representing the edge of the beam. The values of the inclination angle α and the impact angle β are known, so using Eq. (12) we can calculate corresponding values of ρ_{10} and ρ_1 , which for available data give the mean value close to 1.1. If we now adopt $\rho_0 = \rho_1$ we can estimate the average value of the ratio of $\rho_0/\rho_{10} = 1.1$, which we can use as the edge beam correction in detection conditions (Eqs. (13) – (15) and Eqs. (18) – (27)).

3 DATABASES

3.1 Periods

In this paper we consider only the so-called normal radio pulsars. All magnetars, millisecond pulsars and pulsars in binary systems are excluded, since they constitute different evolutionary groups on the $P - \dot{P}$ diagram. Most of pulsar periods P are available in the ATNF³ catalogue (Manchester et al. 2005). Our database was consecutively updated according to new papers publishing new pulsar

discoveries (e.g. Janssen et al. (2009), Keith et al. (2009), Keith et al. (2010)).

At present there are 1830 known radio pulsars, with periods that range from 1.4 ms to 11.8 s. Following arguments expressed by KGM04 we consider only those with periods ranging from 20 ms to 8.5 s, both in our period database and in Monte Carlo simulations. The upper limit of 8.5 s is set by PSR J2144-3933 (Manchester et al. (1996) and Young et al. (1999)) with the longest period observed in radio wavelengths, whereas the lower limit we set at 20 ms. The estimates of initial pulsar period range from 14 ms (Migliazzo et al. 2002) to 140 ms (Kramer et al. 2003a). If the actual shortest period is indeed 14 ms instead of being close to 20 ms, then we miss only two normal pulsars, which is statistically irrelevant. All in all, our period database contains 1520 normal pulsars, 355 more than in the KGM04 database. The distribution of all selected periods is presented in the upper panel of Fig. 3. This sample can be best fitted by the log-normal function expressed by Eq. (11) with parameters $x_0 = -0.30$ and $\sigma = 0.80$, although gamma function (Eq. (8)) with parameters $m = 0.43$ and $a = 2.12$ also gives a reasonable fit (see Table 2 for comparison).

3.2 Pulse-widths

In our simulations we attempt to reproduce the observed distribution of pulse-widths measured at 10% of the maximum intensity level. The observed pulse-width W depends on a number of geometrical (discussed in Section 2) and non-geometrical factors (like scattering, dispersion smearing, sampling or receiver time constant). The influence of the emission geometry (inclination angle α , impact angle β , opening angle $\rho(P)$) on the observed pulse-width W (Eq. (1)) is dominant, however some influence of non-geometrical factors cannot be neglected.

Both GH96 and KGM04 used database that contained about 240 (242 and 238, respectively) pulse-widths that were carefully selected to avoid broadening effects. The trailing part of many profiles with large dispersion measure DM suffer from broadening caused by scattering of radio waves on free electrons in ISM. Our simulations do not take into account scattering, so our sample should be limited to pulsars whose profiles are not significantly broadened. The easiest selection method is to limit the values of dispersion measure but the question is the maximum permissible DM that warrants it? To answer this question we analysed the Fig. 7 in Cordes & Lazio (2003). We found that the limiting value of DM is about 150 pc cm^{-3} and we present our reasoning below.

The typical duty cycle of normal pulsars is $\sim 5\%$, which for our shortest period (20 ms) gives a pulse window of about 1 ms. We assumed arbitrarily the value of 10 per cent (0.1 ms) of this value as the maximum possible broadening due to high DM . According to Fig. 7 in Cordes & Lazio (2003) this corresponds to dispersion measure value $DM \sim 150 \text{ pc cm}^{-3}$. Of course, the number of pulsars with period close to 20 ms in the whole sample is comparatively small, so probably the DM limit can be slightly higher. Increasing the maximum DM value to 170 pc cm^{-3} would extend the number of pulse-widths by less than 10 per cent, which seems to be irrelevant in our statistical analysis. However, for $DM \sim 200$

³ <http://www.atnf.csiro.au/research/pulsar/psrcat>

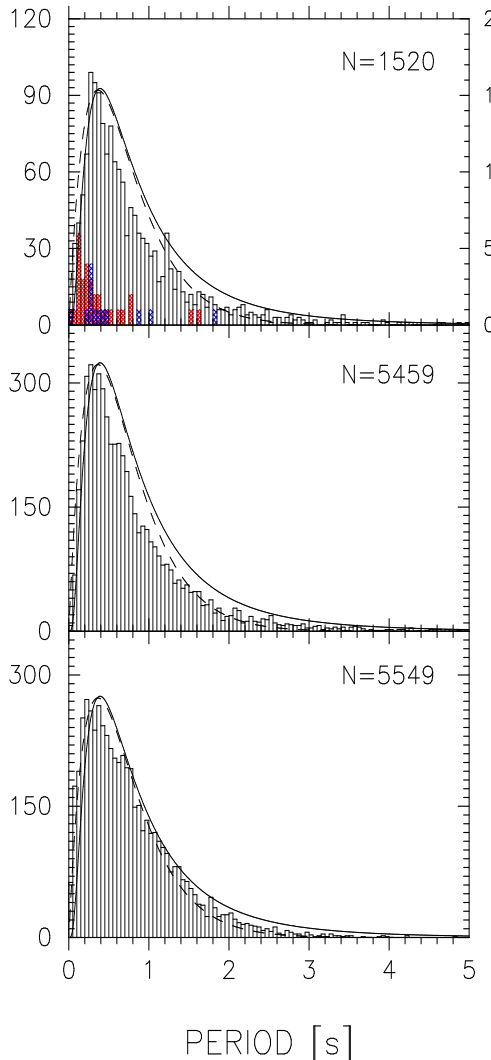


Figure 3. Formal fits of the log-normal (Eq. (11)) and the gamma (Eq. (8)), solid and dashed line respectively, distribution functions to the histogram of 1520 observed (upper panel) and simulated (lower panels) pulsar periods. The ordinate represents the number of observed (upper panel) or simulated (lower panels) pulsars. The upper panel shows also the distribution of inter-pulses according to the right-hand side scale, where blue and red colour corresponds to SP-IP and DP-IP cases, respectively, (as in Fig. 6)). Distribution of the simulated observed pulsar periods generated with the log-normal (middle panel) and the gamma (lower panel) parent period distribution functions with parameters $x_0 = -0.30$, $\sigma = 0.80$ and $m = 0.43$, $a = 2.12$, respectively. In both simulation cases the inclination angle distribution function was that of GH96 (Eq. (6)). The parameter N describes the number of observed and simulated periods.

pc cm⁻³ the pulse broadening would be about 1 ms, which is evidently too much. Thus, we construct our new pulse-width database using the value of 150 pc cm⁻³ as the limit for DM in our sample.

The new database contains pulse-widths used by GH96 and KGM04, extended by pulse-widths from Swinburne Intermediate – Latitude Pulsar Survey (Edwards et al. 2001), Parkes Southern Pulsar Survey I – III (Manchester et al. (1996), Lyne et al. (1988), D’Amico et al. (1998)), Parkes

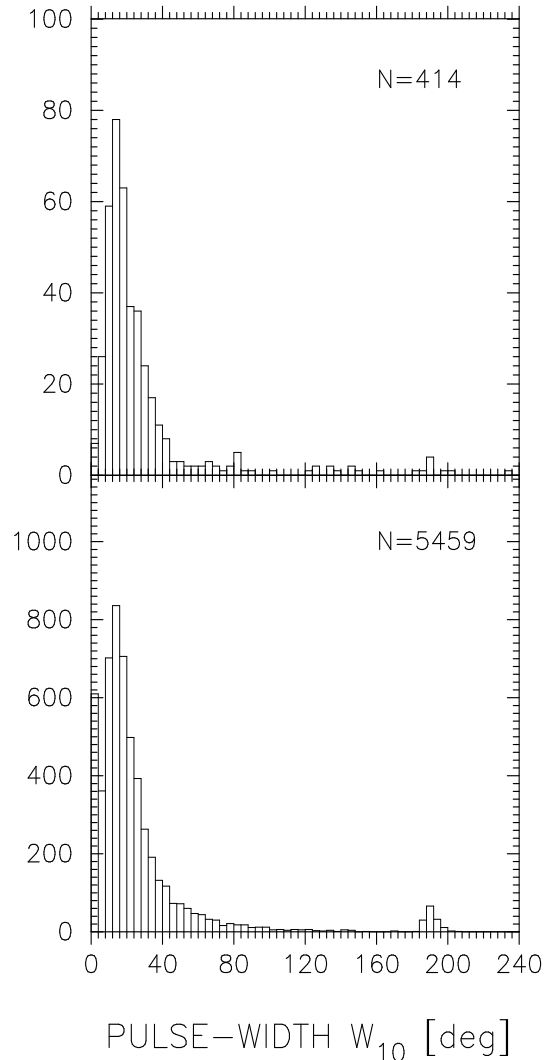


Figure 4. Distribution of 414 pulse-widths W_{10} measurements for pulsars with $DM \leq 150$ pc cm⁻³ (upper panel). The distribution of simulated values is presented in the lower panel. The simulations were performed using the log-normal period distribution (Eq. (11)) and the GH96 inclination angle distribution (Eq. (6)), as this combination gives the best results of the K-S significance test. The parameter N describes the number of observed and simulated periods.

Multibeam Pulsar Survey I – VI (Manchester et al. (2001), Morris et al. (2002), Kramer et al. (2003b), Hobbs et al. (2004), Faulkner et al. (2004), Lorimer et al. (2006) and Keith et al. (2009)). Parkes Southern Pulsar Survey I and II campaigns were carried out at 436 MHz and others on 1.4 GHz, so we had to scale their pulse-widths to 1.4 GHz⁴. After rejecting of all magnetars, milliseconds and binary pulsars 768 normal pulsars remained, among which

⁴ Scaling factor is 0.89 ($= 1.4 \text{ GHz}/0.436 \text{ GHz}$)^{-0.1}. This factor was obtained in the following way: the pulse-width is roughly proportional to the angular radius of the beam ρ , which is proportional to square root of the emission altitude $r_{em}^{1/2}$, which in turn depends on observational frequency ν ($r_{em} = (400 \pm 80) \text{ km } \nu_{\text{GHz}}^{-0.26 \pm 0.09} P_{-15}^{0.07 \pm 0.03} P^{0.30 \pm 0.05}$; Kijak & Gil (1997,

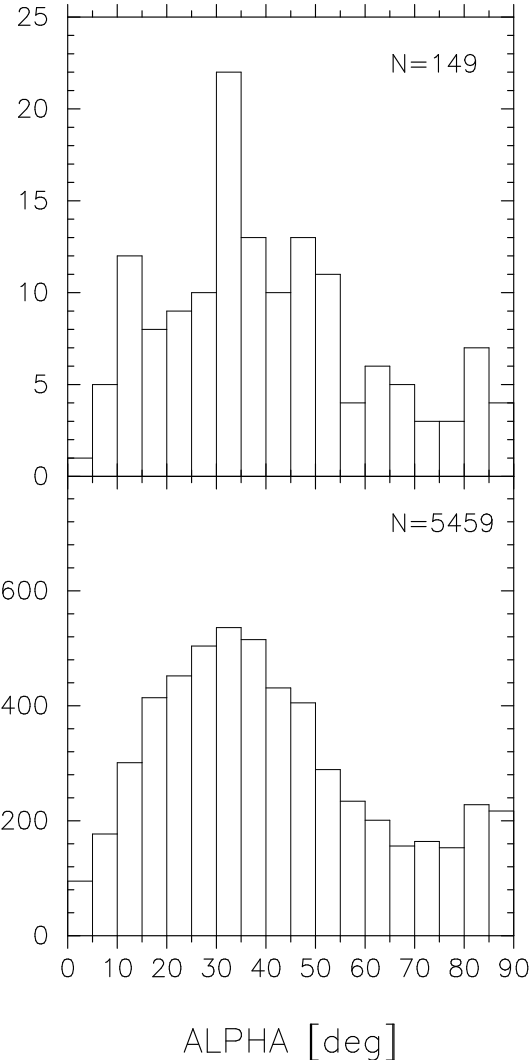


Figure 5. The upper panel shows the distribution of 149 inclination angles α derived from the pulsar polarisation characteristics (data taken from Rankin (1993a) and Rankin (1993b)). The histogram of simulated inclination angles is presented in the lower panel. The simulations were performed using the log-normal period distribution (Eq. (11)) and the GH96 inclination angle distribution (Eq. (6)), as this combination gives the best results of the K-S significance test.

414 had $DM \leq 150$ pc cm $^{-3}$. Thus, our new pulse-width database contains 414 measurements, including 190 from GH96/KGM04 database. Their distribution is presented in the upper panel of Fig. 4.

3.3 Inclination angles

The inclination angle α between the magnetic and the spin pulsar axes is a parameter which cannot be observed but can

(1998)). Thus, the pulse-width can be roughly scaled with the observational frequency ν as $\nu^{-0.1}$.

be derived indirectly. One method is based on the RVM and polarisation data (Lyne & Manchester (1988), R90, Rankin (1993a,b)). It is well known that this method is effective only in a small number of cases with very broad highly polarized profiles. Another, much more effective method was proposed by R90, in which α was derived from the width of the core component measured at the level of 50% maximum intensity (W_{50}^{core})

$$\alpha = \sin^{-1} \left(2^\circ .45 P^{-1/2} / W_{50}^{\text{core}} \right). \quad (29)$$

In our simulation we used database of 149 inclination angles compiled by Rankin (1993a,b). Their distribution is presented in Fig. 5 (upper panel). Unfortunately, the inclination angle database is the only one which was not developed since Rankin's compilation. We would like to advertise here that the validity of the above Equation (29) will be examined statistically in the forthcoming Paper II.

3.4 Interpulses

As a result of discovery of large number of pulsars in recent multibeam surveys a number of cases with interpulse emission also increased from 14 in Taylor et al. (1993) catalogue to 27 in Weltevrede and Johnston (2008a; thereafter WJ08a) up to 44 presented in this paper. The new interpulse database was derived from the sample of 1520 normal pulsars. This database (Table 1) contains 31 double-pole interpulsars (DP-IP) and 13 single-pole interpulsars (SP-IP), which is 2.039% and 0.855% of the total number of normal pulsars, respectively⁵. A clear division into DP and SP interpulses was possible in most cases, based on the pulse profile morphology and/or polarization angle variations (see Section 2.2). It is important to note that the ratio of $N_{\text{SP-IP}}/N_{\text{IP}} = 0.30$ and $N_{\text{DP-IP}}/N_{\text{IP}} = 0.70$ is almost the same as in KGM04 (0.36 and 0.64). The total percentage $\sim 2.90\%$ of interpulsars in the sample of normal pulsars is also unchanged. Thus, it seems that our new database is quite representative for interpulse occurrences in normal pulsars.

To be consistent with our selection of pulsar periods we excluded all millisecond and other recycled pulsars from both the total pulsar sample and from the sample of pulsars with interpulses (this was not done in GH96, who incorrectly estimated rates of interpulse occurrences as a result of this mistake).

All interpulsars (see Table 1) are marked on the $P - \dot{P}$ diagram presented in Fig. 6.

As one can see from this figure DP-IP cases (represented by red dots) lie above 10 Myr line. This means that almost orthogonal rotators are rather young pulsars. On the other hand, SP-IP cases (blue dots) lie between ~ 5 Myr and ~ 500 Myr lines. Thus, the almost aligned rotators have a tendency to be older pulsars. In fact, the average values of P , \dot{P} , τ and B are 0.51 s, 3.49×10^{-15} , 1.55×10^8 yr and 6.88×10^{11} G for SP-IP cases and for DP-IP cases are

⁵ More precisely, the rates of occurrence of SP-IP and DP-IP are $(0.86 \pm 0.24)\%$ and $(2.04 \pm 0.37)\%$, respectively. The errors were estimated $1\sigma = \sqrt{N}/N_{\text{tot}}$, which for SP-IP is $\sqrt{13}/1520 = 0.24\%$ and for DP-IP is $\sqrt{31}/1520 = 0.37\%$ ($N_{\text{tot}} = 1520$ is the number of normal pulsars from which the interpulses were extracted).

Table 1. Table of 44 known interpulses divided into double-pole (DP–IP) and single-pole (SP–IP) cases. Bibliographic marks are following: T/K – KGM04 using Taylor et al. (1993), WJ – Weltevrede & Johnston (2008b), A – D’Amico et al. (1998), M02 – Morris et al. (2002), K03 – Kramer et al. (2003b), H – Hobbs et al. (2004), L – Lorimer et al. (2006), R – Ribeiro (2008)[†], M01 – Manchester et al. (2001), J – Janssen et al. (2009), K09 – Keith et al. (2009), K10 – Keith et al. (2010), C – Camilo et al. (2009), N – new interpulse identified in this work using data from H and L.

No.	Name J	Name B	Period [s]	\dot{P} $[10^{-15}]$	Ratio of amplitudes IP/MP	Separation MP and IP [°]	SP-IP or DP-IP	Bibliography
1.	J0534 + 2200	B0531 + 21	0.033	423	0.6	145	DP	T/K
2.	J0826 + 2637	B0823 + 26	0.531	1.7	0.005	180	DP	T/K
3.	J0828 – 3417	B0826 – 34	1.849	0.99	0.1	180	SP	T/K
4.	J0908 – 4913	B0906 – 49	0.107	15.2	0.24	176	DP	T/K
5.	J0953 + 0755	B0950 + 08	0.253	0.2	0.012	210	SP	T/K
6.	J1057 – 5226	B1055 – 52	0.197	5.8	0.5	205	DP	T/K
7.	J1302 – 6350	B1259 – 63	0.048	2.3	0.75	145	SP	T/K
8.	J1705 – 1906	B1702 – 19	0.299	4.1	0.15	180	DP	T/K
9.	J1722 – 3712	B1719 – 37	0.236	10.9	0.15	180	DP	T/K
10.	J1739 – 2903	B1736 – 29	0.323	7.9	0.4	180	DP	T/K
11.	J1825 – 0935	B1822 – 09	0.769	52.3	0.05	185	DP	T/K
12.	J1851 + 0418	B1848 + 04	0.285	1.1	0.2	200	SP	T/K
13.	J1932 + 1059	B1929 + 10	0.227	1.2	0.018	170	DP	T/K
14.	J1946 + 1805	B1944 + 17	0.441	0.02	0.005	175	SP	T/K
15.	J0905 – 5127		0.346	24.9	0.059	175	DP	WJ
16.	J1126 – 6054	B1124 – 60	0.203	0.03	~0.1	174	DP	WJ
17.	J1611 – 5209	B1607 – 52	0.182	5.2	<0.1	177	DP	WJ
18.	J1637 – 4553	B1634 – 45	0.119	3.2	~0.1	173	DP	WJ
19.	J1549 – 4848		0.288	14.1	~0.3	180	DP	A
20.	J1806 – 1920		0.880	0.017	~1.0	~136	SP	M02
21.	J1828 – 1101		0.072	14.8	~0.3	180	DP	M02
22.	J1913 + 0832		0.134	4.6	~0.6	180	DP	M02
23.	J0834 – 4159		0.121	4.4	~0.25	171	DP	K03
24.	J1713 – 3844		1.600	177.4	~0.25	181	DP	K03
25.	J1843 – 0702		0.192	2.1	~0.44	180	DP	H
26.	J1852 – 0118		0.452	1.8	~0.4	144	SP	H
27.	J1808 – 1726		0.241	0.012	~0.5	~223	SP	L
28.	J1849 + 0409		0.761	21.6	~0.5	181	DP	L
29.	J0831 – 4406		0.312	1.3	~0.05	244	SP	R – K03
30.	J1107 – 5907		0.253	0.09	~0.2	191	SP	R – L
31.	J1424 – 6438		1.024	0.24	~0.12	223	SP	R – K03
32.	J1613 – 5234		0.655	6.6	~0.28	175	DP	R – M01
33.	J1627 – 4706		0.141	1.7	~0.13	171	DP	R – L
34.	J1637 – 4450		0.253	0.58	~0.26	256	SP	R – L
35.	J1842 + 0358		0.233	0.81	~0.23	175	DP	R – L
36.	J1915 + 1410		0.297	0.05	~0.21	186	DP	R – L
37.	J0842 – 4851	B0840 – 48	0.644	9.5	~0.14	180	DP	N – H
38.	J1413 – 6307	B1409 – 62	0.395	7.434	~0.04	~170	DP	N – H
39.	J1737 – 3555	B1734 – 35	0.398	6.12	~0.04	~180	DP	N – H
40.	J1903 + 0925		0.357	36.9	~0.19	~240	SP	N – L
41.	J2047 + 5029		0.446	4.2	~0.6	175	DP	J
42.	J1244 – 6531		1.547	7.2	~0.3	145	DP	K09
43.	J0627 + 0706		0.476	29.9 ^{††}	~0.2	180	DP	K10
44.	J2032 + 4127		0.143	20.1	~0.18	195	DP	C

[†] Items 29 – 36 correspond to interpulses identified by Ribeiro (2008) in the data of K03, L and M01.

^{††} Unpublished value provided by Michael Keith (private communication).

0.39 s, 2.86×10^{-14} , 4.64×10^6 yr and 2.17×10^{12} G. This strongly implies a secular alignment of the magnetic axis towards the spin axis, in agreement with the two humped distribution function of parent inclination angles expressed by Eq. (6). To some extent this is an observational support for results of simulation of the inclination angle α evolution made by WJ08a. These authors argued that the magnetic axis is likely to align from a random distribution at birth with a timescale of $\sim 10^7$ years. It is not clear whether this conclusion is fully consistent with Eq. (6), although the alignment of the magnetic axis seems to be reproduced well in Fig. 6.

4 MONTE CARLO SIMULATIONS OF CONAL EMISSION

We performed Monte Carlo simulation of the pulse-widths W_{10} , pulsar periods P and inclination angles α following a technique developed by KGM04, with a number of important improvements:

1. We used new, generally more numerous databases of pulsar periods (1520 as compared with 1165 in KGM04), pulse-widths (414 versus 238) and interpulses (44 versus 14). The inclination angle database was unchanged with respect to KGM04.

2. The pulse-widths measurements were selected with additional criterion that $DM \leq 150$ pc cm $^{-3}$. This allows avoiding a significant pulse broadening contaminating pulse-width measurements at the low intensity level.

3. The log-normal period distribution proposed by Lorimer et al. (2006) was added to a set of possible trial functions.

4. Beam edge correction in detection conditions was introduced in the form $\rho_0 = 1.1\rho_{10}$ where ρ_{10} is expressed by Eqs. (13) – (15). For more details see Section 2.5.

5. The separation between MP and IP within the ML77 version of SP–IP model is computed exactly from the detection geometry. As one can see from Tab. 1, the minimum (maximum) separation between MP and IP is about 100° (260°). On the other hand, we have the empirical relation for component peaks

$$\rho_s = \begin{cases} 3^\circ.7 P^{-1/2} & \text{for } P > 0.7s \\ 4^\circ.6 P^{-1/2} & \text{for } P \leq 0.7s \end{cases} \quad (30)$$

found by GKS93 (see their Fig. 3), which can be used in Monte Carlo simulations. While using the wide hollow cone version of the SP–IP model (ML77) one can have a problem judging whether the pulse represents just a broad profile or it is already an interpulse case. Thus, beside satisfying the detection condition for the SP–IP (Eq. (22) or Eq. (26)) the simulated pulse-width $W(\rho_s)$ should be larger than 100° (smaller than 260°).

The first test for our software was to reproduce results from KGM04 (using their databases). Results of this test are presented in Table B1 (Appendix B in the on-line materials). After making sure that our programs work correctly, we started new Monte Carlo simulations. They involve a number of subsequent steps described below:

1. Generate the inclination angle α as a random number

with one of the trial parent probability density function $f(\alpha)$ corresponding to Eqs. (3) – (7).

2. Generate the pulsar period of P as a random number with the one of the trial parent probability density function $f(P)$ corresponding to Eqs. (8) – (11).

3. Generate the observer angle ξ as random number with the parent probability density function $f(\xi) = \sin \xi$.

4. Calculate the impact angle $\beta = \xi - \alpha$.

5. Calculate the beam opening angle $\rho_{10}(P)$ at the level of 10% of the maximum intensity with one of the trial distribution function (Eqs. (13) – (15)).

6. Calculate the opening angle ρ_0 corresponding to the edge of the beam $\rho_0 = 1.1\rho_{10}$.

7. Check the detection conditions for each simulated object (Eqs. (20) – (23) for circular and Eqs. (24) – (27) for elliptical beam). If the pulsar is detected then it is added to the total number of detected pulsars N_{det} .

8. Calculate the pulse-width W_{10} according to Eq. (1) for each set of parameters $\rho_{10}(P)$, α and β of the detected pulsar.

9. For each pulsar detected in a simulation run check the detection conditions for occurrence of an interpulse. For DP–IP model Eq. (21) for circular beam or Eq. (25) for elliptical beam were used. For SP–IP model in ML77 version Eq. (22) for circular or Eq. (26) for elliptical beam were used while for G83 version Eq. (23) for circular or Eq. (27) for elliptical beam were used. Moreover, for the ML77 version of the SP–IP model, components separation (Eq. (30)) is checked whether it is in the range of 100° – 260°. If an interpulse is detected then it is added to the number of interpulses N_{DP-IP} or N_{SP-IP} .

10. Record all relevant information like inclination angle α , period P , pulse-width W_{10} and occurrence of the interpulses from one or two magnetic poles.

11. For each set of the probability density function of the inclination angle α , period P and the model of the opening angle ρ_{10} , 50000 objects were created (each having a set of parameters such as: P , α , β , ρ and W). After checking the detection conditions we obtained database of the observed simulated pulsars and distribution of their parameters α , P and W_{10} as well as occurrence of the interpulses from one N_{SP-IP} or two N_{DP-IP} magnetic poles. In order to obtain the statistical significance each simulation run was repeated 10 times and the results were averaged.

12. Judge the statistical significance using the Kolmogorov–Smirnov (K–S) test for the simulated observed pulsars parameters as α , P and W_{10} and observed distribution of these parameters. Record the values of $\mathcal{D}(\alpha)$, $\mathcal{P}(\alpha)$, $\mathcal{D}(P)$, $\mathcal{P}(P)$, $\mathcal{D}(W_{10})$ and $\mathcal{P}(W_{10})$, where \mathcal{D} describes the maximum distance between both cumulative distribution functions and \mathcal{P} is the probability that the two compared distributions are drawn from the same parent distribution.

13. Calculate the beaming fraction defined as $f_b = N_{det}/N_{tot}$ (where N_{det} is the number of detected pulsars in total population of N_{tot} simulated pulsars) and the occurrence of interpulses from one magnetic pole N_{SP-IP}/N_{det} or two magnetic poles N_{DP-IP}/N_{det} , respectively.

14. Change values of free parameters of a given trial period distribution function.

15. Repeat simulations with all possible combinations of distribution probability functions of α , P and ρ_{10} .

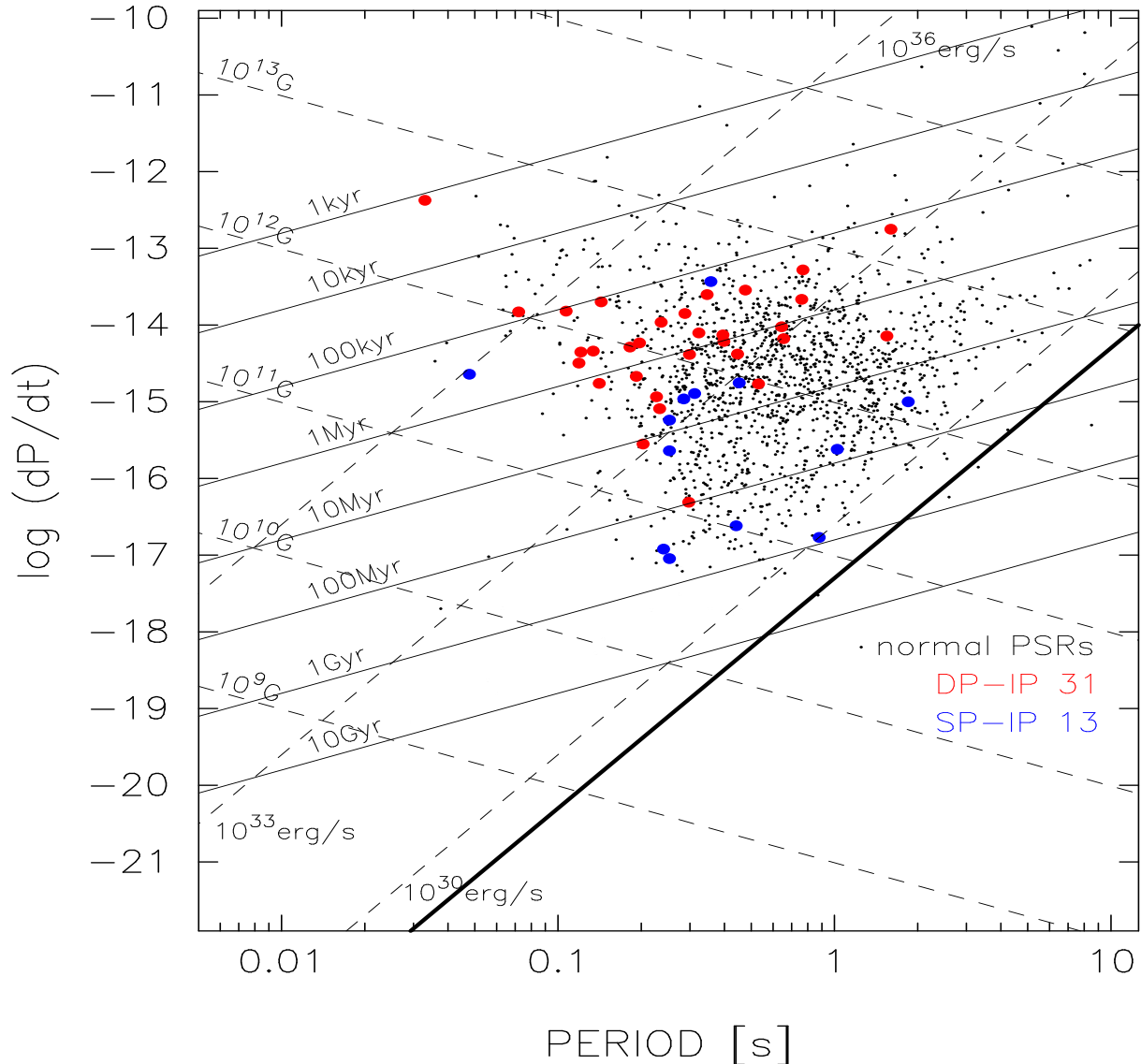


Figure 6. Diagram $P - \dot{P}$ for normal (see Section 3.1) pulsars, including 44 cases with interpulse emission (see Table 1). Black dots represent 1476 normal pulsars, while red and blue circles correspond to 31 double-pole (DP-IP) and 13 single-pole (SP-IP) interpulsars, respectively. Lines of constant magnetic field B , characteristic age τ , spin-down luminosity \dot{E} are shown. The death line ($10^{29} \text{ erg s}^{-1}$) derived by Contopoulos & Spitkovsky (2006) is marked by the thick line. It is easy to notice that SP-IP cases are generally located much closer to the death line than DP-IP cases.

16. Search for good solutions satisfying simultaneously all demanded criteria, that is $\mathcal{P}(\alpha) \geq 0.5\%$, $\mathcal{P}(P) \geq 0.5\%$, $\mathcal{P}(W_{10}) \geq 0.5\%$ as well as the rates of occurrence of SP-IP and DP-IP are at the observed level ($0.86 \pm 0.24\%$) and ($2.04 \pm 0.37\%$) (errors correspond to 1σ level).

We performed Monte Carlo simulation of conal emission of radio pulsars according to procedure described in items 1–16 listed above. We checked 160 (80 for circular and 80 for elliptical beams) different combinations of trial functions for parent distribution periods P , inclination angles α and opening angles ρ_{10} . For each combination of the above distribution functions we searched the two-dimensional grid of free parameters of the period distribution function. It gave the total number of 641 360 single simulation runs. In all solutions we identified "detectable" cases in which all prob-

abilities (of P , α and W_{10}) were greater than 0.005 (0.5%) and occurrence of interpulses were at the observed levels ($2.04 \pm 0.37\%$) for DP-IP and ($0.86 \pm 0.24\%$) for SP-IP. Such solutions we called "a good solution".

In summary, each simulation run including 50000 detection attempts resulted in about 5500 detections (satisfying geometrical detection conditions (Section 2.4)). There were 641 360 simulation runs including all possible combinations of the probability distribution functions (Section 2.1). Among the resulting $\sim 4 \times 10^9$ geometrical detections we found 827 good solutions (as described in item 16 above). These solutions are listed in Tables B2 – B7 and 9 best examples with relatively high K-S probability values are shown in Table 2 (items 1a – 9a). Items 1b – 9b correspond to tests of the luminosity problem described in the Appendix A in the on-line materials.

Table 2. Examples of 9 best simulation results for different distribution functions (Eqs. (6) – (15)) and circular beams. \mathcal{D} and \mathcal{P} are parameters of the Kolmogorov–Smirnov significance test. For symbol description see item 12 in Section 4. Lines denoted by letters a and b correspond to simulations without and with the luminosity problem included, respectively. Notice that for combination (6), (8) and (14) of distribution functions there is only one good solution that could be presented (see Fig. C6).

No.	Distributions Equation numbers	$f(P)$		W_{10}		P		α		DP-IP [%]	SP-IP [%]	f_b
		\mathcal{D}	\mathcal{P}	\mathcal{D}	\mathcal{P}	\mathcal{D}	\mathcal{P}	\mathcal{D}	\mathcal{P}			
1a	(6) (11) (13)	x_0 -0.30	σ 0.80	0.032	0.821	0.018	0.813	0.089	0.196	2.10	0.89	0.108
1b	(6) (11) (13)	-0.30	0.80	0.043	0.738	0.074	0.032	0.093	0.265	2.12	0.82	0.013
2a	(6) (11) (13)	-0.29	0.81	0.035	0.734	0.019	0.797	0.089	0.195	2.26	0.89	0.107
2b	(6) (11) (13)	-0.29	0.81	0.042	0.745	0.068	0.066	0.080	0.431	2.01	0.76	0.013
3a	(6) (11) (14)	-0.19	0.80	0.074	0.029	0.018	0.827	0.084	0.255	2.34	1.09	0.108
3b	(6) (11) (14)	-0.19	0.80	0.066	0.341	0.062	0.122	0.095	0.294	2.01	1.06	0.013
4a	(6) (11) (14)	-0.18	0.81	0.070	0.055	0.019	0.757	0.083	0.271	2.35	1.06	0.107
4b	(6) (11) (14)	-0.18	0.81	0.066	0.326	0.079	0.017	0.090	0.301	2.26	0.91	0.013
5a	(6) (11) (15b)	-0.31	0.77	0.047	0.373	0.029	0.285	0.076	0.362	2.28	1.01	0.110
5b	(6) (11) (15b)	-0.31	0.77	0.044	0.704	0.078	0.023	0.087	0.336	2.13	0.83	0.013
6a	(6) (11) (15b)	-0.28	0.81	0.046	0.393	0.027	0.362	0.084	0.257	2.10	1.01	0.110
6b	(6) (11) (15b)	-0.28	0.81	0.043	0.723	0.089	0.006	0.087	0.335	1.98	0.81	0.014
7a	(6) (8) (13)	m 0.42	a 2.15	0.037	0.649	0.041	0.047	0.083	0.267	2.14	1.05	0.109
7b	(6) (8) (13)	0.42	2.15	0.051	0.546	0.094	0.006	0.083	0.402	2.12	0.74	0.013
8a	(6) (8) (13)	0.45	2.07	0.038	0.623	0.043	0.037	0.092	0.173	2.19	0.96	0.109
8b	(6) (8) (13)	0.45	2.07	0.049	0.576	0.104	0.005	0.088	0.343	2.17	0.76	0.013
9a	(6) (8) (14)	0.38	2.51	0.068	0.065	0.049	0.012	0.111	0.056	2.18	1.12	0.110
9b	(6) (8) (14)	0.38	2.51	0.055	0.470	0.108	0.001	0.105	0.169	2.11	0.885	0.014

5 DISCUSSION

Our new statistical analysis is based on a number of new databases that we compiled from the recently published data. We followed methodology developed by KGM04, which relies on comparison of synthetic and real pulsar data. Our period P database contains 1520 items (we excluded all recycled and binary pulsars) in the range of 0.02 – 8.51 seconds. This database includes 355 more pulsars than recently analysed database compiled by KGM04. We also compiled a new database of pulse-widths W_{10} measured at 10% intensity level. This database contains 414 items, which is 176 more than that of KGM04. There are many more pulse-width measurements available these days, but our database is restricted to pulsars with $DM < 150 \text{ pc cm}^{-3}$, which guarantees avoiding significant external pulse broadening.

Most importantly, we created the largest ever database of interpulse occurrence in pulsar emission. Our database contains 44 pulsars (compared with 14 pulsars in Taylor et al. (1993)/KGM04 database), including 31 cases of DP-IP and 13 cases of SP-IP. Although our IP database is more numerous than any of the previous ones (e.g. KGM04, WJ08a), it seems that the frequencies of occurrence are similar to those occurring in previous smaller databases. In fact, we have 2.90% of total number of IP cases, divided into 2.04% DP-IP and 0.86% SP-IP cases, respectively, in a population of 1520 pulsars. This can be compared with 2.71%, 1.94% and 0.78%, respectively, found in KGM04 database.

One can therefore firmly state that there should be about 3% of IP cases in the population of normal pulsars, including about 2% and 1% of DP-IP and SP-IP cases, respectively.

All pulsars from the period P database for which the value of \dot{P} is known are presented on the $P - \dot{P}$ diagram in Fig. 6. Black dots represent 1476 normal pulsars (without IP emission) while red and blue dots correspond to 31 DP-IP and 13 SP-IP cases, respectively. It is easy to notice that SP-IP cases are much older than DP-IP cases (with mean characteristic age 155 Myr versus 4.6 Myr, respectively). Also SP-IP cases represent weaker magnetic fields than DP-IP cases (6.9×10^{11} versus 2.2×10^{12} G). Assuming reasonable that DP-IP and SP-IP cases represent almost orthogonal (α close to 90°) and almost aligned (α close to 0°) rotators, respectively, one can conclude that the distribution of IP cases on the $P - \dot{P}$ diagram presented in Fig. 6 reveals a secular alignment of the magnetic axis towards the spin axis with a random initial value of the inclination angle. Similar conclusion was reached by Weltevrede & Johnston (2008a) and most recently by Young et al. (2010), although using different statistical arguments. It is interesting to note that Young et al. (2010) reached their conclusion without using interpulse pulsars at all, while these objects were crucial for our analysis. Moreover, Young et al. (2010) argued that the best suitable solution for their simulation is Model II (see their Fig. 9) whereas our simulations seem to prefer their Model III.

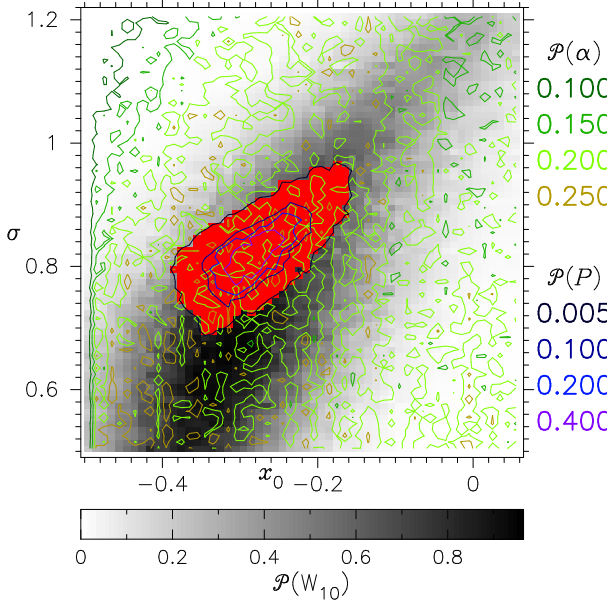


Figure 7. Colour graphic representation of simulation of the best solution of the Monte Carlo simulations corresponding to the following set of trial probability density function: log-normal (Eq. (11)) for periods, GH96 Eq. (6) for inclination angles and Eq. (13) for opening angles. Both axes describe free parameters of the period distribution log-normal function: parameter x_0 on the horizontal axis and the parameter σ on the vertical axis (these parameters are responsible for the location of the maximum and the width of the log-normal function, respectively). Below the main window the narrow bar with the Kolmogorov-Smirnov probabilities $P(W)$ for the pulse-width W_{10} coded in shades of grey is presented (the highest value ~ 0.95 corresponds to K-S probability obtained in this case). On the right hand the scales for K-S probabilities for inclination angles $P(\alpha)$ and for periods $P(P)$ are presented by different colours. Red rectangles in the solution area correspond to solutions simultaneously satisfying all constraints (K-S probabilities $P > 0.005$ for periods, inclination angles and pulse-widths as well as the occurrence of interpulses at the observed levels, i.e. $(0.86 \pm 0.24)\%$ for SP-IP and $(2.04 \pm 0.37)\%$ for DP-IP). Thus all acceptable solutions are represented by red rectangles and their distribution describes errors of the log-normal functions $x_0 = -0.30^{+0.13}_{-0.09}$ and $\sigma = 0.80^{+0.16}_{-0.11}$ (see also Tab.B2).

The SP-IP cases are very interesting. In our simulations we used two models of SP-IP emission. In the classical model of ML77 (Fig. C1) the MP and the IP components result from two cuts of a very wide hollow emission cone. In this model the separation between MP and IP should be frequency dependent (following a spread of dipolar field lines), and its value being close to 180° should be considered accidental (Weltevrede, Wright & Stappers 2007). An alternative SP-IP model was proposed by G83 (Fig. C2). This model is based on the assumption of the double conal structure of the pulsar beam. The line-of-sight of the nearly aligned rotator cuts one cone for the MP and the other one for the IP emission (see Fig. 8 in Kloumann & Rankin (2010) for schematic diagram for PSR B1944+17). This model naturally predicts two important properties: frequency independence of MP – IP separation (equal to 180°) and existence of the bridge of emission between MP and IP. Interestingly, in our Monte Carlo simula-

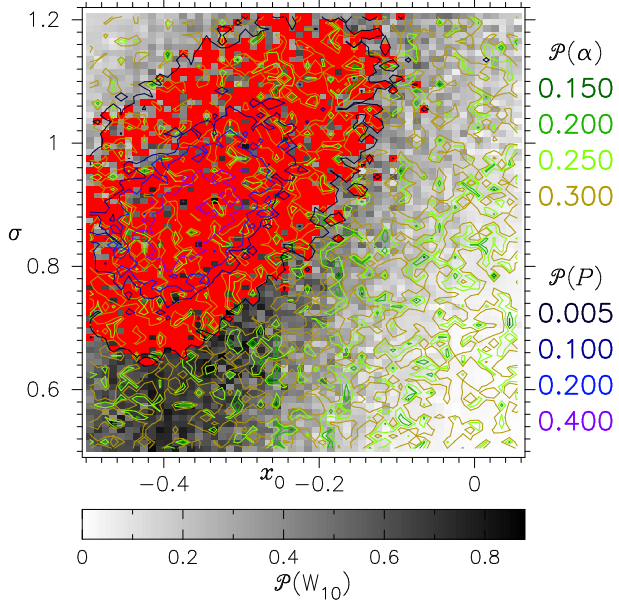


Figure 8. Same as in Fig. 7 but with luminosity problem included in simulations (Appendix A). This figure corresponds to the items 1b and 2b, while Fig. 7 corresponds to the items 1a and 2a in Table 2.

tions we detected more cases corresponding to ML77 model than to G83 model. Therefore, if these simulations are correct, most of the 14 SP-IP cases (about 1% of a total population) should show tendency to frequency dependent separation between MP and IP. Unfortunately, we are not able to verify this conclusion, as most of the available data correspond to a single frequency. However, this should be performed in some suitable project in the future.

A convenient method of graphical representation of each set of trial distribution functions is "a colour map of solutions", example of which is presented in Fig. 7. More plots of this kind are presented in Appendix C. Colour contours represent levels of conformity of the observed and the simulated distributions. The "green" set of colours is used for inclination angles and the "blue" one is used for periods. Their legends are presented on the right-hand side of Fig. 7, which describe the corresponding probability levels $P(\alpha)$ and $P(P)$. The grey bar below the plot represents conformity of the observed and the synthetic distributions for the pulse-width W_{10} in the form of K-S probability $P(W)$. The white colour represents zero probability and the black corresponds to the maximum probability occurring in a given plot. Axes of each plot represent the free parameters of period distribution function (i.e. m and a for the gamma function, x_0 and σ for the log-normal function). The space for good solutions is restricted to the areas where all three probabilities P simultaneously exceed 0.5%. That is why in Fig. 7 and Fig. C3 – C6 all good solutions must lay in darkest blue contour. Moreover, the occurrence of interpulsars in this region must be on the observed level (specified at the end of the previous paragraph), which is marked by red rectangles in Fig. 7. In fact, the good solutions are represented by red rectangles because they are marked only if all required probabilities occur simultaneously. The numerical details of all good solutions are presented in Tables B2 – B6.

Table 3. Number of good solutions for different combination of distribution functions described by Equations: (6) – inclination angle, (11) – log–normal period distribution, (8) – gamma period distribution; (14), (13) and (15b) – opening angle distribution functions.

No.	Distributions	No. of solutions
1	(6) (11) (13)	326
2	(6) (11) (14)	170
3	(6) (11) (15b)	183
4	(6) (8) (13)	147
5	(6) (8) (14)	1

Careful studies of all contour plots (see examples in Fig. 7 and Fig. C3 – C9) and corresponding numerical solutions (Tables B2 – B6) lead to the following conclusions:

1. Solutions satisfying all criteria ($\mathcal{P} > 0.5\%$ for all variables P , α and W_{10} as well as the definition and the occurrence of interpulses at the observed levels) were obtained mainly for the log–normal period distribution function (Eq. (11)) with parameters $x_0 = -0.30^{+0.13}_{-0.09}$ and $\sigma = 0.80^{+0.16}_{-0.11}$ (see Fig. 7). Six best examples corresponding to this function are presented in Table 2 (items 1 – 6). Also the gamma distribution period function (Eq. (8)) with parameters $m = 0.45^{+0.07}_{-0.08}$ and $a = 2.04^{+0.34}_{-0.16}$ (see Fig. C5) seems to be quite good, however the corresponding K–S probabilities are lower than in the log–normal distribution period function case. Four best examples are presented in Table 2 (items 7 – 9). None of the period trial functions (Eqs. (8) – (11)) is perfectly suited to reproduce the observed distributions of our observables. However, the gamma and the log–normal functions are by far the best, with the latter being slightly better, most likely because it reproduces the tail of long periods (see middle panel in Fig. 3) very well.

2. Both the rotation axis and the observer’s direction are randomly distributed in space (see Eq. (2)).

3. The only trial distribution function of the inclination angle that satisfies all constraints is the complicated trigonometric function of GH96 (represented by Eq. (6)). This function has two local maxima, one near 0° (almost aligned rotator) and the other near 90° (almost orthogonal rotator). We do not find support for the modified cosine function of ZJM03 (Eq. (7)), which was derived without taking into account a problem of frequency of occurrence of the IP emission. It is clear that none of the functions represented by Eqs. (3) – (7) reproduces the observed distribution of simulated variables P , W and α as well as the frequency of IP occurrence. However, the function of GH96 represented by Eq. (6) suits the best and is recommended as the model function for the parent distribution of the inclination angles.

4. As a result of simulations performed with suitable parent distribution functions of periods and inclination angles we obtained good solutions for most of the trial model functions for the opening angle. It is not possible to discriminate the opening angle functions using the statistical tools available to us. This is illustrated in Table 3.

5. The average beaming fraction $f_b = N_{det}/N_{tot} \approx 0.1$, where $N_{tot} = 50000$ is the total number of simulated pulsar candidates and N_{det} is the number of detected pulsars in our simulations. This value is close to the one obtained by

TM98 and ZJM03, but lower than those obtained by GH96 and KGM04. One should realize that this factor corresponds to averaging over many pulsar parameters, the most important being pulsar period (for more details see the end of this Section). Moreover, since the pulsar luminosity is not taken into account (some distant pulsars will be too weak to be detected) this value of the beaming fraction should be considered as an upper limit. Once the luminosity problem is considered (see Appendix A for some details) the value of beaming fraction largely decreases, perhaps even to the value as low as 0.02.

As already mentioned this paper is a continuation of our previous attempt to resolve the pulse–width statistics based on the modeling of pulsar geometry (KGM04). Although we improved the numbers and the quality of the observational databases as well as methods of data processing, we are still lacking an analysis of the possible effect of the intrinsic luminosity of radio pulsars on our results. This problem is, however, very difficult and complicated and we will discuss it only superficially, postponing a full treatment to a future paper (see also Appendix A). The proper approach would be to compare the synthetic radio luminosity with the minimum detectable flux achieved in a given pulsar survey, and thus it can be applied only to uniform data sets of pulsars detected in single survey. Our data do not have such a degree of uniformity. However, most surveys were less sensitive to long–period pulsars, as it stems from the nature of the applied Fourier–transform method. Since the interpulse emission (which appears to be the most restrictive constrain in our analysis) occurs mainly at shorter periods (see upper panel in Fig. 3), a possible under–representation of pulsars with longer periods should not significantly affect our general results.

We assumed that the intrinsic pulsar luminosity does not depend significantly on the inclination angle (geometry) but can depend on P and \dot{P} (pulsar evolution). We performed simple test to check possible influence of pulsar geometry and evolution. The result of this test is presented and discussed in Appendix A. However, the main results of this paper were obtained using only geometrical detection conditions, that is every pulsar in the field of view of our hypothetical radiotelescope was detected. It means that each detectable pulsar would be close and bright enough so its radio energy flux would exceed the detection threshold of our hypothetical radio pulsar search campaign. As we argue below (see also Appendix A), omitting the luminosity problem does not affect correctness of our results, at least significantly. However, taking it under consideration would vastly complicate the research programme (especially its computational part) and introduce additional uncertainties decreasing reliability of our conclusions. Also, it is worth emphasizing once more that our statistical studies were in principle limited to geometrical features (inclination angles, pulse–width and structure of the beam), without drawing conclusions depending on the luminosity problem, like the initial periods or the neutron stars birth rates.

The absolute luminosity of pulsar can be written in general form as $L_r = f(P, \dot{P}) = AP^{\alpha_1}\dot{P}^{\alpha_2}$, where A , α_1 and α_2 are free parameters of a model (e.g. Arzoumanian, Chernoff & Cordes, 2002; ACC02 hereafter). Some authors even argue that for given P and \dot{P} the luminosity is constant

i.e. pulsars can be considered as standard candles. Without a detailed discussion we would like to emphasise that each particular approach depends on an adopted model and leads to some problems. For example, from the analysis of observational data ACC02 deduced that luminosity function is $L_r = P^{-1.3} \dot{P}^{0.4} / 10^{-15} 10^{29.3}$ erg s $^{-1}$. This could be considered as an empirical function, but one should realise that the authors used some controversial assumptions about the shape and size of the beam to obtain it, which are not really true in our opinion. However, more important are problems reported by other authors (Gonthier et al. 2004), who tried to use this function in their statistical studies. They noticed that this function gives too many bright pulsars as compared with observations and too high the NS birth rate. For example, Gonthier et al. (2004) used the above function in simulations of γ -ray pulsars detected by EGRET (Thompson 2008) but they had to reduce the amplitude $A = 10^{29.3}$ by factor of 60 (leaving values of α_1 and α_2 unchanged for unknown reasons). Anyway, it is important to realize that a form of the function of absolute pulsar luminosity is not known.

The flux density of a pulsar with luminosity L erg s $^{-1}$ and distance d is $S = (f_b/4\pi)L$ [mJy kpc 2], where f_b is the beaming fraction describing a part of a full sphere illuminated by a pulsar beam. This value of S , calculated with high uncertainty, should be compared with the sensitivity of a radiotelescope expressed as the so-called minimum detectable flux density S_{min} . Detection of pulsar is possible if $S > S_{min}$. We used data from pulsars discovered in more than a dozen surveys, with S_{min} changing from one campaign to another. It is impossible to find a universal, theoretical value of S_{min} corresponding to all pulsars in our sample, and thus it is impossible to find a consistent detection criterion based only on a distance to the pulsar and its luminosity. Apart from uncertainties introduced by this method, the parameter space would be extended enormously by many dimensions such as: distance, direction in the space to the pulsar, inhomogeneities in ISM, luminosity function and beaming fraction. Thus, computationally the problem greatly complicates and the expected benefits are not that high to justify these efforts. Therefore, we used the assumption that each pulsar detected in our "geometrical search" simulations corresponds to a flux density S greater than a hypothetical S_{min} , the value of which we do not specify. Instead, we use geometrical criterion $\rho_0 > \beta$ where $\rho = 1.1\rho_{10}$ and ρ_{10} is calculated from empirical formulae (Eqs. (13) – (15)).

In Appendix A we present a simple test to check how the luminosity problem can affect a validity of our conclusions. We do not intend to find any new model of the intrinsic pulsar luminosity. This is beyond the scope of our paper. Instead, we use a very convenient existing luminosity probability density function presented by RL10, which is best suited for our non-uniform (with respect to sensitivity of different pulsar search campaigns) database. The results of this check are presented in Table 2 (lines 1b – 9b in comparison with lines 1a – 9a) and shortly explained below. We found that most of our conclusions were not significantly changed but the number of pulsar detections dropped by a factor of several (see Appendix A). As a result the actual (but still period averaged) beaming fraction f_b dropped to

a value about 2% (compared with 10% obtained without luminosity).

Therefore, we conclude that the actual beaming fraction f_b (describing a part of the full sphere illuminated by an average pulsar beam) can be significantly lower than 10 %, perhaps even as low as about 2% (see Table 2). This is by a factor of few to several smaller than estimates of the beaming fraction value that can be found in the literature (0.17 – Gunn & Ostriker (1970), 0.16 – GH96, 0.14 – KGM04, 0.12 – ZJM03, 0.1 – TM98, 0.084 – WJ08a). This would suggest that the number of the neutron stars in the Galaxy is much larger than currently estimated. Recent discoveries of Rotating Radio Transients (McLaughlin et al. 2006) seem to support such a point of view. Indeed, it seems that there are 2 – 3 times more RRATs than pulsars in the Galaxy (Keane 2010). RRATs seem to be just a normal radio pulsars in which we detect only strongest subpulses. More than 30 RRATs have been detected so far (Keane et al. 2010), thus an interesting question arises when one should expect first interpulse case in those objects. Our paper shows that there are about 3% of interpulses in normal pulsar population. Thus, among 30 RRATs one should expect one IP case. However, the situation is more complicated than that since in many cases the interpulse is much weaker than the main pulse. From careful analysis of all our interpulse cases we can predict that the first interpulse RRAT will occur when the population of these objects will rise to about 100.

Finally, we would like to comment on the new interpulse case detected in PSR J2007+2722 using Einstein@Home global computing technique (Knispel et al. 2010). This is a 24 ms isolated pulsar with magnetic axis almost aligned to the spin axis. The mean profile covers full 360° pulse window, with two equal amplitude components separated by about 180° (see Fig. 1 in Knispel et al. (2010)). Thus, this case seems to be an ideal example of SP-IP object. However, the authors of the discovery paper argue that this is likely a disrupted recycled pulsar. For this reason we do not include it to our interpulse database. The global computing technique should result in more pulsar discoveries in the near future and we hope that some of them will contain the interpulse emission.

6 CONCLUSIONS

The main results and conclusions of this paper can be summarized as follows:

1. We compiled the largest ever database of 44 pulsars with interpulses, in which we identified 31 (about 2%) double-pole cases and 13 (about 1%) single-pole cases.
2. We found a strong evidence that the magnetic axis aligns with time towards the rotation axis from the originally random orientation.
3. The parent period distribution density function is most likely the log-normal distribution, although the gamma distribution cannot be excluded.
4. The most suitable model distribution function for the inclination angle is the complicated trigonometric function which has two local maxima, one near 0° and the other

near 90° . The former and the latter implies the right rates of IP occurrence, single-pole (almost aligned rotator) and double-pole (almost orthogonal rotator), respectively.

5. The average pulsar beam has an almost perfect circular cross-section.

6. The upper limit for period averaged beaming fraction describing a fraction of the full sphere covered by pulsar beam is about 10%.

ACKNOWLEDGMENTS

This work is partially supported by the Grant 1 P03D 015 29 of the Polish State Committee for Scientific Research and by Polish Research Grants NN 203 2738 33 and NN 203 3919 34. We thank R.N. Manchester for invitation of K.M. to Australia, support and access to the ATNF pulsar data. We also thank M. Kramer for sharing with us unpublished results concerning new interpulse cases. We thank M. Kolodziejczyk for linguistic help. We also thank the anonymous referee for useful comments.

References

- Arzoumanian Z., Chernoff D.F., Cordes J.M., 2002, ApJ, 568, 289 (ACC02)
- Backer D.C., 1976, ApJ, 209, 895
- Biggs J.D., 1990, MNRAS, 245, 514
- Camilo F., Ray P.S., Ransom S.M., et al., 2009, ApJ, 705, 1
- Contopoulos I., Spitkovsky A., 2006, ApJ, 643, 1139
- Cordes J.M., Lazio T.J.W., 2003, astro-ph/0301598
- D'Amico N., Stappers B.W., Bailes M., Martin C.E., Bell J.F., Lyne A.G., Manchester R.N., 1998, MNRAS, 297, 28
- Edwards R.T., Bailes M., van Straten W., Britton M.C., 2001, MNRAS, 326, 358
- Faucher-Giguere C.-A., Kaspi V.M., 2006, ApJ, 643, 332
- Faulkner A.J., Stairs I.H., Kramer M., et al., 2004, MNRAS, 355, 147
- Gil J., 1981, Acta Phys. Polonicae, B12, 1081
- Gil J., 1983, A&A, 127, 267
- Gil J., Gronkowski P., Rudnicki W., 1984, A&A, 132, 312
- Gil J., 1985, ApJ, 299, 154
- Gil J., Kijak J., 1993, A&A, 273, 563
- Gil J., Kijak J., Seiradakis J.H., 1993, A&A, 272, 268, (GKS93)
- Gil J., Han J.L., 1996, ApJ, 458, 265 (GH96)
- Gonthier P.L., Van Guilder R., Harding A.K., 2004, ApJ, 604, 755
- Henry G.R., Paik H.-J., 1969, Nature, 224, 1188
- Gunn J.E., Ostriker J.P., 1970, ApJ, 160, 979
- Hobbs G., Faulkner A., Stairs I.H., et al., 2004, MNRAS, 352, 1439
- Janssen G.H., Stappers B.W., Braun R., et al., 2009, A&A, 498, 223
- Keane E.F., Ludovici D.A., Eatough R.P., Kramer M., Lyne A.G., McLaughlin M.A., Stappers B.W., 2010, MNRAS, 401, 1057
- Keane E.F., 2010, astro-ph.1008.3693
- Keith M.J., Eatough R.P., Lyne A.G., et al., 2009, MNRAS, 395, 837
- Keith M.J., Johnston S., Weltevrede P., Kramer M., 2010, MNRAS, 402, 745
- Kijak J., Gil J., 1997, MNRAS, 288, 631
- Kijak J., Gil J., 1998, MNRAS, 299, 855
- Kloumann I., Rankin J., 2010, astro-ph.1007.1950
- Knispel B., Allen B., Cordes J.M., 2010, astro-ph.1008.2172
- Kolonko M., Gil J., Maciesiak K., 2004, A&A, 428, 943 (KGM04)
- Kramer M., Wielebinski R., Jessner A., Gil J., Seiradakis J.H., 1994, A&AS, 107, 515
- Kramer M., Lyne A.G., Hobbs G., et al., 2003a, ApJ, 593, L31
- Kramer M., Bell J.F., Manchester R.N., et al., 2003b, MNRAS, 342, 1299
- Lorimer D.R., Faulkner A.J., Lyne A.G., et al., 2006, MNRAS, 372, 777
- Lyne A.G., Manchester R.N., 1988, MNRAS, 234, 477
- Lyne A.G., Manchester R.N., Lorimer D.R., et al., 1998, MNRAS, 295, 743L
- Manchester R.N., Lyne A.G., 1977, MNRAS, 181, 761 (ML77)
- Manchester R.N., Taylor J.H., 1977, *Pulsars*
- Manchester R.N., Lyne A.G., D'Amico N., et al., 1996, MNRAS, 279, 1235
- Manchester R.N., Lyne A.G., Camilo F., et al., 2001, MNRAS, 328, 17
- Manchester R.N., Hobbs G.B., Toeh A., Hobbs M., 2005, AJ, 129
- McKinnon M.M., 1993, ApJ, 413, 317
- McLaughlin M., Lyne A.G., Lorimer D.R., et al., 2006, Nature, 439, 817
- Migliazzo J.M., Gaensler B.M., Backer D.C., Stappers B.W., van der Swaluw E., Strom R.G., 2002, ApJ, 567, L141
- Morris D.J., Hobbs G., Lyne A.G., et al., 2002, MNRAS, 335, 275
- Narayan R., Vivekanand M., 1983, A&A, 122, 145
- Prószyński M., 1979, A&A, 79, 8
- Rankin J., 1983, ApJ, 274, 333
- Rankin J., 1990, ApJ, 352, 247 (R90)
- Rankin J., 1993a, ApJ, 405, 285
- Rankin J., 1993b, ApJS, 85, 145
- Ribeiro V.A.R.M., 2008, On the Shape of Pulsar Emission, MSc Thesis, The University of Manchester
- Rickett B.J., Lyne A.G., 1968, Nature, 218, 934
- Ridley J.P., Lorimer D.R., 2010, MNRAS, 404, 1081 (RL10)
- Roberts D.H., Sturrock P.A., 1972, ApJ, 172, 435
- Roberts D.H., Sturrock P.A., 1973, ApJ, 181, 161
- Taylor H., Manchester R.N., Lyne A.G., 1993, ApJS, 88, 529
- Tauris T.M., Manchester R.N., 1998, MNRAS, 298, 625 (TM98)
- Thompson D.J., 2008, Reports on Progress in Physics, 71(11):116901
- Weltevrede P., Wright G.A.E., Stappers B.W., 2007, A&A, 467, 1163
- Weltevrede P., Johnston S., 2008a, MNRAS, 387, 1755 (WJ08a)
- Weltevrede P., Johnston S., 2008b, MNRAS, 391, 1210

Young M.D.T., Chan L.S., Burman R.R., Blair D.G., 2010,
MNRAS, 402, 1329

Young M.D., Manchester R.N., Johnston S., 1999, Nature,
400, 848

Zhang L., Jiang Z.J., Mei D.C., 2003, PASJ, 55, 461
(ZJM03)

ON-LINE MATERIALS

APPENDIX A: LUMINOSITY PROBLEM

To test how the luminosity problem can affect the validity of results and conclusions obtained in our paper we followed the results of Faucher-Giguere & Kaspi (2006), recently presented by Ridley & Lorimer (2010; hereafter RL10). As shown in this paper the radio luminosity can be calculated from

$$\log L = \log L_0 - \log P + 0.5 \log(\dot{P}/10^{-15}) + \delta_L, \quad (\text{A1})$$

where L_0 is 0.18 mJy kpc² and δ_L is randomly chosen from a normal distribution with $\sigma_{\delta_L} = 0.8$. Thus the luminosity L can be calculated when the values of P and \dot{P} are known. We generated pulsar period P as a random deviate with a parent probability density function $f(P)$ corresponding to Eqs. (8) – (11) in Section 2.1. The value of period derivative can be calculated from either Eqs. (9) and (10) in RL10 or by random generation with a distribution in agreement with the observed $P - \dot{P}$ diagram (Fig. 6). We used both methods and made sure that they lead to similar simulation results. For example, we found that L depends very weakly on the inclination angle α which enters into Eq. (9) in RL10.

Once the luminosity $L(P, \dot{P})$ is calculated we can obtain the probability density function

$$f(L) \propto \begin{cases} 0 & L \in [0 \text{ mJy kpc}^2, 0.1 \text{ mJy kpc}^2) \\ L^{-19/15} & L \in [0.1 \text{ mJy kpc}^2, 2.0 \text{ mJy kpc}^2) \\ L^{-2} & L \in [2.0 \text{ mJy kpc}^2, \infty \text{ mJy kpc}^2], \end{cases} \quad (\text{A2})$$

(Eq.(17) in Faucher-Giguere & Kaspi (2006) and Eq.(15) in RL10). This function is illustrated in Fig. A1. Now, we can extend our Monte Carlo simulation procedure by adding to the list of 16 steps listed in Section 4 the detection condition based on the luminosity described above. The procedure was as follows. First, to simplify calculations the function was normalised to unity at the luminosity value equal to 0.1 mJy kpc² (see Fig. A1). This gave the proportionality constant $C = 0.1^{19/15} = 0.05$ in Eq. (A2). For a generated P and \dot{P} the values of L and $f(L)$ were calculated according to Eqs. (A1) and (A2), respectively. The pulsar was counted as detected when the value of $f(L)$ lied below the thick line presented in Fig.A1 (and outside the shadowed area).

The results of the luminosity test are presented in Table 2, where we compare good solutions with (lines 1b – 9b) and without (lines 1a – 9a) luminosity included, respectively. As one can see the only parameter that changed drastically is the beaming fraction f_b , which dropped by a factor of about 8. This is a consequence of much smaller number of detections. However, the interpulse detection at the requested levels still determines the statistical structure of detected pulsar population. This is illustrated in Fig. 8, as compared with Fig. 7.

In this Appendix we attempted to estimate an influence of the pulsar luminosity problem on the geometrical conclusion derived in our paper. We used a luminosity model represented by Eq. (A2) derived by Faucher-Giguere & Kaspi (2006) and presented by RL10. If this equation describes the luminosity density probability function for pulsars in our Galaxy, then the beaming fraction can be as low as about

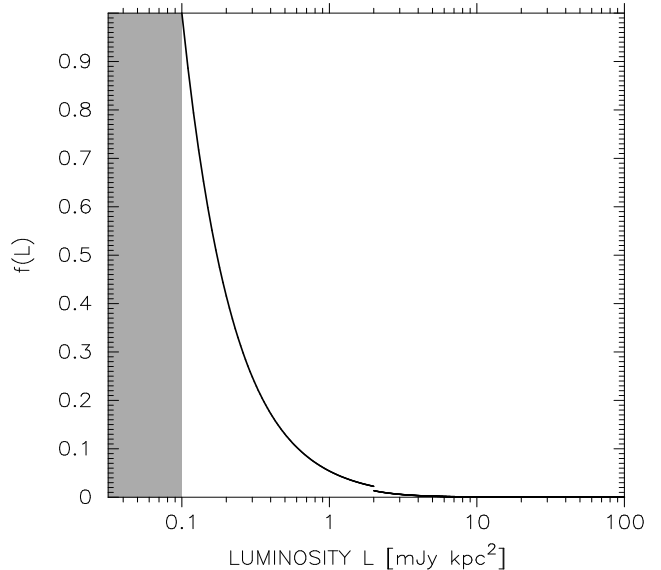


Figure A1. The luminosity probability density function described by Eq. (A2). No pulsar detections are expected in shadowed rectangular area.

2%. The advantage of this rather crude model is a convenience in use and independence of details of different pulsar search campaigns. Anyway, at this point we can firmly conclude that the average pulsar beaming fraction is a number between 0.02 and 0.10 (2% – 10%).

APPENDIX B: TABLES

Table B1: Reproduction of the results from KGM04

Original results from KGM04				Reproduction of KGM04 results in this work		
Parameter	Average	σ	%	Average	σ	%
NOP	6385.3501	70.9845		6399.0098	66.5424	
DP-IP	143.2600	11.8651	2.244	141.2800	11.1410	2.208
SP-IP	41.5600	6.7962	0.651	41.7100	6.4075	0.652
$\mathcal{D}(W_{10})$	0.1270	0.0066		0.1280	0.0060	
$\mathcal{P}(W_{10})$	0.0016	0.0013		0.0012	0.0009	
$\mathcal{D}(P)$	0.0600	0.0067		0.0581	0.0063	
$\mathcal{P}(P)$	0.0038	0.0052		0.0053	0.0077	
$\mathcal{D}(\alpha)$	0.1009	0.0055		0.1001	0.0055	
$\mathcal{P}(\alpha)$	0.1075	0.0344		0.1061	0.0362	
b_f			12.771			12.798
<hr/>						
$m = 0.35$	$a = 2.51$					
NOP	6352.7300	71.2812		6364.2798	72.6219	
DP-IP	141.3400	11.2045	2.225	136.4900	10.5605	2.145
SP-IP	41.0500	5.5766	0.646	42.6500	6.9969	0.670
$\mathcal{D}(W_{10})$	0.1217	0.0066		0.1267	0.0068	
$\mathcal{P}(W_{10})$	0.0029	0.0025		0.0015	0.0013	
$\mathcal{D}(P)$	0.0685	0.0063		0.0626	0.0070	
$\mathcal{P}(P)$	0.0006	0.0015		0.0023	0.0034	
$\mathcal{D}(\alpha)$	0.1013	0.0058		0.0996	0.0059	
$\mathcal{P}(\alpha)$	0.1056	0.0369		0.1095	0.0373	
b_f			12.705			12.729

Table B2: Simulation results of the pulsar beam for opening angle distribution Eq. (13), inclination angle distribution function Eq. (6) and period distribution function Eq. (11). Graphical representation of this class of solutions is represented in Fig. 7.

No.	$f(P)$		W_{10}		P		α		DP-IP [%]	SP-IP [%]	f_b
	x_0	σ	\mathcal{D}	\mathcal{P}	\mathcal{D}	\mathcal{P}	\mathcal{D}	\mathcal{P}			
1	-0.39	0.79	0.044	0.484	0.053	0.008	0.084	0.255	2.17	0.92	0.111
2	-0.38	0.74	0.041	0.533	0.051	0.007	0.089	0.191	2.21	1.00	0.111
3	-0.38	0.75	0.040	0.574	0.052	0.005	0.090	0.188	2.15	0.90	0.109
4	-0.38	0.76	0.039	0.593	0.049	0.016	0.087	0.218	2.00	0.89	0.110
5	-0.38	0.77	0.042	0.512	0.047	0.014	0.086	0.238	2.22	0.97	0.110
6	-0.38	0.78	0.039	0.604	0.046	0.018	0.085	0.244	2.18	0.87	0.110
7	-0.38	0.79	0.047	0.370	0.048	0.010	0.087	0.216	2.20	0.94	0.110
8	-0.38	0.80	0.046	0.414	0.049	0.012	0.086	0.232	2.22	0.97	0.110
9	-0.38	0.81	0.049	0.360	0.050	0.014	0.091	0.182	2.21	1.01	0.110
10	-0.38	0.82	0.048	0.362	0.051	0.007	0.084	0.254	2.27	0.96	0.111
11	-0.37	0.73	0.040	0.572	0.051	0.013	0.088	0.216	2.09	0.85	0.109
12	-0.37	0.74	0.036	0.685	0.047	0.013	0.087	0.218	2.26	0.91	0.109
13	-0.37	0.75	0.038	0.619	0.045	0.022	0.086	0.229	2.12	0.91	0.109
14	-0.37	0.76	0.041	0.535	0.047	0.019	0.088	0.208	2.19	0.94	0.109
15	-0.37	0.77	0.039	0.603	0.044	0.035	0.086	0.232	2.13	0.96	0.109
16	-0.37	0.78	0.040	0.588	0.045	0.020	0.086	0.237	2.07	0.91	0.110
17	-0.37	0.79	0.046	0.417	0.044	0.040	0.089	0.194	2.20	0.99	0.109
18	-0.37	0.80	0.045	0.449	0.041	0.064	0.089	0.201	2.08	0.97	0.110
19	-0.37	0.81	0.047	0.382	0.045	0.020	0.088	0.208	2.20	0.98	0.110
20	-0.37	0.82	0.045	0.438	0.047	0.015	0.085	0.250	2.21	0.96	0.110
21	-0.36	0.72	0.033	0.785	0.048	0.013	0.087	0.220	2.12	0.97	0.108
22	-0.36	0.73	0.033	0.793	0.048	0.009	0.087	0.218	2.21	0.88	0.109
23	-0.36	0.74	0.038	0.617	0.044	0.038	0.091	0.185	2.21	0.89	0.109
24	-0.36	0.75	0.038	0.622	0.045	0.021	0.089	0.198	2.10	0.93	0.109
25	-0.36	0.76	0.038	0.644	0.041	0.055	0.089	0.202	2.19	0.91	0.110
26	-0.36	0.77	0.036	0.694	0.043	0.047	0.083	0.263	2.16	0.96	0.110

No.	$f(P)$		W_{10}		P		α		DP-IP [%]	SP-IP [%]	f_b
	x_0	σ	\mathcal{D}	\mathcal{P}	\mathcal{D}	\mathcal{P}	\mathcal{D}	\mathcal{P}			
27	-0.36	0.78	0.041	0.555	0.040	0.065	0.086	0.229	2.20	0.99	0.110
28	-0.36	0.79	0.045	0.430	0.043	0.049	0.088	0.208	2.14	1.01	0.110
29	-0.36	0.80	0.044	0.463	0.041	0.043	0.084	0.254	2.08	0.97	0.110
30	-0.36	0.81	0.044	0.458	0.041	0.052	0.088	0.220	2.22	0.94	0.110
31	-0.36	0.82	0.041	0.524	0.044	0.033	0.084	0.253	2.08	0.97	0.111
32	-0.36	0.83	0.046	0.403	0.043	0.030	0.087	0.221	2.25	1.08	0.110
33	-0.36	0.84	0.048	0.338	0.049	0.008	0.088	0.209	2.22	1.04	0.111
34	-0.35	0.69	0.032	0.800	0.050	0.010	0.091	0.178	2.07	0.88	0.108
35	-0.35	0.70	0.032	0.802	0.051	0.010	0.093	0.170	2.22	0.96	0.109
36	-0.35	0.71	0.028	0.908	0.045	0.021	0.086	0.237	2.16	0.93	0.108
37	-0.35	0.72	0.031	0.840	0.045	0.029	0.088	0.210	2.18	0.89	0.108
38	-0.35	0.73	0.033	0.772	0.044	0.028	0.088	0.208	2.20	0.91	0.109
39	-0.35	0.74	0.035	0.729	0.041	0.053	0.092	0.177	2.21	0.87	0.109
40	-0.35	0.75	0.033	0.796	0.042	0.033	0.087	0.223	2.21	0.87	0.109
41	-0.35	0.76	0.036	0.693	0.039	0.062	0.090	0.186	2.16	0.88	0.109
42	-0.35	0.77	0.036	0.692	0.040	0.048	0.086	0.222	2.17	0.95	0.110
43	-0.35	0.78	0.042	0.521	0.038	0.070	0.092	0.166	2.18	1.00	0.109
44	-0.35	0.79	0.038	0.612	0.036	0.127	0.085	0.252	2.16	0.96	0.108
45	-0.35	0.80	0.038	0.623	0.035	0.135	0.088	0.210	2.10	0.89	0.109
46	-0.35	0.81	0.041	0.539	0.037	0.092	0.086	0.225	2.26	0.87	0.109
47	-0.35	0.82	0.040	0.574	0.038	0.071	0.086	0.236	2.22	0.98	0.110
48	-0.35	0.83	0.041	0.525	0.042	0.034	0.085	0.243	2.14	0.96	0.110
49	-0.35	0.84	0.045	0.426	0.046	0.016	0.088	0.214	2.28	0.97	0.109
50	-0.35	0.85	0.046	0.410	0.052	0.008	0.086	0.234	2.14	1.04	0.110
51	-0.34	0.69	0.031	0.838	0.050	0.007	0.087	0.221	2.19	0.93	0.108
52	-0.34	0.70	0.025	0.946	0.047	0.018	0.084	0.245	2.16	0.92	0.108
53	-0.34	0.71	0.028	0.897	0.043	0.033	0.083	0.268	2.15	0.85	0.109
54	-0.34	0.72	0.027	0.931	0.040	0.049	0.082	0.278	2.13	0.89	0.108
55	-0.34	0.73	0.032	0.803	0.039	0.058	0.091	0.172	2.12	0.99	0.109
56	-0.34	0.74	0.033	0.773	0.040	0.060	0.088	0.207	2.19	0.95	0.108
57	-0.34	0.75	0.029	0.880	0.038	0.101	0.083	0.263	2.11	0.84	0.109
58	-0.34	0.76	0.034	0.759	0.035	0.159	0.086	0.229	2.03	0.94	0.109
59	-0.34	0.77	0.035	0.704	0.033	0.171	0.084	0.258	2.15	0.90	0.109
60	-0.34	0.78	0.038	0.622	0.034	0.158	0.087	0.212	2.13	0.94	0.108
61	-0.34	0.79	0.041	0.531	0.031	0.248	0.089	0.192	2.11	0.93	0.110
62	-0.34	0.80	0.041	0.534	0.034	0.154	0.088	0.218	2.01	1.01	0.109
63	-0.34	0.81	0.038	0.640	0.035	0.147	0.086	0.233	2.10	0.89	0.109
64	-0.34	0.82	0.041	0.546	0.037	0.089	0.087	0.224	2.23	0.94	0.109
65	-0.34	0.83	0.042	0.514	0.038	0.075	0.083	0.278	2.22	0.99	0.110
66	-0.34	0.84	0.042	0.515	0.042	0.042	0.088	0.211	2.21	1.00	0.109
67	-0.34	0.85	0.043	0.477	0.046	0.022	0.087	0.217	2.19	0.99	0.110
68	-0.34	0.86	0.048	0.354	0.053	0.007	0.087	0.214	2.18	1.01	0.109
69	-0.33	0.70	0.029	0.901	0.046	0.020	0.090	0.180	2.03	0.89	0.108
70	-0.33	0.71	0.028	0.902	0.044	0.020	0.091	0.174	1.95	0.91	0.109
71	-0.33	0.72	0.029	0.887	0.042	0.036	0.087	0.214	2.07	0.86	0.109
72	-0.33	0.73	0.029	0.893	0.038	0.077	0.089	0.203	2.02	0.87	0.108
73	-0.33	0.74	0.031	0.830	0.036	0.103	0.087	0.216	2.10	0.89	0.108
74	-0.33	0.75	0.033	0.784	0.037	0.103	0.090	0.192	2.18	0.91	0.108
75	-0.33	0.76	0.032	0.816	0.031	0.234	0.088	0.213	2.16	0.86	0.108
76	-0.33	0.77	0.029	0.887	0.030	0.273	0.087	0.227	2.06	0.96	0.108
77	-0.33	0.78	0.032	0.802	0.029	0.297	0.089	0.203	2.14	0.97	0.108
78	-0.33	0.79	0.038	0.648	0.028	0.323	0.092	0.169	2.10	0.91	0.109
79	-0.33	0.80	0.037	0.668	0.031	0.211	0.089	0.198	2.10	0.89	0.109
80	-0.33	0.81	0.034	0.764	0.028	0.346	0.086	0.226	2.07	0.94	0.109
81	-0.33	0.82	0.039	0.609	0.030	0.267	0.092	0.168	2.11	0.90	0.109
82	-0.33	0.83	0.041	0.547	0.039	0.062	0.088	0.207	2.31	1.01	0.110
83	-0.33	0.84	0.043	0.479	0.039	0.077	0.088	0.208	2.21	0.95	0.109
84	-0.33	0.85	0.042	0.526	0.046	0.020	0.087	0.219	2.22	0.95	0.109
85	-0.33	0.86	0.045	0.418	0.051	0.010	0.089	0.198	2.16	0.98	0.108
86	-0.32	0.70	0.027	0.937	0.052	0.005	0.084	0.252	2.09	0.82	0.108
87	-0.32	0.71	0.029	0.894	0.047	0.013	0.083	0.257	2.09	0.86	0.107
88	-0.32	0.72	0.027	0.914	0.042	0.034	0.085	0.252	2.04	0.84	0.107
89	-0.32	0.73	0.029	0.899	0.038	0.105	0.083	0.263	2.05	0.98	0.108
90	-0.32	0.74	0.030	0.864	0.037	0.109	0.087	0.220	2.07	0.99	0.107
91	-0.32	0.75	0.030	0.852	0.033	0.170	0.084	0.258	2.16	0.81	0.108

No.	$f(P)$		W_{10}		P		α		DP-IP [%]	SP-IP [%]	f_b
	x_0	σ	\mathcal{D}	\mathcal{P}	\mathcal{D}	\mathcal{P}	\mathcal{D}	\mathcal{P}			
92	-0.32	0.76	0.031	0.835	0.028	0.312	0.085	0.239	2.21	0.86	0.108
93	-0.32	0.77	0.034	0.767	0.029	0.298	0.086	0.231	2.18	0.91	0.108
94	-0.32	0.78	0.036	0.693	0.027	0.389	0.090	0.196	2.06	0.99	0.108
95	-0.32	0.79	0.031	0.842	0.024	0.501	0.085	0.248	2.15	0.99	0.108
96	-0.32	0.80	0.038	0.623	0.027	0.361	0.085	0.243	2.23	0.98	0.109
97	-0.32	0.81	0.036	0.706	0.028	0.364	0.087	0.227	2.07	0.99	0.108
98	-0.32	0.82	0.037	0.645	0.028	0.341	0.084	0.259	2.14	0.97	0.109
99	-0.32	0.83	0.037	0.651	0.032	0.224	0.083	0.270	2.15	0.89	0.110
100	-0.32	0.84	0.041	0.530	0.038	0.087	0.085	0.238	2.20	0.99	0.109
101	-0.32	0.85	0.040	0.565	0.042	0.037	0.090	0.194	2.18	1.02	0.109
102	-0.32	0.86	0.045	0.444	0.045	0.021	0.084	0.254	2.19	0.96	0.108
103	-0.32	0.87	0.042	0.499	0.050	0.018	0.084	0.252	2.17	0.96	0.109
104	-0.31	0.72	0.026	0.952	0.047	0.014	0.090	0.188	1.98	0.86	0.108
105	-0.31	0.73	0.028	0.900	0.041	0.037	0.090	0.189	2.20	0.95	0.108
106	-0.31	0.74	0.029	0.872	0.038	0.078	0.092	0.170	2.15	0.89	0.108
107	-0.31	0.75	0.033	0.785	0.031	0.227	0.089	0.192	2.17	0.92	0.107
108	-0.31	0.76	0.031	0.834	0.028	0.333	0.092	0.165	2.18	0.90	0.107
109	-0.31	0.77	0.029	0.871	0.025	0.480	0.085	0.246	2.21	0.87	0.107
110	-0.31	0.78	0.035	0.726	0.023	0.541	0.092	0.176	2.12	0.92	0.108
111	-0.31	0.79	0.030	0.872	0.021	0.658	0.087	0.212	2.14	0.90	0.109
112	-0.31	0.80	0.032	0.804	0.024	0.537	0.089	0.203	2.24	0.96	0.108
113	-0.31	0.81	0.033	0.777	0.024	0.480	0.091	0.179	2.16	0.93	0.108
114	-0.31	0.82	0.036	0.677	0.026	0.428	0.089	0.204	2.14	0.94	0.108
115	-0.31	0.83	0.036	0.688	0.029	0.330	0.086	0.233	2.21	1.07	0.108
116	-0.31	0.84	0.034	0.757	0.032	0.210	0.088	0.201	2.20	0.95	0.109
117	-0.31	0.85	0.040	0.573	0.037	0.097	0.087	0.224	2.27	0.96	0.108
118	-0.31	0.86	0.043	0.482	0.042	0.041	0.091	0.184	2.20	1.00	0.108
119	-0.31	0.87	0.041	0.539	0.045	0.023	0.093	0.160	2.16	0.98	0.108
120	-0.31	0.88	0.043	0.479	0.053	0.005	0.087	0.212	2.12	1.06	0.109
121	-0.30	0.73	0.027	0.936	0.043	0.034	0.088	0.208	2.16	0.81	0.107
122	-0.30	0.74	0.029	0.875	0.038	0.076	0.087	0.229	2.11	0.86	0.108
123	-0.30	0.75	0.027	0.897	0.035	0.127	0.087	0.225	2.03	0.89	0.107
124	-0.30	0.76	0.027	0.915	0.032	0.250	0.084	0.260	2.13	0.81	0.107
125	-0.30	0.77	0.028	0.903	0.028	0.355	0.087	0.218	2.18	0.85	0.108
126	-0.30	0.78	0.030	0.860	0.026	0.398	0.090	0.196	2.12	0.91	0.108
127	-0.30	0.79	0.029	0.889	0.023	0.579	0.089	0.201	2.16	0.88	0.108
128	-0.30	0.80	0.032	0.821	0.018	0.813	0.089	0.196	2.10	0.89	0.108
129	-0.30	0.81	0.035	0.724	0.021	0.674	0.093	0.166	2.22	0.88	0.108
130	-0.30	0.82	0.034	0.752	0.021	0.650	0.088	0.207	2.25	0.92	0.107
131	-0.30	0.83	0.038	0.635	0.026	0.407	0.091	0.179	2.13	0.94	0.108
132	-0.30	0.84	0.037	0.657	0.034	0.150	0.086	0.227	2.25	1.01	0.108
133	-0.30	0.85	0.039	0.601	0.035	0.150	0.089	0.202	2.11	0.94	0.108
134	-0.30	0.86	0.040	0.587	0.040	0.055	0.091	0.176	2.19	0.98	0.109
135	-0.30	0.87	0.040	0.592	0.044	0.021	0.089	0.208	2.21	0.90	0.109
136	-0.30	0.88	0.044	0.461	0.049	0.009	0.088	0.206	2.26	1.00	0.108
137	-0.29	0.72	0.029	0.887	0.053	0.006	0.091	0.197	2.05	0.82	0.106
138	-0.29	0.73	0.026	0.951	0.050	0.007	0.089	0.209	2.08	0.87	0.107
139	-0.29	0.74	0.027	0.938	0.043	0.037	0.088	0.203	2.11	0.89	0.107
140	-0.29	0.75	0.029	0.892	0.042	0.038	0.092	0.171	2.03	0.83	0.106
141	-0.29	0.76	0.029	0.872	0.035	0.145	0.089	0.198	2.18	0.95	0.107
142	-0.29	0.77	0.029	0.887	0.030	0.303	0.090	0.184	2.08	0.91	0.107
143	-0.29	0.78	0.029	0.894	0.025	0.483	0.087	0.227	2.10	0.88	0.107
144	-0.29	0.79	0.030	0.853	0.023	0.552	0.090	0.179	2.19	0.91	0.107
145	-0.29	0.80	0.030	0.860	0.021	0.670	0.089	0.205	2.11	0.90	0.107
146	-0.29	0.81	0.035	0.734	0.019	0.797	0.089	0.195	2.26	0.89	0.107
147	-0.29	0.82	0.033	0.780	0.022	0.630	0.087	0.223	2.06	0.91	0.108
148	-0.29	0.83	0.033	0.778	0.027	0.392	0.089	0.203	2.13	0.93	0.108
149	-0.29	0.84	0.034	0.759	0.024	0.504	0.088	0.213	2.10	1.00	0.108
150	-0.29	0.85	0.041	0.534	0.036	0.119	0.092	0.164	2.19	0.93	0.107
151	-0.29	0.86	0.037	0.668	0.036	0.103	0.089	0.207	2.20	0.98	0.108
152	-0.29	0.87	0.041	0.537	0.042	0.044	0.093	0.162	2.22	1.03	0.108
153	-0.29	0.88	0.039	0.602	0.042	0.037	0.089	0.200	2.17	0.94	0.108
154	-0.29	0.89	0.043	0.476	0.049	0.014	0.091	0.183	2.31	0.98	0.108
155	-0.28	0.73	0.027	0.914	0.054	0.005	0.087	0.221	2.15	0.88	0.105
156	-0.28	0.74	0.030	0.860	0.049	0.017	0.086	0.231	2.01	0.84	0.106

No.	$f(P)$		W_{10}		P		α		DP-IP [%]	SP-IP [%]	f_b
	x_0	σ	\mathcal{D}	\mathcal{P}	\mathcal{D}	\mathcal{P}	\mathcal{D}	\mathcal{P}			
157	-0.28	0.75	0.028	0.895	0.044	0.030	0.088	0.205	2.09	0.95	0.107
158	-0.28	0.76	0.028	0.908	0.040	0.061	0.088	0.206	2.09	0.89	0.106
159	-0.28	0.77	0.029	0.883	0.036	0.115	0.087	0.224	2.15	0.87	0.107
160	-0.28	0.78	0.028	0.902	0.032	0.217	0.091	0.179	1.97	0.84	0.107
161	-0.28	0.79	0.031	0.855	0.025	0.462	0.089	0.192	2.03	0.82	0.106
162	-0.28	0.80	0.029	0.897	0.024	0.528	0.084	0.258	2.14	0.97	0.107
163	-0.28	0.81	0.028	0.906	0.023	0.577	0.086	0.231	2.00	0.87	0.107
164	-0.28	0.82	0.030	0.836	0.019	0.757	0.086	0.234	2.10	0.94	0.107
165	-0.28	0.83	0.034	0.752	0.022	0.641	0.087	0.217	2.07	0.89	0.107
166	-0.28	0.84	0.034	0.761	0.024	0.489	0.087	0.211	2.17	0.91	0.108
167	-0.28	0.85	0.036	0.684	0.028	0.350	0.085	0.245	2.31	1.00	0.108
168	-0.28	0.86	0.034	0.747	0.034	0.178	0.086	0.230	2.14	0.95	0.108
169	-0.28	0.87	0.039	0.607	0.039	0.076	0.084	0.253	2.16	1.01	0.108
170	-0.28	0.88	0.036	0.686	0.043	0.033	0.090	0.181	2.13	0.93	0.108
171	-0.28	0.89	0.040	0.573	0.046	0.024	0.088	0.205	2.20	1.01	0.108
172	-0.28	0.90	0.039	0.596	0.050	0.009	0.086	0.224	2.09	0.94	0.109
173	-0.27	0.74	0.028	0.906	0.053	0.005	0.086	0.229	2.14	0.85	0.106
174	-0.27	0.75	0.031	0.840	0.045	0.024	0.089	0.211	2.12	0.86	0.105
175	-0.27	0.76	0.030	0.847	0.046	0.018	0.089	0.208	2.03	0.90	0.106
176	-0.27	0.77	0.029	0.865	0.039	0.060	0.090	0.180	2.09	0.89	0.106
177	-0.27	0.78	0.032	0.815	0.037	0.116	0.089	0.201	2.02	0.92	0.107
178	-0.27	0.79	0.031	0.848	0.034	0.173	0.091	0.176	2.10	0.88	0.107
179	-0.27	0.80	0.032	0.832	0.030	0.292	0.089	0.199	2.15	0.90	0.106
180	-0.27	0.81	0.032	0.818	0.027	0.438	0.094	0.154	2.11	0.84	0.106
181	-0.27	0.82	0.031	0.830	0.023	0.543	0.089	0.191	2.21	0.94	0.107
182	-0.27	0.83	0.032	0.802	0.023	0.572	0.091	0.179	2.16	0.92	0.106
183	-0.27	0.84	0.034	0.752	0.026	0.406	0.088	0.203	2.26	0.97	0.107
184	-0.27	0.85	0.032	0.818	0.024	0.494	0.089	0.201	2.12	0.95	0.107
185	-0.27	0.86	0.035	0.711	0.033	0.206	0.093	0.156	2.11	0.98	0.107
186	-0.27	0.87	0.038	0.650	0.036	0.119	0.094	0.149	2.04	0.93	0.107
187	-0.27	0.88	0.040	0.577	0.040	0.069	0.092	0.170	2.15	0.97	0.108
188	-0.27	0.89	0.039	0.607	0.045	0.023	0.093	0.156	2.14	0.96	0.108
189	-0.27	0.90	0.040	0.582	0.046	0.014	0.089	0.205	2.17	0.99	0.107
190	-0.26	0.75	0.029	0.881	0.052	0.006	0.086	0.224	2.20	0.88	0.105
191	-0.26	0.76	0.031	0.838	0.051	0.008	0.086	0.235	2.05	0.86	0.106
192	-0.26	0.77	0.032	0.801	0.045	0.041	0.080	0.307	2.13	0.89	0.106
193	-0.26	0.78	0.030	0.870	0.038	0.088	0.083	0.268	2.05	0.96	0.106
194	-0.26	0.79	0.029	0.893	0.033	0.207	0.087	0.223	2.03	0.91	0.106
195	-0.26	0.80	0.031	0.835	0.031	0.243	0.090	0.198	2.06	0.91	0.106
196	-0.26	0.81	0.033	0.788	0.030	0.277	0.089	0.197	2.11	0.96	0.107
197	-0.26	0.82	0.032	0.826	0.029	0.317	0.085	0.237	2.13	0.88	0.106
198	-0.26	0.83	0.033	0.783	0.022	0.610	0.088	0.215	2.17	0.87	0.107
199	-0.26	0.84	0.032	0.830	0.027	0.416	0.088	0.222	2.12	0.89	0.106
200	-0.26	0.85	0.032	0.816	0.026	0.430	0.087	0.225	2.10	0.93	0.106
201	-0.26	0.86	0.034	0.742	0.028	0.353	0.088	0.209	2.12	0.92	0.107
202	-0.26	0.87	0.036	0.704	0.033	0.204	0.087	0.225	2.01	1.03	0.107
203	-0.26	0.88	0.031	0.853	0.038	0.091	0.081	0.288	2.06	0.91	0.107
204	-0.26	0.89	0.036	0.709	0.039	0.060	0.085	0.243	2.19	0.99	0.107
205	-0.26	0.90	0.035	0.710	0.046	0.017	0.085	0.242	2.11	0.97	0.108
206	-0.26	0.91	0.039	0.607	0.051	0.006	0.087	0.230	2.29	1.01	0.106
207	-0.25	0.76	0.031	0.840	0.052	0.008	0.088	0.206	2.10	0.86	0.105
208	-0.25	0.77	0.030	0.847	0.049	0.011	0.087	0.215	2.18	0.90	0.106
209	-0.25	0.78	0.031	0.810	0.044	0.041	0.086	0.228	2.11	0.83	0.106
210	-0.25	0.79	0.029	0.876	0.040	0.104	0.087	0.216	2.12	0.88	0.106
211	-0.25	0.80	0.030	0.872	0.036	0.108	0.090	0.182	2.04	0.88	0.106
212	-0.25	0.81	0.032	0.825	0.035	0.149	0.091	0.185	2.13	0.86	0.106
213	-0.25	0.82	0.035	0.714	0.034	0.189	0.086	0.228	2.15	0.87	0.106
214	-0.25	0.83	0.031	0.846	0.030	0.339	0.091	0.183	2.15	0.89	0.105
215	-0.25	0.84	0.032	0.791	0.026	0.451	0.084	0.257	2.05	0.93	0.106
216	-0.25	0.85	0.033	0.794	0.028	0.320	0.083	0.259	2.18	0.90	0.107
217	-0.25	0.86	0.032	0.806	0.030	0.255	0.086	0.234	2.05	0.99	0.106
218	-0.25	0.87	0.035	0.720	0.029	0.299	0.088	0.214	2.03	0.90	0.107
219	-0.25	0.88	0.037	0.675	0.032	0.222	0.086	0.229	2.14	0.91	0.107
220	-0.25	0.89	0.033	0.785	0.039	0.071	0.085	0.244	2.05	0.97	0.107
221	-0.25	0.90	0.035	0.737	0.043	0.043	0.086	0.224	2.08	0.98	0.107

No.	$f(P)$		W_{10}		P		α		DP-IP [%]	SP-IP [%]	f_b
	x_0	σ	\mathcal{D}	\mathcal{P}	\mathcal{D}	\mathcal{P}	\mathcal{D}	\mathcal{P}			
222	-0.25	0.91	0.039	0.604	0.047	0.031	0.087	0.223	2.23	0.94	0.107
223	-0.25	0.92	0.038	0.623	0.051	0.007	0.086	0.239	2.09	0.95	0.107
224	-0.25	0.93	0.042	0.520	0.056	0.006	0.087	0.222	2.09	1.01	0.108
225	-0.24	0.77	0.037	0.658	0.057	0.005	0.090	0.183	2.05	0.80	0.106
226	-0.24	0.78	0.033	0.784	0.052	0.009	0.093	0.164	2.12	0.82	0.105
227	-0.24	0.79	0.032	0.825	0.044	0.036	0.094	0.154	2.13	0.91	0.105
228	-0.24	0.80	0.033	0.772	0.044	0.032	0.090	0.184	2.08	0.87	0.106
229	-0.24	0.81	0.032	0.803	0.038	0.094	0.090	0.188	2.14	0.88	0.106
230	-0.24	0.82	0.030	0.860	0.039	0.074	0.089	0.204	2.16	0.88	0.106
231	-0.24	0.83	0.035	0.735	0.033	0.216	0.088	0.207	2.06	0.84	0.106
232	-0.24	0.84	0.031	0.831	0.031	0.281	0.090	0.184	2.11	0.89	0.107
233	-0.24	0.85	0.034	0.768	0.031	0.233	0.091	0.186	2.03	0.99	0.105
234	-0.24	0.86	0.034	0.750	0.029	0.282	0.088	0.221	2.08	0.90	0.106
235	-0.24	0.87	0.033	0.790	0.029	0.287	0.093	0.159	2.10	0.93	0.106
236	-0.24	0.88	0.035	0.715	0.033	0.196	0.090	0.185	2.21	0.94	0.107
237	-0.24	0.89	0.034	0.761	0.034	0.147	0.091	0.177	2.03	0.98	0.107
238	-0.24	0.90	0.036	0.685	0.037	0.092	0.088	0.215	2.11	0.91	0.106
239	-0.24	0.91	0.038	0.646	0.046	0.019	0.088	0.211	2.19	0.99	0.108
240	-0.24	0.92	0.039	0.592	0.050	0.011	0.091	0.170	2.13	0.95	0.107
241	-0.24	0.93	0.040	0.567	0.052	0.005	0.087	0.214	2.15	0.97	0.107
242	-0.23	0.78	0.034	0.761	0.053	0.007	0.089	0.199	2.11	0.91	0.105
243	-0.23	0.80	0.035	0.732	0.052	0.009	0.091	0.175	2.08	0.92	0.105
244	-0.23	0.81	0.036	0.687	0.045	0.030	0.085	0.233	2.03	0.90	0.105
245	-0.23	0.82	0.031	0.847	0.043	0.034	0.090	0.192	2.07	0.91	0.105
246	-0.23	0.83	0.034	0.762	0.039	0.099	0.091	0.178	2.07	0.89	0.106
247	-0.23	0.84	0.032	0.819	0.034	0.183	0.088	0.218	2.15	0.88	0.105
248	-0.23	0.85	0.031	0.835	0.034	0.139	0.089	0.200	2.07	0.89	0.106
249	-0.23	0.86	0.033	0.786	0.036	0.132	0.090	0.191	2.19	0.94	0.106
250	-0.23	0.87	0.034	0.753	0.030	0.245	0.088	0.212	2.09	0.96	0.105
251	-0.23	0.88	0.032	0.810	0.034	0.135	0.088	0.211	2.19	0.96	0.106
252	-0.23	0.89	0.035	0.729	0.035	0.121	0.088	0.209	2.07	0.91	0.106
253	-0.23	0.90	0.036	0.681	0.039	0.069	0.087	0.217	2.20	0.93	0.106
254	-0.23	0.91	0.035	0.737	0.042	0.039	0.089	0.196	2.15	0.90	0.107
255	-0.23	0.92	0.040	0.587	0.046	0.014	0.089	0.196	2.21	0.99	0.106
256	-0.23	0.93	0.038	0.619	0.051	0.011	0.086	0.238	2.25	0.97	0.106
257	-0.22	0.79	0.035	0.735	0.054	0.010	0.088	0.211	1.98	0.85	0.105
258	-0.22	0.80	0.037	0.668	0.054	0.011	0.088	0.213	2.07	0.90	0.105
259	-0.22	0.81	0.035	0.719	0.047	0.014	0.088	0.209	2.02	0.99	0.105
260	-0.22	0.82	0.036	0.706	0.049	0.008	0.085	0.244	2.07	0.88	0.106
261	-0.22	0.83	0.031	0.826	0.048	0.021	0.086	0.230	2.19	0.90	0.106
262	-0.22	0.84	0.036	0.696	0.044	0.050	0.083	0.265	2.21	0.91	0.105
263	-0.22	0.85	0.034	0.753	0.037	0.142	0.084	0.252	2.15	0.87	0.105
264	-0.22	0.86	0.036	0.701	0.035	0.150	0.089	0.199	2.08	0.97	0.105
265	-0.22	0.87	0.033	0.801	0.035	0.139	0.084	0.255	2.14	0.97	0.105
266	-0.22	0.88	0.034	0.750	0.034	0.178	0.088	0.213	2.10	0.91	0.106
267	-0.22	0.89	0.034	0.739	0.036	0.098	0.083	0.268	2.22	0.98	0.106
268	-0.22	0.90	0.035	0.734	0.041	0.052	0.084	0.247	2.10	0.95	0.106
269	-0.22	0.91	0.036	0.712	0.038	0.084	0.087	0.224	2.16	0.97	0.106
270	-0.22	0.92	0.034	0.759	0.042	0.040	0.085	0.239	2.17	0.95	0.106
271	-0.22	0.93	0.036	0.699	0.047	0.016	0.085	0.243	2.13	0.96	0.106
272	-0.21	0.82	0.038	0.626	0.054	0.006	0.093	0.166	2.02	0.85	0.105
273	-0.21	0.83	0.035	0.731	0.050	0.027	0.090	0.192	2.13	0.81	0.105
274	-0.21	0.84	0.035	0.721	0.051	0.009	0.094	0.149	2.06	0.91	0.104
275	-0.21	0.85	0.034	0.769	0.043	0.077	0.091	0.175	2.10	0.89	0.106
276	-0.21	0.86	0.034	0.759	0.040	0.059	0.088	0.209	2.09	0.91	0.105
277	-0.21	0.87	0.033	0.781	0.040	0.069	0.090	0.188	2.13	0.88	0.106
278	-0.21	0.88	0.035	0.730	0.038	0.069	0.091	0.184	2.03	0.95	0.106
279	-0.21	0.89	0.036	0.697	0.041	0.051	0.087	0.220	2.11	0.95	0.106
280	-0.21	0.90	0.035	0.716	0.038	0.075	0.091	0.185	2.12	0.92	0.106
281	-0.21	0.91	0.036	0.694	0.041	0.043	0.090	0.198	2.04	0.90	0.106
282	-0.21	0.92	0.038	0.633	0.042	0.038	0.092	0.168	2.18	0.98	0.106
283	-0.21	0.93	0.037	0.678	0.045	0.019	0.092	0.167	2.15	1.04	0.107
284	-0.21	0.94	0.036	0.709	0.049	0.010	0.091	0.188	2.07	0.92	0.106
285	-0.21	0.95	0.034	0.759	0.049	0.008	0.086	0.235	2.19	0.98	0.107
286	-0.20	0.83	0.037	0.661	0.053	0.007	0.087	0.226	1.99	0.86	0.105

No.	$f(P)$		W_{10}		P		α		DP-IP [%]	SP-IP [%]	f_b
	x_0	σ	\mathcal{D}	\mathcal{P}	\mathcal{D}	\mathcal{P}	\mathcal{D}	\mathcal{P}			
287	-0.20	0.84	0.037	0.670	0.049	0.030	0.089	0.196	2.15	0.92	0.105
288	-0.20	0.85	0.035	0.729	0.047	0.013	0.083	0.263	2.24	0.91	0.105
289	-0.20	0.86	0.037	0.672	0.046	0.031	0.088	0.211	2.04	0.84	0.105
290	-0.20	0.87	0.036	0.705	0.043	0.033	0.091	0.188	2.09	0.93	0.105
291	-0.20	0.88	0.037	0.665	0.041	0.046	0.086	0.231	2.09	0.93	0.105
292	-0.20	0.89	0.038	0.627	0.039	0.088	0.091	0.185	2.12	1.01	0.105
293	-0.20	0.90	0.034	0.743	0.040	0.069	0.088	0.214	2.21	0.96	0.106
294	-0.20	0.91	0.037	0.670	0.042	0.054	0.092	0.171	2.14	0.88	0.105
295	-0.20	0.92	0.036	0.701	0.042	0.041	0.088	0.205	2.21	0.89	0.105
296	-0.20	0.93	0.038	0.635	0.044	0.028	0.091	0.182	2.05	0.93	0.106
297	-0.20	0.94	0.035	0.719	0.047	0.017	0.089	0.203	2.16	0.94	0.106
298	-0.20	0.95	0.038	0.622	0.049	0.009	0.089	0.201	2.14	0.97	0.106
299	-0.19	0.85	0.037	0.668	0.050	0.008	0.091	0.170	2.10	1.01	0.104
300	-0.19	0.86	0.039	0.618	0.051	0.007	0.087	0.214	2.16	0.86	0.104
301	-0.19	0.87	0.038	0.621	0.049	0.018	0.085	0.238	2.16	0.95	0.105
302	-0.19	0.88	0.037	0.682	0.047	0.016	0.088	0.218	2.19	0.94	0.104
303	-0.19	0.89	0.040	0.591	0.046	0.032	0.083	0.275	2.06	0.96	0.104
304	-0.19	0.90	0.037	0.655	0.043	0.042	0.085	0.247	2.14	0.87	0.105
305	-0.19	0.91	0.037	0.672	0.045	0.029	0.086	0.231	2.06	0.95	0.105
306	-0.19	0.92	0.038	0.641	0.045	0.022	0.089	0.203	2.04	0.93	0.105
307	-0.19	0.93	0.036	0.700	0.044	0.022	0.087	0.221	2.25	0.87	0.105
308	-0.19	0.94	0.036	0.704	0.048	0.011	0.086	0.229	1.92	0.90	0.106
309	-0.19	0.95	0.038	0.620	0.052	0.005	0.085	0.239	2.14	1.02	0.106
310	-0.18	0.87	0.037	0.661	0.050	0.010	0.089	0.192	2.10	0.86	0.105
311	-0.18	0.88	0.037	0.649	0.050	0.013	0.090	0.189	2.14	0.88	0.104
312	-0.18	0.89	0.039	0.599	0.051	0.009	0.090	0.197	2.10	0.90	0.104
313	-0.18	0.90	0.038	0.651	0.047	0.025	0.087	0.214	2.05	0.91	0.105
314	-0.18	0.91	0.040	0.577	0.049	0.011	0.086	0.229	2.11	0.91	0.105
315	-0.18	0.92	0.036	0.712	0.047	0.020	0.091	0.177	2.07	0.96	0.105
316	-0.18	0.93	0.035	0.724	0.046	0.019	0.086	0.233	2.21	0.95	0.105
317	-0.18	0.94	0.036	0.696	0.049	0.008	0.088	0.207	2.03	0.96	0.106
318	-0.18	0.95	0.040	0.585	0.051	0.008	0.087	0.224	2.13	0.93	0.105
319	-0.18	0.96	0.036	0.701	0.052	0.007	0.089	0.199	1.98	0.91	0.106
320	-0.17	0.88	0.040	0.571	0.051	0.006	0.089	0.198	2.20	0.90	0.104
321	-0.17	0.90	0.040	0.590	0.052	0.007	0.087	0.225	2.14	0.93	0.105
322	-0.17	0.91	0.037	0.678	0.048	0.013	0.088	0.210	2.00	0.89	0.104
323	-0.17	0.92	0.038	0.619	0.050	0.006	0.090	0.190	2.13	0.97	0.105
324	-0.17	0.93	0.040	0.562	0.052	0.006	0.086	0.229	2.14	0.92	0.104
325	-0.17	0.94	0.039	0.588	0.049	0.009	0.087	0.218	2.12	0.95	0.105
326	-0.17	0.95	0.041	0.538	0.049	0.010	0.088	0.204	2.13	0.89	0.105

Table B3: Simulation results of the pulsar beam for opening angle distribution Eq. (14), inclination angle distribution function Eq. (6) and period distribution function Eq. (11). Graphical representation of this class of solutions is represented in Fig. C3.

No.	$f(P)$		W_{10}		P		α		DP-IP [%]	SP-IP [%]	f_b
	x_0	σ	\mathcal{D}	\mathcal{P}	\mathcal{D}	\mathcal{P}	\mathcal{D}	\mathcal{P}			
1	-0.29	0.75	0.087	0.008	0.051	0.005	0.086	0.235	2.22	1.04	0.112
2	-0.28	0.72	0.078	0.020	0.049	0.010	0.081	0.287	2.29	1.06	0.111
3	-0.28	0.73	0.076	0.027	0.049	0.009	0.079	0.313	2.38	1.03	0.111
4	-0.28	0.74	0.076	0.027	0.049	0.011	0.078	0.338	2.25	0.99	0.111
5	-0.28	0.78	0.089	0.005	0.048	0.014	0.084	0.253	2.21	1.06	0.113
6	-0.27	0.69	0.062	0.112	0.050	0.007	0.072	0.427	2.36	1.05	0.109
7	-0.27	0.70	0.065	0.094	0.049	0.009	0.075	0.381	2.36	0.97	0.110
8	-0.27	0.71	0.070	0.049	0.049	0.010	0.075	0.382	2.27	1.05	0.111
9	-0.27	0.72	0.072	0.040	0.049	0.012	0.076	0.363	2.33	0.96	0.111
10	-0.27	0.73	0.077	0.029	0.047	0.015	0.079	0.327	2.27	1.04	0.110
11	-0.27	0.74	0.075	0.037	0.047	0.015	0.072	0.429	2.33	1.07	0.111
12	-0.27	0.75	0.079	0.018	0.046	0.023	0.076	0.374	2.34	1.06	0.110
13	-0.27	0.76	0.080	0.019	0.042	0.044	0.075	0.386	2.31	1.07	0.111
14	-0.27	0.77	0.083	0.014	0.045	0.024	0.075	0.385	2.38	1.07	0.112
15	-0.26	0.69	0.063	0.108	0.052	0.007	0.082	0.285	2.18	1.00	0.109
16	-0.26	0.70	0.062	0.110	0.049	0.010	0.079	0.323	2.21	1.03	0.110

No.	$f(P)$		W_{10}		P		α		DP-IP [%]	SP-IP [%]	f_b
	x_0	σ	\mathcal{D}	\mathcal{P}	\mathcal{D}	\mathcal{P}	\mathcal{D}	\mathcal{P}			
17	-0.26	0.71	0.065	0.080	0.044	0.023	0.076	0.359	2.28	1.06	0.111
18	-0.26	0.72	0.069	0.060	0.044	0.034	0.074	0.399	2.35	1.05	0.111
19	-0.26	0.73	0.075	0.029	0.041	0.047	0.083	0.267	2.29	1.01	0.111
20	-0.26	0.74	0.069	0.055	0.039	0.082	0.079	0.321	2.19	1.04	0.110
21	-0.26	0.76	0.076	0.033	0.040	0.051	0.078	0.331	2.26	1.07	0.111
22	-0.26	0.77	0.080	0.015	0.042	0.038	0.075	0.373	2.39	1.06	0.111
23	-0.26	0.79	0.087	0.010	0.040	0.061	0.080	0.308	2.32	1.08	0.111
24	-0.25	0.70	0.061	0.127	0.050	0.009	0.081	0.296	2.26	1.00	0.109
25	-0.25	0.71	0.062	0.106	0.044	0.022	0.075	0.388	2.27	1.00	0.110
26	-0.25	0.72	0.066	0.079	0.041	0.047	0.081	0.300	2.31	1.05	0.110
27	-0.25	0.73	0.067	0.065	0.041	0.039	0.079	0.314	2.23	0.97	0.110
28	-0.25	0.74	0.071	0.053	0.041	0.052	0.080	0.305	2.32	0.96	0.110
29	-0.25	0.75	0.073	0.039	0.038	0.077	0.079	0.313	2.27	1.02	0.110
30	-0.25	0.76	0.077	0.024	0.038	0.085	0.080	0.298	2.31	1.05	0.110
31	-0.25	0.77	0.080	0.017	0.038	0.085	0.080	0.305	2.38	1.09	0.111
32	-0.25	0.78	0.081	0.016	0.036	0.144	0.079	0.316	2.36	1.06	0.111
33	-0.25	0.79	0.082	0.012	0.038	0.093	0.079	0.313	2.35	1.08	0.111
34	-0.24	0.70	0.058	0.176	0.051	0.005	0.079	0.332	2.25	0.94	0.109
35	-0.24	0.71	0.056	0.192	0.047	0.015	0.077	0.350	2.08	0.99	0.109
36	-0.24	0.72	0.063	0.102	0.042	0.036	0.081	0.288	2.27	0.93	0.109
37	-0.24	0.73	0.066	0.094	0.038	0.086	0.081	0.291	2.19	1.03	0.110
38	-0.24	0.74	0.067	0.074	0.038	0.075	0.083	0.271	2.25	1.05	0.110
39	-0.24	0.75	0.069	0.062	0.032	0.198	0.082	0.273	2.22	1.08	0.110
40	-0.24	0.76	0.076	0.025	0.036	0.100	0.084	0.249	2.30	1.04	0.110
41	-0.24	0.77	0.072	0.042	0.032	0.213	0.081	0.287	2.27	1.01	0.110
42	-0.24	0.78	0.078	0.026	0.031	0.234	0.083	0.272	2.34	1.06	0.110
43	-0.24	0.80	0.082	0.013	0.034	0.154	0.082	0.280	2.26	1.09	0.111
44	-0.23	0.71	0.056	0.198	0.050	0.010	0.082	0.275	2.23	1.01	0.108
45	-0.23	0.72	0.060	0.138	0.047	0.019	0.082	0.284	2.29	0.98	0.109
46	-0.23	0.73	0.063	0.110	0.039	0.055	0.081	0.292	2.27	1.00	0.109
47	-0.23	0.74	0.065	0.098	0.033	0.170	0.079	0.323	2.29	0.98	0.110
48	-0.23	0.75	0.070	0.054	0.032	0.191	0.085	0.248	2.32	1.08	0.110
49	-0.22	0.72	0.057	0.171	0.049	0.014	0.080	0.308	2.28	0.97	0.108
50	-0.22	0.73	0.061	0.122	0.042	0.035	0.084	0.254	2.38	1.05	0.107
51	-0.22	0.74	0.064	0.105	0.041	0.051	0.082	0.286	2.34	1.08	0.108
52	-0.22	0.75	0.066	0.075	0.032	0.209	0.084	0.255	2.30	1.06	0.109
53	-0.22	0.76	0.072	0.048	0.029	0.261	0.083	0.274	2.35	1.04	0.109
54	-0.22	0.78	0.069	0.062	0.027	0.387	0.080	0.302	2.25	1.08	0.110
55	-0.21	0.73	0.056	0.189	0.049	0.011	0.082	0.286	2.21	1.03	0.108
56	-0.21	0.74	0.059	0.150	0.042	0.048	0.080	0.301	2.15	1.06	0.108
57	-0.21	0.75	0.064	0.100	0.035	0.154	0.082	0.283	2.28	1.02	0.108
58	-0.21	0.76	0.065	0.085	0.033	0.189	0.082	0.282	2.22	0.98	0.109
59	-0.21	0.77	0.067	0.076	0.026	0.386	0.081	0.293	2.26	1.04	0.108
60	-0.21	0.78	0.069	0.051	0.024	0.503	0.080	0.301	2.24	1.07	0.109
61	-0.21	0.79	0.071	0.046	0.022	0.621	0.082	0.281	2.27	1.06	0.109
62	-0.21	0.80	0.074	0.032	0.023	0.546	0.081	0.295	2.28	1.08	0.109
63	-0.21	0.83	0.084	0.012	0.032	0.212	0.083	0.264	2.38	1.06	0.110
64	-0.20	0.73	0.058	0.166	0.051	0.005	0.081	0.294	2.19	0.94	0.107
65	-0.20	0.74	0.055	0.209	0.047	0.022	0.075	0.379	2.24	0.97	0.107
66	-0.20	0.75	0.061	0.117	0.041	0.051	0.075	0.379	2.12	1.07	0.108
67	-0.20	0.76	0.063	0.110	0.032	0.199	0.076	0.371	2.20	1.06	0.108
68	-0.20	0.77	0.068	0.068	0.028	0.324	0.076	0.365	2.18	1.05	0.108
69	-0.20	0.79	0.072	0.038	0.020	0.732	0.077	0.347	2.29	1.04	0.109
70	-0.20	0.80	0.072	0.040	0.022	0.601	0.078	0.342	2.35	1.09	0.109
71	-0.20	0.81	0.076	0.025	0.023	0.544	0.076	0.366	2.35	1.07	0.109
72	-0.20	0.82	0.080	0.017	0.025	0.489	0.083	0.271	2.35	1.06	0.109
73	-0.19	0.74	0.056	0.185	0.049	0.015	0.080	0.328	2.22	1.06	0.107
74	-0.19	0.75	0.059	0.158	0.041	0.051	0.080	0.302	2.22	0.98	0.108
75	-0.19	0.76	0.063	0.104	0.035	0.122	0.085	0.235	2.32	1.03	0.107
76	-0.19	0.77	0.062	0.125	0.032	0.254	0.081	0.295	2.30	1.02	0.107
77	-0.19	0.79	0.071	0.050	0.020	0.702	0.080	0.318	2.36	1.09	0.108
78	-0.19	0.80	0.074	0.029	0.018	0.827	0.084	0.255	2.34	1.09	0.108
79	-0.19	0.82	0.078	0.023	0.025	0.461	0.082	0.288	2.38	1.09	0.109
80	-0.19	0.83	0.080	0.019	0.028	0.330	0.076	0.363	2.37	1.09	0.109
81	-0.18	0.75	0.052	0.261	0.050	0.006	0.079	0.324	2.21	0.98	0.106

No.	$f(P)$		W_{10}		P		α		DP-IP [%]	SP-IP [%]	f_b
	x_0	σ	\mathcal{D}	\mathcal{P}	\mathcal{D}	\mathcal{P}	\mathcal{D}	\mathcal{P}			
82	-0.18	0.76	0.056	0.178	0.045	0.028	0.080	0.304	2.27	0.96	0.106
83	-0.18	0.77	0.062	0.118	0.034	0.151	0.080	0.305	2.32	0.98	0.107
84	-0.18	0.78	0.064	0.094	0.031	0.248	0.083	0.266	2.37	1.05	0.106
85	-0.18	0.79	0.068	0.060	0.027	0.378	0.082	0.290	2.27	1.01	0.107
86	-0.18	0.80	0.068	0.059	0.020	0.704	0.084	0.252	2.27	1.00	0.107
87	-0.18	0.81	0.070	0.055	0.019	0.757	0.083	0.271	2.35	1.06	0.107
88	-0.17	0.75	0.056	0.196	0.052	0.007	0.084	0.252	2.14	0.90	0.106
89	-0.17	0.76	0.057	0.172	0.047	0.023	0.083	0.274	2.36	0.97	0.106
90	-0.17	0.77	0.058	0.163	0.041	0.054	0.079	0.317	2.28	0.97	0.105
91	-0.17	0.78	0.061	0.132	0.034	0.182	0.081	0.298	2.16	0.99	0.106
92	-0.17	0.79	0.061	0.133	0.034	0.184	0.082	0.286	2.19	1.02	0.107
93	-0.17	0.80	0.062	0.104	0.026	0.455	0.080	0.306	2.21	1.03	0.106
94	-0.17	0.81	0.065	0.097	0.025	0.517	0.080	0.313	2.23	1.01	0.107
95	-0.17	0.83	0.077	0.025	0.023	0.555	0.083	0.268	2.29	1.05	0.108
96	-0.17	0.84	0.074	0.036	0.027	0.408	0.083	0.276	2.34	1.07	0.108
97	-0.17	0.85	0.080	0.018	0.034	0.166	0.081	0.289	2.39	1.08	0.108
98	-0.16	0.76	0.053	0.230	0.052	0.005	0.080	0.300	2.23	1.00	0.106
99	-0.16	0.77	0.057	0.175	0.047	0.031	0.082	0.283	2.25	0.96	0.106
100	-0.16	0.78	0.059	0.155	0.040	0.068	0.079	0.316	2.30	1.03	0.105
101	-0.16	0.79	0.060	0.128	0.034	0.173	0.081	0.292	2.23	0.97	0.107
102	-0.16	0.80	0.067	0.064	0.031	0.218	0.084	0.247	2.22	1.08	0.106
103	-0.16	0.81	0.067	0.080	0.025	0.468	0.082	0.289	2.21	1.07	0.107
104	-0.16	0.82	0.070	0.061	0.023	0.553	0.081	0.292	2.26	1.04	0.107
105	-0.16	0.83	0.072	0.047	0.021	0.674	0.083	0.271	2.31	1.09	0.107
106	-0.16	0.89	0.087	0.008	0.053	0.005	0.083	0.275	2.35	1.06	0.109
107	-0.15	0.77	0.053	0.231	0.053	0.006	0.083	0.273	2.23	0.94	0.105
108	-0.15	0.78	0.059	0.141	0.045	0.025	0.089	0.194	2.39	0.98	0.106
109	-0.15	0.79	0.059	0.145	0.041	0.073	0.088	0.215	2.24	0.94	0.106
110	-0.15	0.80	0.064	0.096	0.033	0.187	0.089	0.200	2.15	1.01	0.107
111	-0.15	0.81	0.066	0.078	0.031	0.225	0.083	0.268	2.38	1.07	0.107
112	-0.15	0.82	0.063	0.112	0.030	0.306	0.082	0.283	2.23	1.07	0.107
113	-0.15	0.83	0.069	0.072	0.023	0.598	0.083	0.269	2.32	1.04	0.106
114	-0.14	0.77	0.052	0.255	0.053	0.009	0.081	0.286	2.25	0.98	0.105
115	-0.14	0.78	0.054	0.232	0.052	0.010	0.079	0.322	2.20	0.97	0.105
116	-0.14	0.79	0.060	0.146	0.044	0.027	0.081	0.303	2.25	1.00	0.106
117	-0.14	0.80	0.057	0.169	0.039	0.066	0.077	0.349	2.27	0.97	0.106
118	-0.14	0.81	0.062	0.114	0.036	0.185	0.080	0.313	2.29	1.04	0.106
119	-0.14	0.82	0.067	0.078	0.032	0.249	0.083	0.270	2.22	0.96	0.106
120	-0.14	0.86	0.077	0.028	0.029	0.315	0.080	0.318	2.33	1.09	0.107
121	-0.13	0.79	0.060	0.137	0.051	0.005	0.083	0.267	2.26	1.06	0.104
122	-0.13	0.80	0.057	0.165	0.041	0.067	0.078	0.337	2.25	1.04	0.105
123	-0.13	0.81	0.061	0.139	0.041	0.064	0.082	0.279	2.19	1.06	0.105
124	-0.13	0.83	0.067	0.080	0.028	0.346	0.088	0.209	2.26	1.09	0.106
125	-0.13	0.84	0.065	0.079	0.029	0.350	0.079	0.324	2.28	1.07	0.106
126	-0.12	0.81	0.060	0.135	0.046	0.031	0.081	0.290	2.35	0.99	0.104
127	-0.12	0.82	0.059	0.147	0.040	0.070	0.083	0.266	2.29	0.97	0.104
128	-0.12	0.83	0.065	0.085	0.036	0.141	0.083	0.263	2.26	0.97	0.105
129	-0.12	0.85	0.073	0.039	0.030	0.309	0.083	0.260	2.41	1.06	0.106
130	-0.12	0.86	0.069	0.058	0.031	0.237	0.081	0.289	2.31	1.06	0.106
131	-0.12	0.87	0.072	0.045	0.028	0.308	0.079	0.329	2.26	1.08	0.106
132	-0.11	0.81	0.056	0.181	0.052	0.007	0.079	0.338	2.20	0.95	0.104
133	-0.11	0.82	0.060	0.142	0.047	0.019	0.082	0.281	2.27	1.02	0.104
134	-0.11	0.83	0.060	0.141	0.044	0.038	0.079	0.322	2.16	0.99	0.105
135	-0.11	0.84	0.061	0.128	0.038	0.090	0.077	0.358	2.23	1.04	0.105
136	-0.11	0.85	0.067	0.076	0.036	0.131	0.078	0.335	2.32	1.03	0.105
137	-0.11	0.86	0.070	0.053	0.030	0.261	0.085	0.239	2.25	1.06	0.105
138	-0.10	0.83	0.060	0.139	0.047	0.022	0.087	0.219	2.25	1.01	0.105
139	-0.10	0.84	0.059	0.152	0.044	0.038	0.083	0.270	2.26	0.99	0.104
140	-0.10	0.85	0.062	0.115	0.041	0.069	0.084	0.255	2.33	1.01	0.104
141	-0.10	0.86	0.065	0.084	0.036	0.114	0.081	0.294	2.22	1.03	0.106
142	-0.09	0.82	0.059	0.150	0.056	0.017	0.081	0.294	2.26	0.98	0.103
143	-0.09	0.83	0.056	0.184	0.049	0.010	0.077	0.348	2.21	1.01	0.104
144	-0.09	0.84	0.060	0.131	0.049	0.010	0.078	0.345	2.34	1.01	0.104
145	-0.09	0.85	0.063	0.111	0.047	0.034	0.080	0.325	2.31	1.05	0.103
146	-0.09	0.86	0.064	0.089	0.045	0.028	0.079	0.311	2.24	1.01	0.104

No.	$f(P)$		W_{10}		P		α		DP-IP [%]	SP-IP [%]	f_b
	x_0	σ	\mathcal{D}	\mathcal{P}	\mathcal{D}	\mathcal{P}	\mathcal{D}	\mathcal{P}			
147	-0.09	0.87	0.067	0.077	0.037	0.120	0.078	0.341	2.37	1.03	0.104
148	-0.09	0.88	0.068	0.063	0.039	0.065	0.078	0.336	2.21	1.08	0.105
149	-0.09	0.89	0.074	0.033	0.035	0.121	0.081	0.296	2.29	1.08	0.105
150	-0.08	0.84	0.060	0.152	0.054	0.007	0.079	0.324	2.33	1.03	0.103
151	-0.08	0.85	0.061	0.125	0.051	0.010	0.078	0.326	2.33	1.06	0.104
152	-0.08	0.87	0.067	0.069	0.038	0.082	0.080	0.302	2.30	1.05	0.104
153	-0.08	0.91	0.077	0.025	0.040	0.047	0.079	0.327	2.33	1.06	0.105
154	-0.07	0.85	0.058	0.165	0.054	0.010	0.083	0.270	2.15	1.00	0.102
155	-0.07	0.87	0.064	0.095	0.045	0.030	0.086	0.231	2.29	1.06	0.104
156	-0.07	0.88	0.065	0.086	0.042	0.041	0.086	0.226	2.28	1.03	0.104
157	-0.07	0.89	0.067	0.082	0.039	0.073	0.082	0.288	2.27	1.02	0.104
158	-0.07	0.93	0.082	0.013	0.045	0.020	0.083	0.269	2.40	1.07	0.105
159	-0.06	0.86	0.060	0.131	0.052	0.005	0.085	0.240	2.21	1.07	0.103
160	-0.06	0.87	0.063	0.106	0.050	0.015	0.084	0.250	2.27	0.99	0.104
161	-0.06	0.88	0.066	0.079	0.047	0.016	0.085	0.247	2.29	0.99	0.103
162	-0.06	0.89	0.067	0.071	0.045	0.020	0.083	0.284	2.24	1.02	0.104
163	-0.06	0.90	0.073	0.038	0.043	0.043	0.090	0.195	2.20	1.07	0.103
164	-0.06	0.91	0.070	0.052	0.043	0.036	0.081	0.302	2.19	1.07	0.104
165	-0.05	0.91	0.069	0.058	0.047	0.014	0.082	0.281	2.38	1.05	0.104
166	-0.05	0.92	0.076	0.026	0.043	0.043	0.084	0.248	2.29	1.09	0.104
167	-0.04	0.90	0.066	0.081	0.052	0.010	0.083	0.275	2.23	1.08	0.102
168	-0.03	0.93	0.072	0.041	0.051	0.016	0.088	0.211	2.34	1.06	0.103
169	-0.03	0.94	0.071	0.047	0.050	0.009	0.083	0.273	2.28	1.09	0.104
170	-0.02	0.91	0.070	0.056	0.052	0.008	0.081	0.299	2.28	1.02	0.102

Table B4: Simulation results of the pulsar beam for opening angle distribution Eq. (15b), inclination angle distribution function Eq. (6) and period distribution function Eq. (11). Graphical representation of this class of solutions is represented in Fig. C4.

No.	$f(P)$		W_{10}		P		α		DP-IP [%]	SP-IP [%]	f_b
	x_0	σ	\mathcal{D}	\mathcal{P}	\mathcal{D}	\mathcal{P}	\mathcal{D}	\mathcal{P}			
1	-0.38	0.78	0.063	0.104	0.052	0.005	0.080	0.302	2.27	1.02	0.113
2	-0.37	0.75	0.057	0.194	0.051	0.006	0.083	0.267	2.23	1.03	0.112
3	-0.37	0.76	0.062	0.109	0.051	0.006	0.085	0.242	2.25	1.06	0.112
4	-0.37	0.77	0.062	0.114	0.051	0.009	0.082	0.285	2.22	1.08	0.112
5	-0.37	0.78	0.065	0.088	0.051	0.005	0.083	0.266	2.19	1.01	0.113
6	-0.36	0.74	0.058	0.167	0.049	0.013	0.085	0.247	2.30	1.00	0.112
7	-0.36	0.75	0.058	0.166	0.051	0.005	0.083	0.263	2.18	1.03	0.112
8	-0.36	0.76	0.058	0.168	0.047	0.014	0.083	0.264	2.30	1.00	0.113
9	-0.36	0.77	0.058	0.173	0.049	0.016	0.078	0.334	2.29	1.04	0.113
10	-0.35	0.71	0.045	0.425	0.050	0.007	0.082	0.280	2.26	1.03	0.111
11	-0.35	0.72	0.047	0.382	0.051	0.009	0.083	0.273	2.29	0.96	0.111
12	-0.35	0.73	0.053	0.250	0.049	0.008	0.081	0.295	2.26	1.00	0.111
13	-0.35	0.74	0.055	0.220	0.047	0.015	0.086	0.231	2.29	0.98	0.112
14	-0.35	0.75	0.053	0.234	0.048	0.011	0.081	0.293	2.29	0.96	0.111
15	-0.35	0.76	0.055	0.214	0.045	0.021	0.083	0.261	2.20	0.97	0.112
16	-0.35	0.77	0.060	0.132	0.046	0.013	0.082	0.282	2.24	1.05	0.113
17	-0.35	0.80	0.063	0.105	0.046	0.018	0.085	0.240	2.17	1.01	0.112
18	-0.35	0.81	0.065	0.092	0.051	0.011	0.084	0.254	2.33	1.05	0.112
19	-0.34	0.70	0.043	0.482	0.050	0.009	0.082	0.279	2.24	1.01	0.110
20	-0.34	0.71	0.043	0.491	0.046	0.017	0.080	0.318	2.23	0.93	0.111
21	-0.34	0.72	0.043	0.474	0.045	0.021	0.081	0.292	2.20	0.97	0.111
22	-0.34	0.73	0.052	0.269	0.045	0.020	0.089	0.198	2.23	1.07	0.111
23	-0.34	0.74	0.052	0.269	0.046	0.019	0.086	0.231	2.22	1.03	0.111
24	-0.34	0.75	0.050	0.297	0.044	0.032	0.082	0.280	2.19	0.92	0.112
25	-0.34	0.76	0.054	0.215	0.041	0.064	0.086	0.234	2.13	1.07	0.112
26	-0.34	0.77	0.058	0.165	0.039	0.063	0.084	0.260	2.27	1.00	0.112
27	-0.34	0.78	0.062	0.113	0.040	0.052	0.086	0.222	2.24	1.04	0.111
28	-0.34	0.79	0.064	0.096	0.039	0.062	0.087	0.212	2.23	1.04	0.113
29	-0.34	0.81	0.061	0.120	0.048	0.010	0.085	0.236	2.17	1.01	0.112
30	-0.33	0.70	0.042	0.499	0.048	0.010	0.083	0.264	2.10	0.96	0.110
31	-0.33	0.71	0.047	0.376	0.047	0.012	0.085	0.235	2.04	0.99	0.111
32	-0.33	0.72	0.047	0.383	0.043	0.034	0.081	0.294	2.17	0.92	0.111

No.	$f(P)$		W_{10}		P		α		DP-IP [%]	SP-IP [%]	f_b
	x_0	σ	\mathcal{D}	\mathcal{P}	\mathcal{D}	\mathcal{P}	\mathcal{D}	\mathcal{P}			
33	-0.33	0.73	0.044	0.460	0.041	0.052	0.082	0.276	2.11	0.95	0.111
34	-0.33	0.74	0.051	0.271	0.042	0.034	0.080	0.302	2.20	0.98	0.111
35	-0.33	0.75	0.052	0.281	0.043	0.031	0.082	0.286	2.22	1.02	0.111
36	-0.33	0.76	0.052	0.271	0.037	0.100	0.079	0.320	2.23	0.98	0.111
37	-0.33	0.77	0.049	0.345	0.037	0.115	0.079	0.320	2.18	1.08	0.111
38	-0.33	0.78	0.053	0.257	0.037	0.087	0.082	0.283	2.21	1.06	0.111
39	-0.33	0.79	0.060	0.138	0.036	0.100	0.085	0.243	2.20	1.04	0.112
40	-0.33	0.80	0.059	0.143	0.042	0.038	0.081	0.287	2.21	1.02	0.112
41	-0.33	0.81	0.057	0.171	0.041	0.053	0.079	0.317	2.18	1.08	0.112
42	-0.33	0.82	0.064	0.089	0.047	0.016	0.085	0.245	2.26	1.01	0.112
43	-0.32	0.69	0.040	0.573	0.051	0.005	0.083	0.273	2.24	0.93	0.110
44	-0.32	0.70	0.041	0.532	0.048	0.010	0.082	0.278	2.13	0.90	0.110
45	-0.32	0.71	0.041	0.530	0.042	0.039	0.083	0.258	2.17	0.94	0.110
46	-0.32	0.72	0.041	0.539	0.039	0.056	0.086	0.236	2.11	0.91	0.109
47	-0.32	0.73	0.044	0.456	0.038	0.071	0.081	0.297	2.17	1.08	0.110
48	-0.32	0.74	0.048	0.349	0.042	0.058	0.086	0.236	2.15	1.07	0.110
49	-0.32	0.75	0.047	0.371	0.037	0.089	0.082	0.281	2.27	0.91	0.110
50	-0.32	0.76	0.049	0.315	0.034	0.135	0.083	0.262	2.28	0.96	0.111
51	-0.32	0.77	0.057	0.183	0.036	0.105	0.085	0.247	2.22	1.02	0.111
52	-0.32	0.78	0.056	0.222	0.034	0.164	0.088	0.212	2.17	1.07	0.111
53	-0.32	0.80	0.061	0.125	0.038	0.083	0.084	0.263	2.32	1.07	0.112
54	-0.32	0.83	0.064	0.092	0.049	0.014	0.081	0.294	2.23	1.07	0.113
55	-0.31	0.69	0.037	0.659	0.054	0.006	0.080	0.320	2.17	0.86	0.109
56	-0.31	0.70	0.039	0.609	0.049	0.009	0.079	0.322	2.28	0.91	0.109
57	-0.31	0.71	0.040	0.570	0.044	0.025	0.081	0.298	2.16	0.88	0.109
58	-0.31	0.72	0.039	0.599	0.041	0.043	0.082	0.282	2.07	0.95	0.110
59	-0.31	0.73	0.045	0.436	0.036	0.094	0.083	0.271	2.27	1.02	0.110
60	-0.31	0.74	0.049	0.350	0.041	0.049	0.085	0.245	2.23	0.99	0.110
61	-0.31	0.75	0.050	0.307	0.034	0.150	0.081	0.289	2.31	1.00	0.110
62	-0.31	0.76	0.049	0.328	0.032	0.190	0.084	0.247	2.30	0.97	0.110
63	-0.31	0.77	0.047	0.373	0.029	0.285	0.076	0.362	2.28	1.01	0.110
64	-0.31	0.78	0.056	0.192	0.031	0.219	0.083	0.262	2.20	1.05	0.110
65	-0.31	0.79	0.051	0.288	0.029	0.271	0.079	0.314	2.25	1.01	0.112
66	-0.31	0.81	0.057	0.173	0.038	0.085	0.084	0.243	2.23	1.09	0.111
67	-0.31	0.82	0.061	0.128	0.043	0.042	0.082	0.278	2.23	1.09	0.111
68	-0.30	0.70	0.039	0.603	0.052	0.007	0.084	0.257	2.20	0.89	0.109
69	-0.30	0.71	0.037	0.647	0.049	0.012	0.082	0.280	2.13	0.90	0.110
70	-0.30	0.72	0.037	0.677	0.043	0.032	0.082	0.272	2.14	0.87	0.110
71	-0.30	0.73	0.042	0.515	0.037	0.094	0.082	0.274	2.23	0.91	0.110
72	-0.30	0.74	0.044	0.448	0.037	0.093	0.081	0.298	2.18	0.93	0.110
73	-0.30	0.75	0.042	0.528	0.034	0.154	0.080	0.307	2.11	0.99	0.110
74	-0.30	0.76	0.041	0.553	0.034	0.143	0.079	0.325	2.24	0.89	0.110
75	-0.30	0.77	0.044	0.451	0.031	0.216	0.080	0.299	2.24	0.98	0.111
76	-0.30	0.78	0.050	0.319	0.032	0.196	0.085	0.243	2.22	1.03	0.110
77	-0.30	0.79	0.049	0.314	0.030	0.257	0.082	0.284	2.22	0.99	0.110
78	-0.30	0.80	0.055	0.206	0.030	0.242	0.083	0.267	2.24	1.00	0.111
79	-0.30	0.81	0.056	0.189	0.035	0.141	0.088	0.211	2.34	1.02	0.111
80	-0.30	0.82	0.059	0.143	0.037	0.092	0.083	0.257	2.33	1.06	0.111
81	-0.30	0.83	0.063	0.119	0.044	0.032	0.086	0.231	2.26	1.08	0.111
82	-0.29	0.71	0.036	0.704	0.051	0.006	0.083	0.262	2.22	0.94	0.109
83	-0.29	0.72	0.040	0.571	0.048	0.019	0.086	0.254	2.12	0.91	0.108
84	-0.29	0.73	0.035	0.736	0.042	0.041	0.081	0.299	2.15	0.98	0.109
85	-0.29	0.74	0.042	0.519	0.038	0.087	0.081	0.291	2.23	0.97	0.110
86	-0.29	0.75	0.042	0.508	0.039	0.078	0.085	0.244	2.06	0.94	0.109
87	-0.29	0.76	0.047	0.374	0.033	0.169	0.080	0.303	2.29	1.05	0.110
88	-0.29	0.77	0.047	0.379	0.031	0.216	0.082	0.273	2.17	1.03	0.109
89	-0.29	0.78	0.048	0.345	0.027	0.378	0.079	0.329	2.20	1.02	0.109
90	-0.29	0.79	0.051	0.276	0.029	0.280	0.082	0.276	2.30	1.06	0.110
91	-0.29	0.80	0.052	0.267	0.030	0.253	0.082	0.296	2.17	1.04	0.110
92	-0.29	0.81	0.057	0.172	0.031	0.239	0.081	0.295	2.34	1.05	0.110
93	-0.29	0.82	0.056	0.196	0.037	0.094	0.080	0.304	2.16	1.03	0.111
94	-0.29	0.83	0.058	0.161	0.045	0.031	0.083	0.268	2.25	1.07	0.112
95	-0.28	0.72	0.038	0.626	0.050	0.009	0.086	0.226	2.16	0.93	0.109
96	-0.28	0.73	0.037	0.655	0.046	0.030	0.083	0.267	2.22	0.95	0.108
97	-0.28	0.74	0.037	0.673	0.046	0.030	0.083	0.273	2.08	0.92	0.109

No.	$f(P)$		W_{10}		P		α		DP-IP [%]	SP-IP [%]	f_b
	x_0	σ	\mathcal{D}	\mathcal{P}	\mathcal{D}	\mathcal{P}	\mathcal{D}	\mathcal{P}			
98	-0.28	0.75	0.042	0.506	0.040	0.067	0.084	0.250	2.20	1.04	0.109
99	-0.28	0.76	0.044	0.448	0.038	0.088	0.087	0.223	2.13	0.97	0.109
100	-0.28	0.77	0.042	0.502	0.037	0.095	0.085	0.250	2.25	0.99	0.110
101	-0.28	0.78	0.046	0.405	0.031	0.254	0.090	0.188	2.03	0.93	0.110
102	-0.28	0.79	0.049	0.326	0.030	0.253	0.087	0.213	2.08	0.93	0.109
103	-0.28	0.80	0.049	0.330	0.030	0.270	0.084	0.261	2.23	1.06	0.110
104	-0.28	0.81	0.046	0.393	0.027	0.362	0.084	0.257	2.10	1.01	0.110
105	-0.28	0.82	0.052	0.275	0.030	0.235	0.084	0.246	2.23	1.06	0.110
106	-0.28	0.83	0.057	0.166	0.035	0.142	0.085	0.236	2.18	1.01	0.110
107	-0.28	0.84	0.056	0.196	0.041	0.048	0.087	0.216	2.30	1.03	0.111
108	-0.27	0.74	0.036	0.692	0.050	0.020	0.079	0.324	2.21	0.97	0.108
109	-0.27	0.75	0.038	0.627	0.047	0.028	0.082	0.284	2.24	0.93	0.108
110	-0.27	0.76	0.039	0.607	0.047	0.020	0.081	0.299	2.12	0.98	0.108
111	-0.27	0.77	0.042	0.507	0.040	0.070	0.082	0.283	2.21	0.98	0.109
112	-0.27	0.78	0.042	0.534	0.039	0.124	0.080	0.304	2.10	1.04	0.109
113	-0.27	0.79	0.046	0.391	0.040	0.082	0.082	0.281	2.20	0.98	0.110
114	-0.27	0.80	0.047	0.384	0.037	0.109	0.080	0.304	2.22	0.99	0.109
115	-0.27	0.81	0.052	0.271	0.034	0.183	0.085	0.241	2.22	0.96	0.109
116	-0.27	0.82	0.052	0.266	0.031	0.233	0.080	0.298	2.26	1.02	0.110
117	-0.27	0.83	0.052	0.276	0.035	0.124	0.084	0.261	2.27	1.06	0.109
118	-0.26	0.74	0.032	0.801	0.057	0.005	0.082	0.277	2.03	0.91	0.108
119	-0.26	0.75	0.038	0.620	0.050	0.006	0.084	0.251	2.28	0.97	0.108
120	-0.26	0.76	0.036	0.667	0.053	0.006	0.083	0.264	2.12	0.94	0.109
121	-0.26	0.77	0.038	0.623	0.046	0.021	0.079	0.316	2.20	0.96	0.108
122	-0.26	0.78	0.044	0.455	0.045	0.030	0.080	0.303	2.14	1.03	0.109
123	-0.26	0.79	0.042	0.509	0.038	0.092	0.083	0.268	2.11	1.00	0.108
124	-0.26	0.80	0.045	0.452	0.036	0.134	0.086	0.244	2.17	1.06	0.108
125	-0.26	0.81	0.049	0.341	0.036	0.123	0.086	0.231	2.19	1.07	0.109
126	-0.26	0.82	0.046	0.397	0.036	0.113	0.082	0.286	2.23	0.98	0.109
127	-0.26	0.83	0.053	0.237	0.032	0.185	0.087	0.220	2.29	1.05	0.110
128	-0.26	0.84	0.052	0.260	0.038	0.071	0.087	0.233	2.19	1.04	0.110
129	-0.26	0.85	0.053	0.239	0.041	0.050	0.083	0.272	2.24	1.09	0.109
130	-0.26	0.86	0.058	0.157	0.045	0.031	0.084	0.246	2.26	1.06	0.109
131	-0.25	0.76	0.037	0.661	0.054	0.006	0.085	0.235	2.21	0.91	0.108
132	-0.25	0.77	0.040	0.582	0.051	0.013	0.082	0.276	2.25	0.98	0.109
133	-0.25	0.78	0.042	0.499	0.049	0.016	0.080	0.299	2.17	0.93	0.109
134	-0.25	0.79	0.043	0.485	0.045	0.043	0.082	0.280	2.24	0.96	0.108
135	-0.25	0.80	0.044	0.443	0.042	0.043	0.085	0.239	2.08	1.01	0.109
136	-0.25	0.81	0.049	0.351	0.040	0.071	0.087	0.221	2.20	0.99	0.109
137	-0.25	0.82	0.046	0.410	0.041	0.054	0.084	0.256	2.26	0.97	0.109
138	-0.25	0.83	0.051	0.281	0.035	0.176	0.089	0.204	2.25	1.03	0.108
139	-0.25	0.84	0.049	0.346	0.037	0.079	0.082	0.290	2.17	1.04	0.109
140	-0.25	0.85	0.052	0.275	0.040	0.064	0.082	0.284	2.29	1.06	0.110
141	-0.25	0.87	0.058	0.171	0.046	0.019	0.083	0.276	2.17	1.02	0.109
142	-0.25	0.88	0.060	0.131	0.050	0.009	0.083	0.270	2.22	1.06	0.110
143	-0.24	0.79	0.043	0.486	0.048	0.013	0.090	0.184	2.21	1.02	0.107
144	-0.24	0.80	0.040	0.555	0.048	0.014	0.087	0.225	2.19	0.94	0.108
145	-0.24	0.81	0.046	0.397	0.043	0.043	0.086	0.232	2.25	1.01	0.108
146	-0.24	0.82	0.047	0.375	0.045	0.028	0.084	0.262	2.21	0.98	0.109
147	-0.24	0.83	0.047	0.363	0.038	0.101	0.084	0.247	2.16	0.98	0.109
148	-0.24	0.84	0.050	0.307	0.037	0.115	0.087	0.213	2.22	1.02	0.110
149	-0.24	0.86	0.052	0.277	0.041	0.043	0.084	0.258	2.20	1.04	0.109
150	-0.24	0.88	0.055	0.212	0.048	0.011	0.087	0.213	2.37	1.09	0.109
151	-0.23	0.81	0.039	0.603	0.051	0.009	0.083	0.268	2.10	1.03	0.108
152	-0.23	0.82	0.047	0.393	0.049	0.012	0.087	0.228	2.20	1.02	0.108
153	-0.23	0.83	0.047	0.384	0.045	0.032	0.089	0.203	2.15	1.07	0.108
154	-0.23	0.84	0.047	0.364	0.038	0.099	0.086	0.227	2.23	0.99	0.108
155	-0.23	0.85	0.050	0.306	0.040	0.052	0.086	0.225	2.17	1.08	0.109
156	-0.23	0.86	0.055	0.211	0.042	0.040	0.086	0.229	2.32	1.08	0.109
157	-0.23	0.89	0.060	0.141	0.052	0.006	0.086	0.224	2.19	1.07	0.109
158	-0.22	0.79	0.037	0.677	0.059	0.008	0.088	0.214	2.06	0.95	0.107
159	-0.22	0.83	0.045	0.446	0.054	0.006	0.086	0.231	2.29	1.00	0.108
160	-0.22	0.84	0.043	0.468	0.047	0.025	0.082	0.277	2.27	1.05	0.108
161	-0.22	0.85	0.050	0.308	0.041	0.062	0.087	0.225	2.22	0.98	0.108
162	-0.22	0.90	0.055	0.201	0.049	0.011	0.085	0.244	2.26	1.09	0.109

No.	$f(P)$		W_{10}		P		α		DP-IP [%]	SP-IP [%]	f_b
	x_0	σ	\mathcal{D}	\mathcal{P}	\mathcal{D}	\mathcal{P}	\mathcal{D}	\mathcal{P}			
163	-0.21	0.83	0.042	0.529	0.054	0.011	0.088	0.206	2.19	0.91	0.107
164	-0.21	0.85	0.048	0.357	0.047	0.036	0.091	0.177	2.21	1.03	0.108
165	-0.21	0.86	0.047	0.377	0.044	0.025	0.086	0.222	2.19	1.04	0.108
166	-0.21	0.87	0.048	0.358	0.042	0.045	0.090	0.193	2.20	1.03	0.109
167	-0.20	0.84	0.045	0.437	0.054	0.014	0.083	0.264	2.27	1.03	0.107
168	-0.20	0.85	0.046	0.409	0.051	0.006	0.079	0.321	2.33	1.05	0.107
169	-0.20	0.86	0.048	0.340	0.049	0.014	0.083	0.275	2.12	0.99	0.108
170	-0.20	0.87	0.049	0.331	0.046	0.018	0.085	0.248	2.24	1.07	0.108
171	-0.20	0.88	0.048	0.351	0.044	0.024	0.080	0.306	2.15	1.08	0.107
172	-0.19	0.87	0.045	0.444	0.051	0.014	0.080	0.306	2.28	1.08	0.108
173	-0.19	0.90	0.055	0.219	0.047	0.017	0.080	0.316	2.23	1.03	0.108
174	-0.18	0.87	0.045	0.413	0.053	0.006	0.085	0.239	2.15	0.99	0.107
175	-0.18	0.88	0.050	0.318	0.051	0.014	0.087	0.228	2.24	1.00	0.107
176	-0.18	0.89	0.050	0.335	0.052	0.007	0.086	0.248	2.27	1.09	0.107
177	-0.18	0.90	0.052	0.255	0.047	0.021	0.083	0.266	2.14	1.06	0.107
178	-0.18	0.91	0.053	0.254	0.049	0.010	0.084	0.262	2.20	1.07	0.107
179	-0.17	0.88	0.049	0.345	0.054	0.005	0.086	0.234	2.31	1.05	0.106
180	-0.17	0.89	0.050	0.286	0.054	0.007	0.086	0.231	2.24	1.05	0.107
181	-0.17	0.90	0.053	0.243	0.051	0.007	0.085	0.247	2.25	1.09	0.107
182	-0.17	0.91	0.049	0.333	0.050	0.008	0.086	0.227	2.16	1.05	0.107
183	-0.16	0.92	0.054	0.213	0.051	0.009	0.085	0.238	2.32	1.06	0.107

Table B5: Simulation results of the pulsar beam for opening angle distribution Eq. (13), inclination angle distribution function Eq. (6) and period distribution function Eq. (8). Graphical representation of this class of solutions is represented in Fig. C6.

No.	$f(P)$		W_{10}		P		α		DP-IP [%]	SP-IP [%]	f_b
	x_0	σ	\mathcal{D}	\mathcal{P}	\mathcal{D}	\mathcal{P}	\mathcal{D}	\mathcal{P}			
1	0.37	2.32	0.036	0.687	0.049	0.008	0.088	0.206	2.13	0.96	0.110
2	0.37	2.33	0.038	0.634	0.050	0.005	0.090	0.189	2.18	0.94	0.110
3	0.37	2.35	0.035	0.729	0.049	0.007	0.091	0.177	2.07	0.92	0.109
4	0.37	2.36	0.036	0.690	0.050	0.006	0.090	0.181	2.06	0.89	0.109
5	0.37	2.37	0.032	0.797	0.049	0.009	0.086	0.231	2.21	0.98	0.109
6	0.37	2.38	0.033	0.760	0.051	0.007	0.086	0.234	2.22	0.96	0.109
7	0.38	2.26	0.041	0.554	0.051	0.005	0.088	0.206	2.20	0.99	0.110
8	0.38	2.27	0.039	0.601	0.049	0.007	0.089	0.208	2.20	0.97	0.110
9	0.38	2.28	0.041	0.549	0.049	0.007	0.092	0.173	2.19	0.97	0.110
10	0.38	2.29	0.041	0.547	0.048	0.010	0.090	0.180	2.20	0.98	0.109
11	0.38	2.30	0.036	0.696	0.049	0.008	0.090	0.184	2.14	0.98	0.110
12	0.38	2.31	0.035	0.731	0.047	0.014	0.089	0.200	2.19	0.98	0.109
13	0.38	2.32	0.033	0.778	0.047	0.012	0.091	0.179	2.07	0.88	0.109
14	0.38	2.33	0.034	0.736	0.048	0.010	0.093	0.155	2.08	0.99	0.109
15	0.38	2.34	0.033	0.776	0.050	0.008	0.091	0.176	2.18	0.91	0.108
16	0.38	2.35	0.034	0.749	0.051	0.008	0.093	0.167	2.21	0.90	0.109
17	0.38	2.36	0.030	0.851	0.052	0.006	0.094	0.150	2.09	0.93	0.108
18	0.39	2.19	0.051	0.287	0.050	0.006	0.096	0.138	2.20	1.03	0.111
19	0.39	2.22	0.039	0.609	0.048	0.010	0.091	0.173	2.15	0.95	0.110
20	0.39	2.23	0.040	0.573	0.047	0.012	0.093	0.159	2.16	0.98	0.110
21	0.39	2.24	0.039	0.603	0.047	0.012	0.090	0.182	2.16	0.95	0.110
22	0.39	2.25	0.034	0.766	0.046	0.016	0.089	0.202	2.16	1.01	0.109
23	0.39	2.26	0.036	0.700	0.046	0.014	0.089	0.207	2.14	0.94	0.109
24	0.39	2.27	0.034	0.735	0.044	0.022	0.090	0.185	2.15	0.98	0.109
25	0.39	2.28	0.034	0.744	0.045	0.020	0.092	0.164	2.14	1.02	0.109
26	0.39	2.29	0.033	0.787	0.045	0.017	0.089	0.204	2.09	1.05	0.108
27	0.39	2.30	0.030	0.873	0.049	0.010	0.085	0.234	2.11	0.88	0.108
28	0.39	2.31	0.030	0.842	0.052	0.005	0.088	0.220	2.07	0.94	0.108
29	0.40	2.13	0.050	0.289	0.050	0.006	0.088	0.209	2.19	1.03	0.112
30	0.40	2.14	0.050	0.316	0.051	0.006	0.090	0.186	2.20	1.01	0.111
31	0.40	2.15	0.051	0.282	0.050	0.007	0.094	0.153	2.15	1.00	0.112
32	0.40	2.16	0.045	0.442	0.048	0.009	0.093	0.160	2.05	1.08	0.111
33	0.40	2.17	0.041	0.532	0.047	0.011	0.090	0.185	2.13	0.93	0.110
34	0.40	2.18	0.044	0.461	0.044	0.018	0.092	0.170	2.24	0.96	0.111
35	0.40	2.19	0.039	0.589	0.044	0.023	0.088	0.205	2.21	1.01	0.111

No.	$f(P)$		W_{10}		P		α		DP-IP [%]	SP-IP [%]	f_b
	x_0	σ	\mathcal{D}	\mathcal{P}	\mathcal{D}	\mathcal{P}	\mathcal{D}	\mathcal{P}			
36	0.40	2.20	0.040	0.559	0.044	0.020	0.091	0.182	2.23	0.99	0.109
37	0.40	2.21	0.037	0.656	0.045	0.018	0.092	0.170	2.16	0.99	0.110
38	0.40	2.22	0.039	0.602	0.045	0.019	0.095	0.142	2.20	0.97	0.109
39	0.40	2.23	0.038	0.640	0.043	0.028	0.091	0.183	2.14	0.97	0.109
40	0.40	2.24	0.033	0.774	0.045	0.024	0.089	0.198	2.13	0.96	0.109
41	0.40	2.25	0.033	0.784	0.049	0.011	0.093	0.158	2.07	0.98	0.109
42	0.40	2.26	0.034	0.770	0.047	0.020	0.090	0.183	2.18	0.96	0.108
43	0.40	2.27	0.034	0.737	0.049	0.013	0.091	0.182	2.16	1.05	0.109
44	0.40	2.28	0.030	0.871	0.053	0.005	0.091	0.172	2.06	0.92	0.108
45	0.41	2.10	0.048	0.338	0.049	0.007	0.089	0.203	2.23	1.05	0.111
46	0.41	2.11	0.045	0.432	0.047	0.010	0.090	0.180	2.23	1.01	0.112
47	0.41	2.13	0.047	0.375	0.044	0.025	0.089	0.203	2.14	1.06	0.110
48	0.41	2.14	0.044	0.451	0.042	0.029	0.090	0.188	2.23	0.98	0.109
49	0.41	2.15	0.044	0.433	0.043	0.030	0.091	0.178	2.23	0.96	0.110
50	0.41	2.16	0.041	0.540	0.042	0.030	0.091	0.181	2.18	0.98	0.110
51	0.41	2.17	0.038	0.633	0.041	0.037	0.088	0.206	2.23	0.96	0.109
52	0.41	2.18	0.038	0.641	0.042	0.033	0.089	0.201	2.09	1.01	0.109
53	0.41	2.19	0.039	0.604	0.042	0.032	0.093	0.166	2.11	1.02	0.110
54	0.41	2.20	0.034	0.746	0.043	0.030	0.090	0.191	2.11	0.97	0.109
55	0.41	2.21	0.036	0.698	0.045	0.031	0.090	0.190	2.20	0.92	0.109
56	0.41	2.22	0.037	0.656	0.047	0.016	0.095	0.147	2.10	1.04	0.108
57	0.41	2.23	0.031	0.832	0.050	0.023	0.088	0.209	2.14	0.94	0.108
58	0.41	2.24	0.031	0.842	0.053	0.006	0.090	0.182	2.19	0.96	0.108
59	0.42	2.06	0.045	0.413	0.051	0.006	0.083	0.270	2.25	1.05	0.113
60	0.42	2.07	0.047	0.386	0.049	0.008	0.085	0.251	2.29	1.08	0.110
61	0.42	2.08	0.047	0.377	0.048	0.009	0.085	0.248	2.22	1.04	0.111
62	0.42	2.09	0.045	0.422	0.045	0.019	0.085	0.240	2.19	1.03	0.110
63	0.42	2.11	0.040	0.555	0.042	0.033	0.083	0.257	2.25	1.02	0.110
64	0.42	2.12	0.043	0.488	0.041	0.041	0.082	0.279	2.29	0.99	0.110
65	0.42	2.13	0.041	0.542	0.041	0.040	0.086	0.238	2.21	1.03	0.109
66	0.42	2.14	0.038	0.623	0.039	0.053	0.090	0.187	2.17	0.96	0.109
67	0.42	2.15	0.037	0.649	0.041	0.047	0.083	0.267	2.14	1.05	0.109
68	0.42	2.16	0.037	0.649	0.041	0.040	0.086	0.231	2.24	0.99	0.108
69	0.42	2.17	0.037	0.663	0.042	0.041	0.084	0.257	2.16	1.03	0.109
70	0.42	2.18	0.036	0.675	0.046	0.025	0.085	0.238	2.13	0.88	0.109
71	0.42	2.19	0.032	0.805	0.054	0.006	0.083	0.265	2.20	0.92	0.108
72	0.42	2.20	0.034	0.766	0.051	0.008	0.087	0.218	2.26	0.95	0.108
73	0.43	2.05	0.048	0.354	0.045	0.018	0.093	0.163	2.24	1.03	0.111
74	0.43	2.06	0.045	0.433	0.044	0.023	0.089	0.192	2.10	1.02	0.111
75	0.43	2.07	0.046	0.409	0.042	0.029	0.090	0.188	2.17	0.95	0.110
76	0.43	2.08	0.042	0.520	0.042	0.038	0.091	0.174	2.17	0.97	0.110
77	0.43	2.09	0.038	0.621	0.039	0.050	0.084	0.252	2.07	1.05	0.110
78	0.43	2.10	0.038	0.615	0.041	0.038	0.083	0.261	2.21	1.00	0.109
79	0.43	2.11	0.040	0.571	0.043	0.035	0.088	0.210	2.16	0.88	0.109
80	0.43	2.12	0.038	0.618	0.040	0.052	0.089	0.197	2.15	1.00	0.109
81	0.43	2.13	0.037	0.646	0.047	0.023	0.090	0.187	2.20	1.00	0.109
82	0.43	2.14	0.032	0.815	0.047	0.021	0.087	0.222	2.07	0.97	0.108
83	0.43	2.15	0.034	0.759	0.048	0.018	0.089	0.194	2.19	0.98	0.109
84	0.43	2.16	0.037	0.675	0.050	0.011	0.091	0.176	2.19	0.96	0.109
85	0.44	2.01	0.051	0.294	0.050	0.014	0.091	0.180	2.13	1.03	0.111
86	0.44	2.02	0.046	0.408	0.048	0.012	0.092	0.165	2.23	1.01	0.111
87	0.44	2.03	0.048	0.349	0.046	0.016	0.090	0.185	2.38	1.08	0.111
88	0.44	2.04	0.042	0.502	0.044	0.024	0.092	0.172	2.20	1.03	0.111
89	0.44	2.05	0.043	0.480	0.043	0.032	0.089	0.197	2.17	1.08	0.110
90	0.44	2.06	0.040	0.576	0.042	0.034	0.093	0.160	2.16	0.98	0.110
91	0.44	2.07	0.040	0.568	0.041	0.040	0.091	0.179	2.21	1.04	0.110
92	0.44	2.08	0.037	0.644	0.043	0.033	0.089	0.193	2.11	0.96	0.110
93	0.44	2.09	0.033	0.771	0.040	0.049	0.086	0.227	2.18	0.98	0.109
94	0.44	2.10	0.035	0.715	0.042	0.034	0.092	0.173	2.13	0.97	0.109
95	0.44	2.11	0.038	0.625	0.045	0.026	0.091	0.182	2.15	0.93	0.109
96	0.44	2.12	0.034	0.754	0.049	0.011	0.091	0.175	2.25	1.04	0.109
97	0.44	2.13	0.037	0.665	0.054	0.005	0.093	0.167	2.18	1.00	0.108
98	0.45	1.99	0.047	0.366	0.051	0.005	0.092	0.169	2.22	1.01	0.110
99	0.45	2.01	0.044	0.457	0.048	0.014	0.093	0.158	2.12	1.03	0.110
100	0.45	2.02	0.043	0.466	0.046	0.017	0.092	0.170	2.29	1.01	0.111

No.	$f(P)$		W_{10}		P		α		DP-IP [%]	SP-IP [%]	f_b
	x_0	σ	\mathcal{D}	\mathcal{P}	\mathcal{D}	\mathcal{P}	\mathcal{D}	\mathcal{P}			
101	0.45	2.03	0.042	0.514	0.043	0.026	0.095	0.142	2.11	1.08	0.109
102	0.45	2.04	0.037	0.674	0.039	0.066	0.088	0.208	2.11	0.96	0.109
103	0.45	2.05	0.041	0.555	0.040	0.055	0.092	0.172	2.11	1.02	0.110
104	0.45	2.06	0.040	0.584	0.047	0.015	0.095	0.146	2.19	1.00	0.109
105	0.45	2.07	0.038	0.623	0.043	0.037	0.092	0.173	2.19	0.96	0.109
106	0.45	2.08	0.035	0.739	0.050	0.013	0.094	0.152	2.14	1.01	0.109
107	0.45	2.09	0.033	0.771	0.049	0.019	0.089	0.199	2.09	1.04	0.108
108	0.46	1.97	0.045	0.426	0.048	0.010	0.089	0.192	2.18	1.00	0.111
109	0.46	1.98	0.043	0.477	0.049	0.007	0.086	0.237	2.11	1.09	0.110
110	0.46	1.99	0.042	0.504	0.048	0.011	0.090	0.193	2.14	1.01	0.109
111	0.46	2.00	0.041	0.544	0.045	0.020	0.089	0.206	2.27	0.97	0.109
112	0.46	2.01	0.039	0.613	0.043	0.034	0.086	0.228	2.12	0.99	0.109
113	0.46	2.02	0.042	0.502	0.044	0.026	0.090	0.191	2.09	1.05	0.110
114	0.46	2.03	0.038	0.639	0.044	0.030	0.090	0.188	2.11	0.96	0.110
115	0.46	2.04	0.037	0.654	0.046	0.018	0.092	0.166	2.17	0.97	0.109
116	0.46	2.05	0.033	0.778	0.048	0.014	0.088	0.210	2.09	1.00	0.109
117	0.47	1.95	0.045	0.440	0.050	0.007	0.087	0.236	2.19	0.97	0.110
118	0.47	1.96	0.045	0.437	0.051	0.006	0.089	0.198	2.15	1.04	0.110
119	0.47	1.97	0.039	0.603	0.047	0.014	0.083	0.264	2.09	0.93	0.109
120	0.47	1.98	0.042	0.520	0.046	0.017	0.088	0.205	2.25	1.01	0.109
121	0.47	1.99	0.041	0.530	0.045	0.018	0.089	0.198	2.21	0.99	0.110
122	0.47	2.00	0.042	0.514	0.048	0.016	0.085	0.236	2.13	1.05	0.109
123	0.47	2.01	0.039	0.603	0.046	0.017	0.089	0.214	2.19	0.97	0.109
124	0.47	2.02	0.036	0.704	0.051	0.007	0.087	0.226	2.10	1.05	0.108
125	0.47	2.03	0.036	0.701	0.050	0.013	0.087	0.218	2.06	0.96	0.109
126	0.47	2.05	0.037	0.678	0.056	0.006	0.086	0.241	2.16	0.99	0.108
127	0.48	1.91	0.048	0.355	0.053	0.009	0.095	0.140	2.23	1.07	0.110
128	0.48	1.93	0.043	0.467	0.051	0.008	0.089	0.200	2.17	1.04	0.110
129	0.48	1.95	0.042	0.525	0.046	0.019	0.088	0.211	2.25	0.97	0.109
130	0.48	1.96	0.040	0.560	0.046	0.016	0.087	0.218	2.34	0.97	0.110
131	0.48	1.97	0.040	0.582	0.045	0.023	0.090	0.191	2.17	1.00	0.109
132	0.48	1.98	0.037	0.678	0.046	0.020	0.089	0.196	2.24	1.02	0.109
133	0.48	2.00	0.034	0.754	0.052	0.007	0.085	0.251	2.07	1.03	0.108
134	0.48	2.01	0.035	0.721	0.055	0.008	0.087	0.225	2.17	0.99	0.108
135	0.49	1.93	0.042	0.518	0.047	0.013	0.087	0.220	2.29	0.92	0.109
136	0.49	1.94	0.043	0.466	0.047	0.013	0.089	0.203	2.24	0.96	0.109
137	0.49	1.95	0.035	0.716	0.046	0.015	0.083	0.275	2.17	1.00	0.109
138	0.49	1.97	0.038	0.643	0.049	0.011	0.089	0.206	2.22	1.01	0.108
139	0.50	1.91	0.042	0.515	0.049	0.008	0.091	0.183	2.21	0.96	0.109
140	0.50	1.92	0.041	0.531	0.047	0.012	0.087	0.215	2.19	1.04	0.109
141	0.50	1.93	0.038	0.625	0.050	0.009	0.089	0.200	2.19	0.97	0.108
142	0.51	1.88	0.044	0.455	0.052	0.005	0.094	0.153	2.10	1.04	0.110
143	0.51	1.89	0.041	0.548	0.050	0.007	0.091	0.180	2.20	1.08	0.108
144	0.51	1.90	0.038	0.619	0.051	0.006	0.090	0.195	2.20	1.02	0.108
145	0.51	1.91	0.036	0.685	0.052	0.005	0.089	0.198	2.22	0.93	0.109
146	0.52	1.89	0.039	0.601	0.054	0.006	0.090	0.191	2.11	1.02	0.108
147	0.52	1.90	0.040	0.589	0.052	0.005	0.086	0.234	2.19	0.99	0.108

Table B6: Simulation results of the pulsar beam for opening angle distribution Eq. (14), inclination angle distribution function Eq. (6) and period distribution function Eq. (8). Graphical representation of this class of solutions is represented in Fig. C5.

No.	$f(P)$		W_{10}		P		α		DP-IP [%]	SP-IP [%]	f_b
	x_0	σ	\mathcal{D}	\mathcal{P}	\mathcal{D}	\mathcal{P}	\mathcal{D}	\mathcal{P}			
1	0.38	2.51	0.071	0.047	0.049	0.009	0.083	0.266	2.29	1.07	0.110

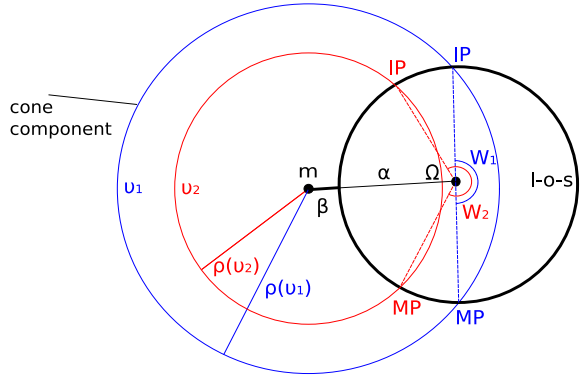


Figure C1. Model of the single-pole interpulse – ML77 version. Two cones of average emission corresponding to frequencies ν_1 (blue) and $\nu_2 > \nu_1$ (red) with an opening angle $\rho(\nu_1) > \rho(\nu_2)$ are marked schematically. For a given α and β angles the l-o-s (marked by the black circle) cuts the radiation cones twice. In this figure it is assumed that at frequency ν_1 MP and IP are separated about $W_1 = 180^\circ$ of longitude. However with increasing frequency the separation W will be different ($W_2 > W_1$ for the presented geometry). This frequency dependence of MP–IP separation is the main difference between ML77 and G83 (presented in Fig. C2) versions of SP–IP models.

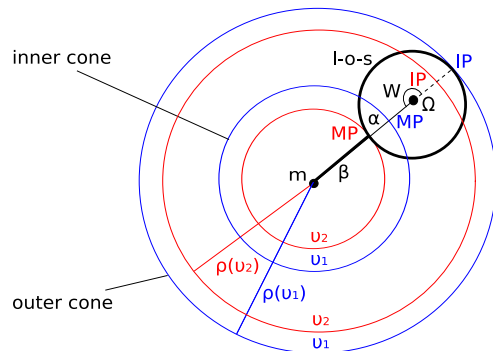


Figure C2. Model of the single-pole interpulse for two nested hollow cones (or inner core surrounded by the cone) – G83 version. In this case the mean pulsar beam consist of core and cone or two nested, coaxial cones (blue circles for frequency ν_1 and red circles of frequency $\nu_2 > \nu_1$). For a given α and β angles the l-o-s (black circle) cuts through both cones. The inner and the outer cone is responsible for the occurrence of the MP and the IP, respectively. For different (higher) observational frequency ν_2 (red circles) the opening angle $\rho(\nu_1) > \rho(\nu_2)$. However, this version of the SP–IP model the MP–IP separation W is frequency independent and equal to 180° of longitude.

APPENDIX C: FIGURES

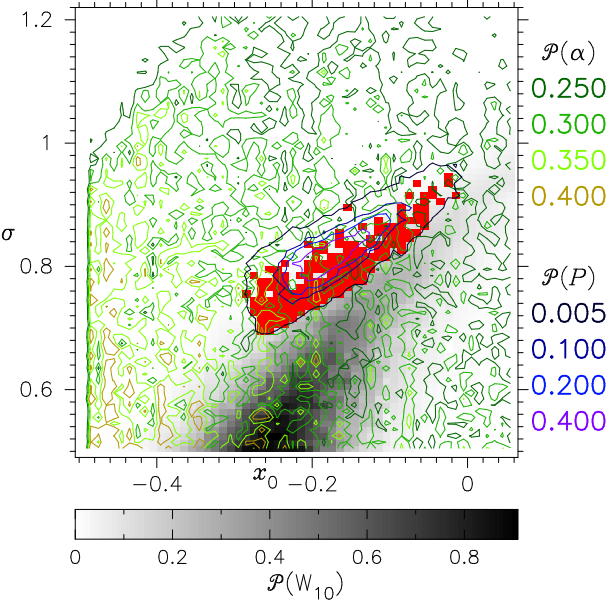


Figure C3. As in Fig. 7 but for opening angles described by Eq. (14). All acceptable solutions are represented by red rectangles and their distribution describes errors of the log–normal functions $x_0 = -0.18^{+0.16}_{-0.11}$ and $\sigma = 0.81^{+0.13}_{-0.12}$ (see also Tab.B3).

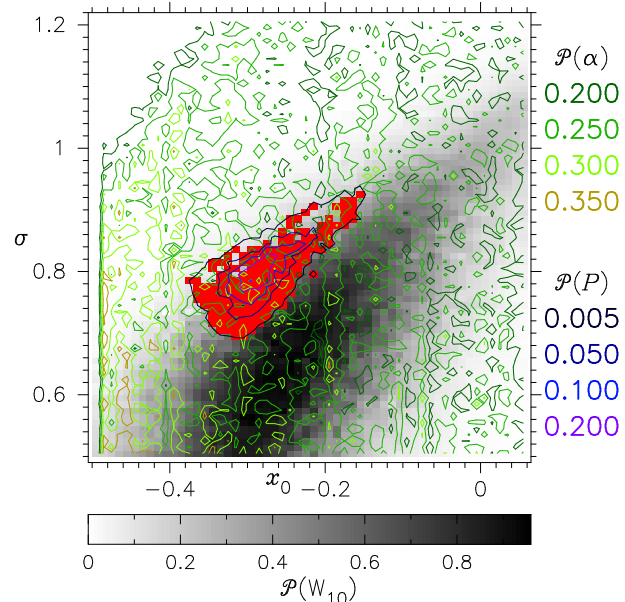


Figure C4. As in Fig. 7 but for opening angles described by Eq. (15b). All acceptable solutions are represented by red rectangles and their distribution describes errors of the log–normal functions $x_0 = -0.29^{+0.13}_{-0.09}$ and $\sigma = 0.79^{+0.13}_{-0.10}$ (see also Tab.B4).

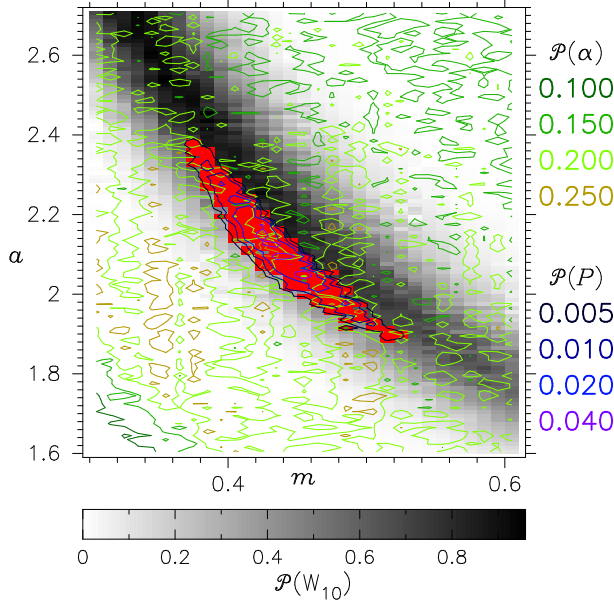


Figure C5. As in Fig. 7 but for period distribution function Eq. (8) and opening angles described by Eq. (13). All acceptable solutions are represented by red rectangles and their distribution describes errors of the gamma functions $m = 0.45^{+0.07}$ and $a = 2.04^{+0.34}_{-0.16}$ (see also Tab.B5).

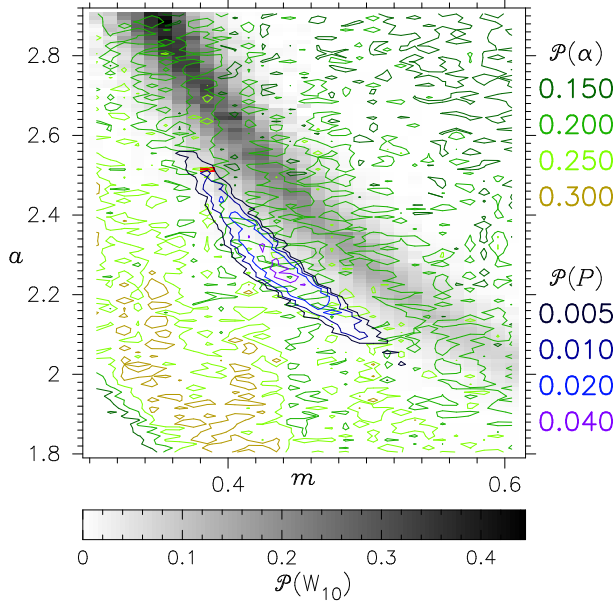


Figure C6. As in Fig. C5 but for opening angles described by Eq. (14). The only one acceptable solution is represented by red rectangle with the gamma function parameters $m = 0.38$ and $a = 2.51$ (see also Tab.B6).

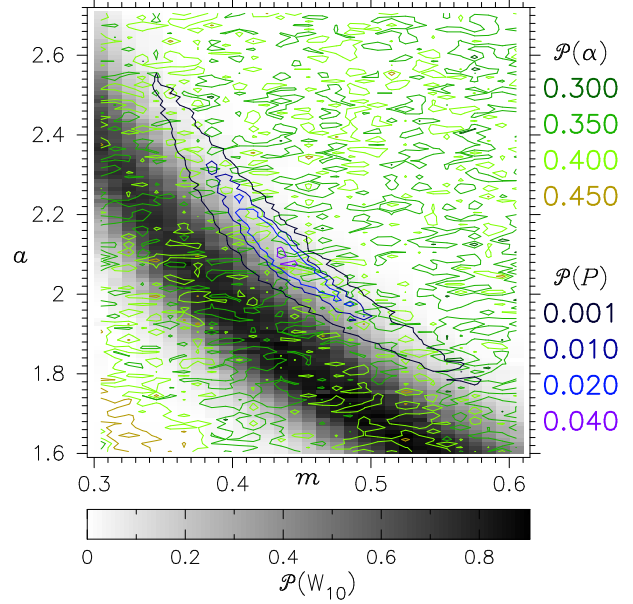


Figure C7. As in Fig. 7 but for period distribution function Eq. (7) and opening angles described by Eq. (13). Notice that no interpulses were found.

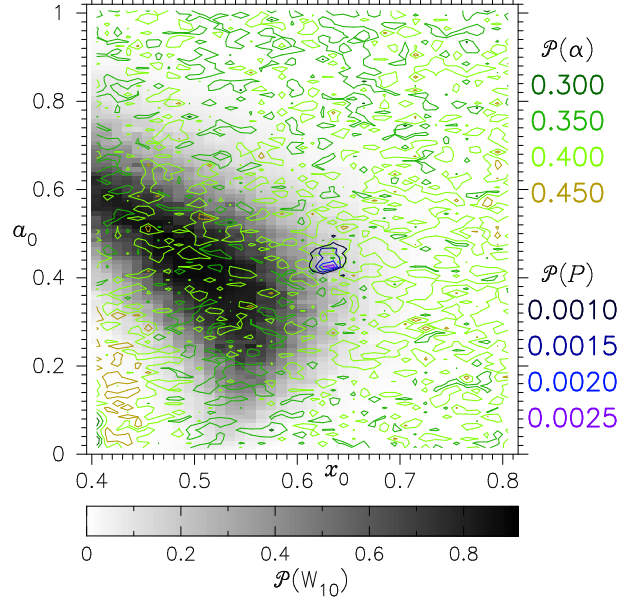


Figure C8. As in Fig. C7 but for period distribution function Eq. (9). Notice that no interpulses were found.

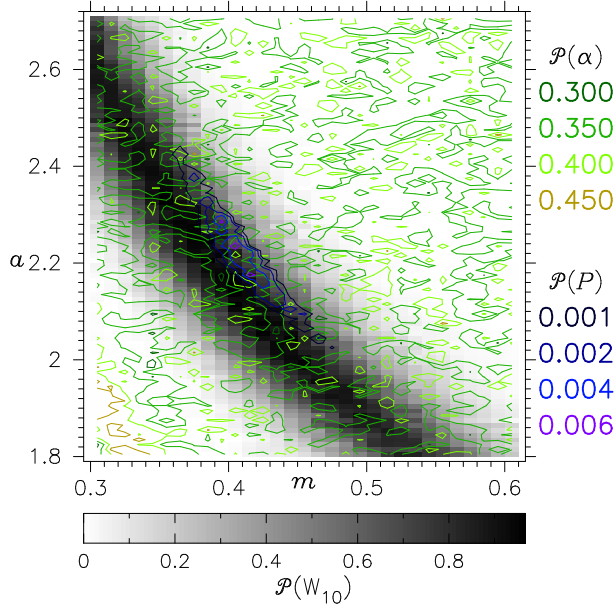


Figure C9. As in Fig. C7 but for opening angles described by Eq. (15b). Notice that no interpulses were found.

This paper has been typeset from a $\text{\TeX}/\text{\LaTeX}$ file prepared by the author.